MASTERARBEIT | MASTER'S THESIS

Titel | Title

p53 aggregation: a prognostic biomarker and drug target?

verfasst von | submitted by

Lena Marie Hauser BSc

angestrebter akademischer Grad | in partial fulfilment of the requirements for the degree of

Master of Science (MSc)

Wien | Vienna, 2024

Studienkennzahl lt. Studienblatt | Degree programme code as it appears on the student record sheet:	UA 066 834
Studienrichtung lt. Studienblatt | Degree programme as it appears on the student record sheet:	Masterstudium Molekulare Biologie
Betreut von | Supervisor:	ao. Univ.-Prof. Dr. Robert Zeillinger

Abstract

The tumor suppressor protein p53, coined the “guardian of the genome”, has shown to be an important mechanistic factor in the development and progression of ovarian cancer and breast cancer. However, mutated p53 is currently neither a drug target nor used as biomarker for treatment guidance in both cancers. Protein aggregation is a well-known contributor to specific neurodegenerative diseases with misfolded proteins causing protein loss-of-function and the disruption of protein homeostasis. Recently, new research has shown that in cancer, multiple tumor suppressor proteins show intrinsic aggregation tendencies, including p53. In response, multiple drugs have been developed that target p53 aggregation, like ReACp53. By binding to an aggregation-prone sequence, ReACp53 attempts to stabilize the wild-type structure of p53, thereby restoring its functionality. This work aims to test the efficacy of ReACp53 in breast cancer cell lines. Additionally, this work aims to look at p53 aggregation as a possible prognostic marker in ovarian cancer. Both projects include the Proximity Ligation Assay (PLA) method, which has a high specificity and sensitivity for detecting protein-protein interaction and can be used for fixed cells and formalin-fixed paraffin-embedded (FFPE) tissue, making it ideal for the analysis of cell lines and patient samples. The PLA has been adapted with two antibody combinations: p53-binding antibody with the oligomer-binding antibody A11 or p53-antibody with the amyloid fibril-binding antibody OC. To further elucidate ReACp53 sensitivity mechanisms in the course of this work, real-time polymerase chain reaction and immunofluorescence were done to measure the expression levels of *TP53*, Δ40p53, Δ133p53, *TP63,* and *TP73* and protein level of p53, p63, and p73 in breast cancer cell lines. We have shown that ReACp53 reduces both oligomer and fibril p53 aggregation. Additionally, ReACp53 increases p63 levels and reduces p73 levels. ReACp53 treatment also led to a small increase in apoptotic cells. We have also shown that fibril p53 aggregation is a statistically significant prognostic marker for progression-free survival in high-grade serous ovarian cancer. In our cohort, patients with intermediate and high fibril p53 staining have longer progression-free survival. If these findings are validated in future studies with larger patient cohorts, it could re-evaluate how we approach p53 aggregation as not only a prognostic marker, but also re-evaluate the relevance of current treatment approaches aiming to reduce p53 aggregation in ovarian cancer.

Zusammenfassung

Das Tumorsuppressorprotein p53, auch genannt “Wächter des Genoms“, ist ein wichtiger Faktor in der Entstehung und Entwicklung von Eierstock- und Brustkrebs. Jedoch ist mutiertes p53 aktuell weder ein Behandlungsziel noch wird es eingesetzt als Biomarker für Behandlungsentscheidungen in beiden Krebsarten. Proteinaggregation ist üblicherweise bekannt für dessen Rolle in neurodegenerativen Erkrankungen, in denen inkorrekt gefaltete Proteine ihre Funktion verlieren und die Proteinhomöostase destabilisieren. Neueste Forschung hat gezeigt, dass mehrere Tumorsuppressorproteine ein intrinsisches Potential zur Proteinaggregation zeigen, inklusive p53. Daraufhin wurden neue Wirkstoffe entwickelt, die p53-Aggregation beeinflussen, wie zum Beispiel ReACp53. In dem ReACp53 die aggregationsanfällige Sequenz von p53 bindet, unterstützt es die Faltung zur Wildtyp-Struktur von p53 und stellt somit wieder die Funktionsfähigkeit von p53 her. Diese Arbeit testet die Funktionsfähigkeit von ReACp53 in Brustkrebs-Zelllinien. Zusätzlich wird in dieser Arbeit untersucht, ob p53-Aggregation ein möglicher prognostischer Biomarker bei Eierstockkrebs ist. In beiden Projekten wird die Färbemethode „Proximity Ligation Assay“ verwendet, welche eine hohe Spezifität und Sensitivität aufweist, um Protein-Protein Interaktionen zu visualisieren. Die Methode kann sowohl bei formalinfixiertem als auch bei formalinfixiertem, paraffineingebettetem Material verwendet werden, was sie ideal für die Analyse von Zelllinien und Patientengewebe macht. Der Proximity Ligation Assay wurde hier mit zwei verschiedenen Antikörperkombination verwendet: ein p53-bindender Antikörper mit dem oligomer-bindenden Antikörper A11 und ein p53-bindender Antikörper mit dem fibrillär-bindenden Antikörper OC. Im Laufe der Arbeit wurde ebenfalls quantitative Polymerasenkettenreaktion und Immunofluoreszenz verwendet um die Genexpressionslevels von *TP53,* Δ40p53, Δ133p53*, TP63 and TP73* und die Proteinlevel von p53, p63 und p73 in den Brustkrebs-Zelllinien zu charakterisieren. Wir konnten zeigen, dass ReACp53 die Menge an sowohl oligomerer als auch fibrillärer p53-Aggregation reduziert. Zusätzlich erhöht ReACp53 die Menge an p63 und senkt die Menge an p73. Die Menge an apoptotischen Zellen wird ebenfalls durch ReACp53 erhöht. Wir konnten zeigen, dass p53-Aggregation ein signifikanter prognostischer Biomarker für progressionsfreies Überleben in hochgradig serösem Eierstockkrebs ist. In unserer Kohorte zeigen Patientinnen mit mittlerer oder hoher fibrillärer p53-Aggregationsmenge ein längeres progressionsfreies Überleben. Sollten diese Ergebnisse in Studien mit größerer Patientenmenge bestätigt werden können, würde dies eine neue Herangehensweise an p53-Aggregation anstoßen. Dies gilt sowohl für p53-Aggregation als prognostischer Marker, als auch für p53 Aggregation als Ziel von Wirkstoffen, die p53-Aggregation in Eierstockkrebs verringern sollen.

Acknowledgements

First and foremost, I would like to express my deepest gratitude to Prof. Dr. Robert Zeillinger for giving me the opportunity to work in his laboratory and for his critical support throughout this research.

I am also sincerely thankful to Nicole Heinzl, PhD, whose patience, mentorship, and insightful feedback helped not only shape this work but my attitude towards research. Her guidance was essential to my progress and growth, and I am eternally grateful for the opportunity to have learned from her.

I would like to thank Eva Welsch for being my unwavering moral support and providing much-needed humor through both the good and tough times.

I would also like to extend my appreciation to all the members of the Molecular Oncology laboratory for creating such a positive work environment.

I am deeply grateful to my family and friends for their unwavering support throughout this journey. I am especially grateful for my Mom without whose support and determination I wouldn't have made it this far.

A special thanks goes to my partner, Thomas, whose constant encouragement and belief in me have been a source of strength during this entire process.

Affidavit

I hereby declare,

that I have authored the present master thesis independently, did not use any sources other than those indicated, and did not receive any unauthorized assistance,

that I have not previously submitted this master thesis topic in any form, in this country or any other, for academic credit,

and that this work is identical to the one assessed by the registered supervisor.

The practical work for the real-time PCR was done by Eva Schuster and Dr. Eva Obermayr, who kindly provided the results for this work. The assembly of the tissue microarrays was done by the Department of Pathology, Charité Berlin pertaining to the clinical trial EUDARIO and the Department of Gynecological Pathology, General Hospital Vienna.

Wien / Vienna

September 2024

Contents

1. Introduction

1.1 p53

Throughout years of research, a variety of molecular mechanisms involved in cancer formation and progression have been identified. Within these, the tumor suppressor gene *TP53* often takes center stage due to a mutation rate of 50 % across all human cancer cases.[1] *TP53* is located on chromosome 17p13.1 and encodes the tumor suppressor protein p53.[2] The full-length human p53 (FLp53) protein consists of 393 amino acids (aa), has a molecular weight of 53 kDa and can be divided into three structural domains (Figure 1).[3,4] The N-terminal region (aa 1-94) contains: the transactivation domain 1 (TAD1; aa 1-40), transactivation domain 2 (TAD2, aa 40-69), and a proline-rich region (PRR, aa 64-94). The second structural domain is the central DNA-binding domain (DBD, aa 94-292), which is characterized by its highly evolutionary conservation. The C-terminal region (aa 292-393) is divided into a tetramerization or oligomerization domain (OD, aa 325-356) and a regulatory C-terminal domain (CTD, aa 356-393).[4] The C-terminal region also includes the nuclear localization signal domain (aa 305-322).[3]

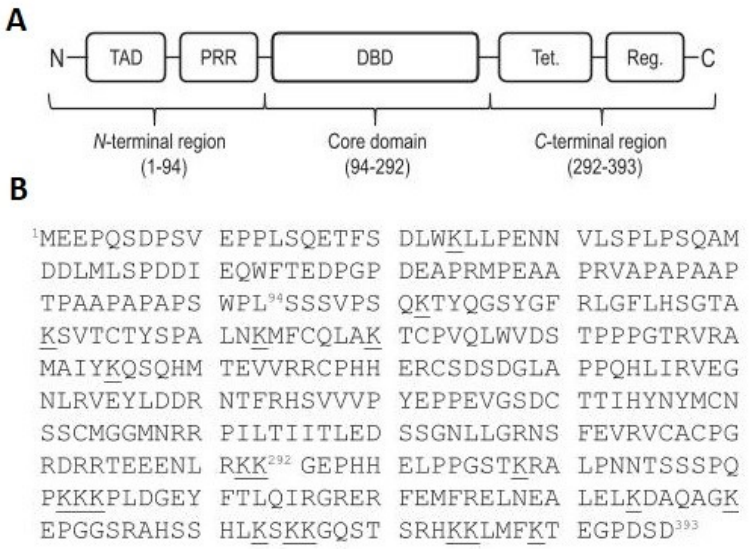

Figure 1 :(A) Scheme of the domains of human p53 protein. The numbers refer to the corresponding amino acids. (B) Amino acid sequence of human p53 protein. Lysines are underscored. Figure adapted from Artl et al. (2015)[5].

So far, 12 isoforms of the protein p53 have been identified. The four major isoforms of the N-terminal are full-length p53, Δ40p53, Δ133p53, and Δ160p53. Each can have the C-terminal alternative splice variants α,β, and γ.[6] The isoform Δ40p53 is generated either through initiation of translation in exon 4 or alternative splicing of intron 2, while Δ133p53 and Δ160p53 are generated through a second promoter in intron 4. The Δ40p53 isoform lacks the first

transactivation domain but retains the second, while the Δ133p53 and Δ160p53 isoform only retain part of the DNA-binding domain and the C-terminus.[6,7] The different isoforms have been implicated in multiple important cellular processes, including oxidative stress, cell cycle arrest, senescence, apoptosis, DNA double-strand break repair, NF-κB signaling, JAK-STAT signaling, and interferon signaling.[8,9] Additionally, these isoforms are differentially expressed in healthy and cancerous tissue. P53 isoforms have been shown to have significant clinical relevance for different types of cancer, with FLp53γ, Δ133p53α, and Δ133p53β being implicated in breast cancer and Δ40p53 and Δ133p53α being involved in ovarian cancer.[6]

Like many other transcription factors, p53 relies on zinc binding to stabilize the complete structure and its DNA-recognizing elements.[10] While the DBD is stably folded, the TAD and CTD contain intrinsically disordered domains.[11] These domains make up 37% of the full-length protein and make it difficult to study the folded structure of p53 by conventional methods, like crystallography or nuclear magnetic resonance (NMR) analysis.[4,5] These regions are majorly affected by post-translational modifications (PTM) and, therefore, play a number of important roles in p53 activity and tetramerization.[4] p53 activity can be separated into its function as a pioneer transcription factor and its transcription factor-independent activity.[12] During homeostasis, p53 is maintained at a low level through a high protein turnover. Two essential negative regulators of p53 are MDM2 and MDMX. While MDM2 is an E3 ligase targeting p53 for ubiquitination and subsequent proteasomal degradation, MDMX regulates p53 by directly inhibiting its transcriptional activity.[13,14] Ubiquitination by MDM2 occurs mostly at the C-terminal lysine residues of p53.[11] Besides MDM2 and MDMX, several other E3 ligases have been associated with p53 degradation, including Pirh2, Cop1, TRIM proteins, CHIP, RBCK1 and ARF-BP1.[13] Ubiquitination of p53 is often connected with its transport into the cytoplasm, due to mono-ubiquitination revealing the nuclear export sequence within the C-terminus of p53.[14] In the cytoplasm, it is recognized as a target for degradation by proteasomes.[13] The p53 protein can undergo many additional PTMs like phosphorylation, acetylation, methylation, SUMOylation, NEDDylation, O-GlcNAcylation, ADP-ribosylation, UFMylation, hydroxylation, β-hydroxybutyr-ylation, sulfation, and isoLG adduction. Many of these are reversible, and different types of stress signals induce different types and sites of PTM. While many PTMs have been proven to regulate p53 *in vitro*, the situation *in vivo* is less clearly understood and prompts further investigation.[11] The classical model of p53 activation describes the phosphorylation of p53 by sensor proteins such as ATM, ATR, Chk1, Chk2, HIPK2, DNA-PK, and p14ARF in response to cellular stress, like DNA damage, hypoxia, oncogene activation, translational stress or metabolic changes.[11,15,16] Phosphorylation at the amino acids S15, T18, and S20 inhibits p53 binding to MDM2 and thereby the negative regulation of p53 by MDM2 while simultaneously promoting the interaction with transcription co-factors like CREB-binding protein or the histone acetyltransferase p300.[11,12] This

stabilizes p53 protein levels and leads to a tetramerization (dimerization of dimers) of the protein, which promotes binding to DNA target sites.[12,17] Tetrameric p53 binds DNA cooperatively, with genes involved in cell cycle arrest less dependent on cooperative p53 binding than genes involved in initiating apoptosis. This suggests that intermolecular p53 interactions play a role in deciding cell fate after DNA damage.[12,18] Besides cell cycle arrest and apoptosis, p53 is also involved in senescence, genome stability, metabolism, ferroptosis, stem cell dynamics, cell competition, metastasis, and immunity.[11] Genome-wide analysis has shown that p53 regulates some target genes directly, however the majority is regulated indirectly. *CDKN1A* is a direct p53 target gene and encodes the cyclin-dependent kinase inhibitor p21. When p21 blocks the activity of cyclin-dependent kinases, DREAM (DP, RB-like, E2F4, and MuvB) and RB:E2F transrepressor complexes are activated, which ultimately leads to a stable cell cycle arrest (senescence).[19] Other p53 transcriptional target genes include the proapoptotic Bcl-2 family proteins PUMA (p53-upregulated modifier of apoptosis), NOXA, BID, BAX, and BAK, amongst others.[20,21] These proteins regulate mitochondrial outer membrane permeabilization (MOMP), which releases apoptogenic proteins like cytochrome-c into the cytosol.[21] This ultimately leads to the activation of caspase-3 and caspase-7, which cleave more than a thousand different proteins, either activating or degrading them. The enzymatic activity leads to the display of a typical apoptotic phenotype characterized by chromatin condensation, cell shrinkage, and membrane blebbing.[22] The transcription factor-independent activity of p53 is mainly characterized by p53 directly binding to BAX and BAK, releasing it from their negative regulators Bcl-2 and Bcl-xL.[14] In total, a variety of mechanisms exist to control p53 through regulation of its protein activity, stability, and subcellular localization.[23]

The physiological function of p53 depends greatly on the DNA-binding domain, which is further accentuated by the observation that approximately 95% of tumor-related *TP53* gene mutations occur in this domain. Additionally, 73% of *TP53* mutations are missense mutations, affecting important regulatory contacts, which leads to a disruption of the tertiary structure.[16,24] Mutations that destabilize the Zn^{2+} binding impair the DBD structure and, therefore, shift the p53 protein into pre-aggregational states.[24] In general, *TP53* mutations can be separated into class I structural and class II contact mutations. While structural mutations cause a lower thermodynamic stability that results in an unfolded structure compared to wild type p53, contact mutations lead to an impairment in DNA binding site recognition. Some mutations have been named “hotspot” mutations due to their increased frequency, accounting for 28% of all *TP53* mutations.[16,25] These hotspot mutations and their class are depicted in Table 1.

Table 1: Table of hotspot mutations most common in TP53 and their structural or contact mutation classification.[1]

Hotspot Mutation	Structural / Contact Mutation
R175H	Structural
G245S	Structural
R248Q	Structural and Contact
R248W	Contact
R249S	Structural
R273H	Contact
R282H	Structural

The outcome of mutations can have vastly different effects on p53 behavior. These outcomes are categorized into loss-of-function (LOF), dominant-negative (DN), and gain-of-function (GOF). In LOF of p53, the physiological activity of wild-type p53 is lost, and it no longer performs tumor-suppressive functions like cell cycle arrest, DNA repair, and apoptosis. Due to the tetrameric folding of p53, mutant p53 can exert a dominant negative effect on wild-type p53 by binding and inhibiting its function. Some mutations have been identified as resulting in a GOF phenotype like promoting enhanced migration, invasion, and metastasis, where p53 no longer acts as a tumor suppressor but rather as an oncogene.[16,26] Stabilization and aggregation of p53 have been speculated to be a potential driver of this GOF behavior.[24]

1.2 p63 and p73

The p53 family is comprised of p53, p63, and p73, and all three proteins show high sequence similarity, with the DBD exhibiting 60 % sequence homology between them.[27,28] Each of the p53 family members contains an N-terminal TAD, a central DBD, and an OD. Additionally, p63 and p73 can contain a C-terminal domain with a sterile alpha motif domain and a transactivation inhibitory domain (Figure 2). *TP63* is located on the distal long arm of the human chromosome 3q27, whereas *TP73* is located on the short arm of chromosome 1p36.[29,30] Both, *TP63* and *TP73*, possess two distinct promoters, one located upstream of exon 1 (P1) and the other located within the intron sequence 3 (P2). If the transcription starts from the P1 promoter, the full-length or N-terminal acidic TA domain (*TAp63* and *TAp73*) will be transcribed. If the transcription, however, starts at the promoter region P2, this TA domain is missing (*ΔNp63* and *ΔNp73*). Additionally, C-terminal splicing can give rise to a variety of p63 and p73 isoforms, with seven isotypes identified for p73 (α, β, γ, δ, ε, ζ and η) and three types identified for p63 (α, β and γ).[28] The α-isoforms of both proteins are most abundantly expressed in nearly all human tissues.[31]

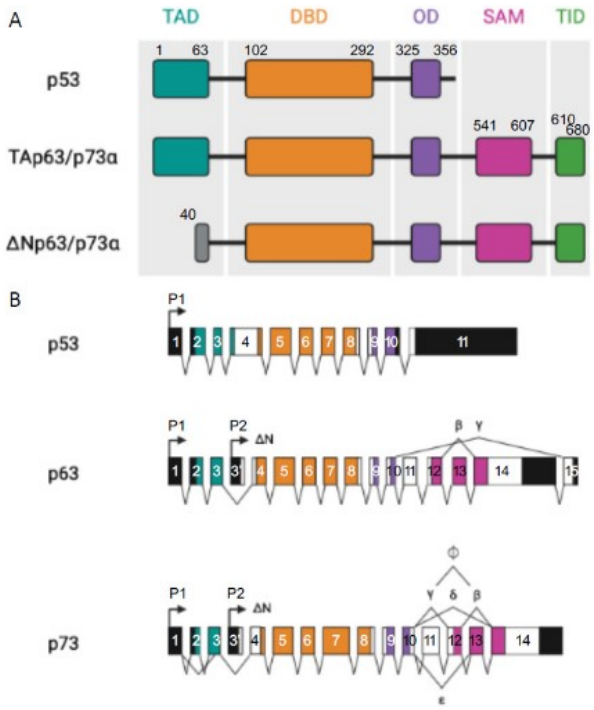

Figure 2: Schematic depiction of p53 family members. (A) Depiction of the p53, TAp63/TAp73 and ΔNp63/ΔNp73 isoforms with their domains. Transactivation domain (TAD, turquoise), DNA-binding domain (DBD, orange), Oligomerization domain (OD, purple), Sterile alpha-motif (pink), Transactivation inhibitory domain (TID, green). (B) Depiction of the p53, p63 and p73 exons. P depicts the promoters, the boxes indicate exons and the lines indicate introns. Adapted from Rodriguez Calleja et al. (2022)[29]

In both proteins, the N-terminal acidic TA isoform is associated with pro-apoptotic and anti-oncogenic activity, while the ΔNp63 and ΔNp73 isoforms are associated with being pro-oncogenic.[32,33] Both TAp63 and ΔNp63 are important regulators of epidermal development and epithelial stem cell maintenance, whereas p73 regulates core genes involved in intercellular adhesion, extracellular matrix interactions, and cell migration.[30,34] ΔNp63 is a key oncogenic driver in squamous cell carcinoma due to 80% of head and neck squamous cell carcinomas showing an amplification of the p63 gene, with ΔNp63α being the most prevalent isoform.[28,33] ΔNp73 overexpression is a factor for poor prognosis in multiple cancers, including ovarian cancer and advanced-stage breast cancer. ΔNp73 isoform expression has been associated with chemoresistance through upregulation of the ATP-binding cassette transporter family, and ΔNp73 isoforms are key regulators in the epithelial-to-mesenchymal transition by inducing a mesenchymal phenotype, which is vital in the development of circulating tumor cells and metastasis.[35] While p53 is mutated in approximately 50 % of cancer cases, p63 and p73 are rarely mutated in cancers.[25] Multiple studies found that when mutated p53 forms aggregates, the dominant-negative effect does not only affect wild-type p53 but also extends to p63 and p73. Wild type p53 does not form oligomers with p63 or p73 *in vivo*, however mutated p53 co-aggregates with p63 and p73, inhibiting their function.[33,36]

1.3 Protein aggregation

Protein functionality is intrinsically linked to its structure. Protein folding is determined by the properties of the amino acid side chains, the environment, protein concentration, and protein folding chaperones, amongst other factors. Most of the intrinsic folding properties of a protein are determined by its free energies. The native folded state of a protein has a lower free energy than its unfolded state in a given environment and is, therefore, thermodynamically preferred.[37] However, some proteins are so-called intrinsically disordered proteins that do not have a fixed three-dimensional structure due to the lack of a global energy minimum but instead multiple folding states with similar energy minima that are separated by low energy barriers.[38] While native protein folding depends on intramolecular interactions between the side chains of the amino acid sequence and its environment, the structure of amyloid states is influenced by intermolecular interactions of the backbone that is common to all protein structures. This so-called cross-β conformation is defined by the intermolecular β-sheets pairing together with their side chains interlinking in an alternating pattern.[39] The cross β-sheet formation of aggregates is highly stable, making it difficult to remove them. The formation of aggregation structures starts with the presence of aggregation-prone regions (APR). On average, 20 % of residues in protein sequences have aggregation propensity. APRs in a protein are called its intrinsic aggregation propensity, while the actual aggregation propensity is additionally influenced by environmental conditions, the protein's concentration, and the conformational landscape of the protein itself. Proteins with the APR folded away from the surface are more aggregation-resistant than proteins with their APR close to the surface. To reduce the aggregation propensity of proteins, APRs are directly flanked by aggregation gatekeepers. These are charged residues and beta-structure breakers. However, these aggregation gatekeepers come at a cost to the native stability of the protein, as each gatekeeper reduces the thermodynamic stability by ~0.5 kcal/mol. Apart from the reduction of stability, they are also likely to slow down native protein folding due to their removal of sidechain charges.[40] The formation of amyloids can be separated into multiple phases. In the commonly accepted nucleation theory, the rate-limiting first step is the nucleation. The nucleation describes the initial formation where the interfacial energy cost of creating a solid phase (amyloid) in a liquid (aqueous cell environment) needs to be overcome. If a preformed amyloid is used as the starting point for aggregation formation, it is called seeding.[39] After this critical nucleation barrier is overcome, the continuous aggregation becomes energetically favorable, and the amyloid grows by monomer addition.[41] These aggregates can grow into oligomers, smaller and more globular-like protein aggregates. Oligomers can be separated into two categories depending on whether they are competent to form fibrils ("on-pathway") or not ("off-pathway"). Fibrils are defined by the repeating structure of β-strands running perpendicular to the fibril axis. In comparison to oligomers, fibrils are significantly elongated. When the quantity

of fibrils makes them visible under light microscopy, the aggregation structure is referred to as plaques.[42]

1.4 p53 aggregation in cancer

Protein aggregation has been proposed as a key driver in multiple neurodegenerative diseases.[41] Aggregation of proteins like amyloid-β, tau, α-synuclein, and SOD-1 has been proven to occur in diseases like Alzheimer's disease, Parkinson's disease, and amyotrophic lateral sclerosis. Outside of neurological diseases, aggregation seems to be implicated in diseases like diabetes type-2 and cancer.[43] The aggregation prediction algorithm TANGO detected two peptide sequences in p53 with higher amyloidogenic potential (aa 250-257 and aa 327-332).[44] The majority of p53 aggregation develops due to an underlying mutation.[45] These mutations trigger a conformational change that exposes the aggregation-prone sequence in p53, which destabilizes the conformation towards the point of phase separation and then aggregation.[45,46] Aggregates of p53 exist in an dynamic equilibrium together with natively folded p53.[47] This equilibrium can also be influenced by the interaction of p53 with DNA and RNA, which have been shown to modulate p53 aggregation.[46] p53 aggregation was found in multiple cancer types, including breast and ovarian cancer in vivo.[48,49] Generally, p53 can aggregate in the nucleus as well as in the cytoplasm.[50,51] *TP53* structure mutations generally lead to a loss-of-function phenotype where the protein cannot perform its function due to a conformational change resulting in decreased stability, protein unfolding, impaired zinc-binding, and, ultimately, aggregation.[43] Furthermore, mutated p53 aggregates can exert a dominant-negative effect on wild-type p53 due to the co-aggregation and, thereby, inactivation of wild-type p53. Not only can mutated p53 co-aggregate with wild-type p53, but some studies report a co-aggregation with p63 and p73 and chaperons.[52] Additionally, p53 aggregation has also been shown to induce histone acetylation through CREB-binding protein and STAT2 recruitment to promoter sites of genes regulating cell proliferation and motility.[50] When p53 aggregation is located in the cytoplasm, it adds to the cellular stress triggered by the unfolded protein response, which further destabilizes the cell.[26] All these processes can then add towards GOF effects, including chemoresistance, increased tumor invasiveness, metabolic reprogramming, angiogenesis, increased migration, stem cell expansion, and tissue remodeling.[50,52,53] Cytoplasmic p53 aggregation does not only hinder the transportation of functional p53 into the nucleus but is also immune to proteasome-mediated degradation.[51] This is why concepts for therapeutic approaches involve autophagy-mediated degradation of p53 aggregates to free wild-type p53 and p63 and p73.[52] In recent years, studies have been published that postulate the idea of "prion-like p53", similar to infectious prion-particles known from diseases like Creutzfeldt-Jakob's disease or

Bovine Spongiform Encephalopathy.[54] Forget et al. have shown that extracellular p53 aggregates can enter cells via macropinocytosis and induce the aggregation of endogenous wild-type p53.[55] However, this has also been challenged, with studies showing that the effect of imprinting an aggregational state onto wild-type p53 can be fully recovered by changing the ratio of aggregated and wild-type p53.[56]

1.5 Aggregation detection methods

1.5.1 Fluorescent Dyes

Fluorescent dyes are available that undergo a spectral shift after binding to aggregation structures. Congo Red has been one of the most widely used. Binding to amyloids leads to a strong increase in red fluorescent light at ~614 nm, which is detectable with standard fluorescence microscopy filters. The limitations of Congo Red include varying results due to section thickness, insensitivity towards small amounts of amyloids, and false-positive signal due to the mounting medium. Another fluorescent dye widely used in practice is Thioflavin T. The fluorescent signal intensity is determined by the inhibited rotation of the aniline ring when bound to amyloid structures and is detectable at 480 nm. The specificity of Thioflavin T results should always be verified since binding to globular proteins like albumin can also produce a fluorescent signal.[57]

1.5.2 P53-Seprion ELISA

Enzyme-linked immunosorbent assay (ELISA) is a detection method where the specificity of antibody binding is used, which allows for high-sensitivity detection.[58] The Seprion-ELISA is a modified variant of an ELISA where the antibody at the bottom of the well is replaced by a Seprion Ligand. This Seprion Ligand is a polyionic polymer that, combined with the provided capture buffer, can bind amyloid aggregates, while monomeric protein is removed by washing. After amyloid binding, a primary antibody binding to p53 is added, followed by a secondary antibody conjugated with horseradish peroxidase (HRP). The enzymatic reaction catalyzed by HRP results in a color change proportional to the amount of bound p53 antibody. This allows for specific quantitative p53-amyloid detection.[59] However, the p53-Seprion ELISA can only be used with fresh-frozen material, which is difficult to obtain in a clinical setting.[60]

1.5.3 Native Western Blot

A native western blot employs the standard method of western blotting with a non-denaturing gel-electrophoresis beforehand. This allows for the retention of the amyloid structure. Together with a p53 antibody, p53 aggregates can be identified due to their higher molecular weight. [61]

1.5.4 Conformation–specific antibodies

The most widely used conformation-specific antibodies are the antibodies A11 and OC. The antibody A11 is raised against pre-fibrillar oligomers, while the antibody OC binds fibrils.[60] These conformation-dependent antibodies can be used in a variety of methods, including co-immunoprecipitation, co-immunofluorescence (co-IF), and Proximity Ligation Assay (PLA). Co-immunofluorescence is a method where the immunofluorescent staining is done with two different antibodies binding to different proteins. In the case of p53 aggregation, an anti-p53 antibody and a conformation-dependent antibody are used. These antibodies are either conjugated with different fluorophores or secondary labeled antibodies are added. The regions where both fluorescent signals are present are implicated to contain p53 aggregates.[49] However, this is not reliable as both epitopes do not necessarily need to be present in the same molecule to produce a signal.[60] This is improved with the Proximity Ligation Assay, where both antibodies need to bind in the proximity of less than 40 nm to each other. After the primary antibodies are bound close to each other, antibodies directed against the primary antibodies' fixed region coupled with an oligonucleotide fragment, so-called probes, are added. The oligonucleotide fragments then hybridize and are amplified through rolling circle amplification. These DNA circles can then be visualized with fluorescence-labeled oligonucleotides.[62]

1.6 Drugs targeting p53 aggregation

Since p53 aggregation was found to play a role in tumorigenesis, considerable efforts have been made to find a drug that specifically targets p53 aggregation and potentially restores wild type p53 function. One potential candidate is the tripyridylamide ADH-6. This cationic α-helix mimetic imitates the topography of α-helices and thereby serves as an effective antagonist for protein-protein interactions. ADH-6 dissolves mutant p53 aggregates in multiple p53 mutated human cancer cell lines and shrinks tumor size in mice xenografts without damaging surrounding healthy tissue.[63] Already in clinical use is the drug arsenic trioxide (ATO), which is approved for the treatment of acute promyelocytic leukemia. Recently, it has been found that ATO stabilizes p53 through covalent binding. In patient-derived xenograft models in mice, ATO reduced tumor size by 42.9% at a similar rate to the cisplatin positive control, whereas p21 upregulation was mainly found in the ATO-treated mice.[64] The polyphenol resveratrol has been tested in breast cancer cell

lines to specifically reduce mutant p53 aggregation and reduce viability and migration of MDA-MB-231 cells *in vitro*.[65] As already mentioned, p53 has a sequence stretch between the amino acids 250-257 that is highly aggregation-prone. Soragni et al. have developed a small peptide drug called Re-Activate p53 (ReACp53) that specifically binds to the amino acids 252-258 (LTIITLE) in the p53 sequence and thereby attempts to restore wild-type p53 structure. The amino acid sequence of ReACp53 itself consists of the aggregation inhibiting portion LTRITLE, with the arginine in position 3 inhibiting a peptide aggregation of ReACp53 itself and an N-terminal poly-9-arginine cell-penetrating tag to ensure cellular uptake of ReACp53.[66] Lei et al. have shown that for the *TP53* mutation R175H, ReACp53 specifically binds to the target region via hydrophobic interactions and forms salt bridges and hydrogen bonds, decreasing the exposure of the aggregation-prone region.[67] Additionally, ReACp53 and the R175H mutated p53 form a strong positive net charge, which discourages wild-type p53 protein to bind and, therefore, pushes the folding equilibrium of p53 towards a functional, wild-type like conformation.[66,67] *In vitro*, ReACp53 treatment induced cell death in mutant p53 organoids but not in wild-type p53 organoids. Additionally, ReACp53-treated mutant p53 organoids showed upregulated transcription of wild type p53 targets.[66] In prostate cancer cell lines, ReACp53 altered p53 cellular localization, increased mitochondrial membrane potential, and increased the association between p53 protein and the apoptosis-inducing Bcl-2 family proteins. Additionally, ReACp53 sensitized p53 mutant-bearing prostate cancer cells toward antiandrogen therapy.[68] In high-grade serous ovarian cancer cell lines, ReACp53 treatment increased apoptosis, measured by annexin V, and showed additive effects in combination with carboplatin therapy.[69]

1.7 Breast cancer

1.7.1 Incidence

In 2022, breast cancer (BC) was the most common cancer amongst women and the 2nd most common cancer worldwide, with 23.8 % and 11.5 % of all cancer cases, respectively. In women, breast cancer is the leading cause of cancer death. The highest age-standardized incidence rates of breast cancer in women are in Australia-New Zealand, Northern America, and Northern Europe, while the lowest rates are in Middle Africa, South Central Asia, and Eastern Africa.[70] According to a meta-analysis by Maajani et al. (2019), the 5-year survival rate for breast cancer decreases from 86 % in Stage I to 32 % in Stage IV. Women in developed countries have a better average 5-year survival rate of 76 %, compared to 69 % for women in developing countries.[71] The most important risk factor is sex, with 99 % of breast cancer cases occurring in women and 1 % in men.[72] Another critical risk factor is age. From 2015 to 2019, 29 % of female breast cancer cases in the US were diagnosed in the age group 60-69, closely followed by 50-59 with 22 % and 70-79 with 21 % of cases.[73] Additionally, the more aggressive triple-negative breast cancer subtype is more often diagnosed in women under 40 years of age, while the most common subtype for women above >70 years of age is Luminal A.[74] It is believed that less than 10 % of breast cancer cases are caused by predisposing germ-line mutations, such as *BRCA1* and *BRCA2* mutations. However, the risk doubles for women whose closest relative has been diagnosed and rises to 3-6x if two close relatives have been diagnosed.[72] Besides *BRCA1* and *BRCA2*, other high penetrance genes like *TP53*, *CDH1*, *PTEN,* and *STK11* are also correlated with a higher risk of breast cancer. In general, risk factors can be divided into modifiable and non-modifiable risk factors. Next to sex, age, family history, and genetics, other non-modifiable risk factors include ethnicity, (lack of or late) pregnancy, and higher density of breast tissue. Modifiable risk factors are hormone replacement therapy, low physical activity, obesity, alcohol intake, and smoking, amongst others.[74]

1.7.2 Diagnosis

Currently, the most effective screening method for breast cancer detection is mammography. While randomized trials reported that mammography screenings reduced breast cancer mortality by 15-25 %, meta-analyses of observational studies reported a mortality reduction of 13-23 %.[75] The age group that benefits the most from mammography screenings are women aged 60-69 years old.[76] The majority of national screening programs in Europe offer bi-annual screenings for women over 50 years of age.[77] The negative aspects of mammography include false-positive diagnoses, radiation exposure, pain, anxiety, and other potential psychological stress factors.[76] Most commonly, breast cancer presents as a breast lump. However, it may also be accompanied by other symptoms such as breast swelling, changes in size or shape, skin changes, nipple changes, and breast pain.[78]

1.7.3 Histology and Staging

There are two common histological classification systems for breast cancer. The first system was defined by Perou and Sorlie, based on the gene expression signature of 50 genes (PAM50) and includes the subtypes of "Luminal A", "Luminal B", "HER-2 enriched", "Claudin-low", "Basal-like" and "Normal-like". The second system is called the "Surrogate intrinsic types" and is defined by histology and the immunohistochemistry expression of key proteins, like estrogen receptor (ER), progesterone receptor (PR), human epidermal growth factor receptor 2 (HER2) and the proliferation marker Ki-67.[79] Since the surrogate intrinsic types are used more widely in a clinical setting to guide treatment decision and are used to classify cell lines that emerged from patient samples, this system will be used in the following work. In Table 2, each surrogate intrinsic type is defined by its receptor profile.

Table 2: Overview of the histological subtypes of breast cancer, adapted from Harbeck et al.(2019)[79]

Breast Cancer subtype	Receptor profile	Percentage of diagnoses
Luminal A-like	ER +, PR +, HER2-, low Ki-67	60-70 %
Luminal B-like Her2-	ER +, PR ±, HER2-, high Ki-67	10-20 %
Luminal B-like Her2+	ER +, PR ±, HER2+, high Ki-67	13-15 %
HER2+	ER-, PR-, HER2+	
Triple negative	ER-, PR-, HER2-	10-15 %

In addition to histology staging, disease staging (shown in Table 3) is also an important factor to consider when evaluating treatment decisions.

Table 3: Overview of staging of breast cancer, adapted from Karim et al. (2023)[80]

Stage	Stage 0	Stage I	Stage II	Stage III	Stage IV
Name	Noninvasive ductal carcinoma in situ	Invasive ductal carcinoma			Metastatic breast cancer
Description	Tumor cells in breast duct have not spread to surrounding breast tissue	Tumor spreading in breast tissue, <2 cm in diameter	Tumor 2-5 cm in diameter	Tumor >5 cm in diameter with spread to auxiliary lymph nodes	Tumor spread beyond breast tissue. Preferential metastasis in brain, lungs, liver and bones

1.7.4 Therapy

Patients with an operable, early breast cancer without metastatic spread first undergo surgery. Systemic therapy can be given in advance (neo-adjuvant) to reduce tumor size prior to removal for patients with large tumor sizes and/or a triple-negative subtype. Patients with ER and/or PR positive disease should undergo endocrine therapy to block ER and/or PR activity. Systemic therapy can also be given after surgery (adjuvant) if the surgical outcome and/or biomarkers indicate a higher risk of recurrence. Maintenance therapy for luminal-like subtypes involves endocrine therapy for a minimum duration of 5 years, while maintenance therapy for the Her2-positive subtype includes mainly anti-Her2 targeting therapy like T-DM1 and other antibody-drug conjugates (ADC).[81,82] Maintenance therapy for triple-negative breast cancer includes mostly chemotherapy in combination with bevacizumab or alone until disease progression or unacceptable toxicity.[81]

1.7.4.1 Surgery

As previously mentioned, in cases of breast cancer without metastasis, patients who are deemed operable undergo surgery to remove the tumor tissue. Currently, the trend in surgery leans towards breast-conserving surgery (BCS), where only tumor tissue is removed together with the preservation of healthy breast tissue.[74] BCS is done with plastic surgery techniques such as the "round-block" procedure or the "V-mammoplasty". BCS is thereby replacing the previous technique of mastectomy. Mastectomy surgery removes breast tissue as a whole and can be followed by breast reconstruction with either implant surgery or autologous tissue breast reconstruction. Advanced breast cancer includes an inoperable locally advanced tumor with or without distant metastasis. In patients with Stage IV BC, the removal of metastasis is being debated but presents an option for selected patients.[79]

1.7.4.2 Radiation

Post-operative radiation is combined with BCS, and randomized trials have confirmed that long-term mortality rates are similar in patients who underwent BCS and radiation to patients who underwent a mastectomy only. For patients who underwent a mastectomy, post-operative radiation is indicated when clinical and pathological factors point towards an intermediate to high risk of local reoccurrence. Radiation techniques have considerably improved in recent years with the aim of reducing acute or long-term toxicity. These techniques aim to reduce dose non-homogeneity, which in turn reduces complication rates associated with radiation therapy, such as acute skin desquamation, oedema, fibrosis, or negative cosmetic effects. Additionally, techniques applied by the patient, such as a prone position and deep-inspiration breath holding, help reduce toxicity to the heart in left-side breast cancer or in patients with a larger breast size.[76]

1.7.4.3 Systemic therapies

1.7.4.3.1 Endocrine therapies

For patients with breast cancer of the subtype Luminal A or Luminal B, the standard of care includes endocrine therapy that aims to reduce estrogen levels or prevent stimulation by estrogen.[74] The treatment duration is indicated for at least 5 years after surgery and might be used as neo-adjuvant or adjuvant treatment.[74,76] Three main groups of medication have been approved: selective estrogen receptor modulators (tamoxifen, toremifene), selective estrogen receptor degraders (fulvestrant), and aromatase inhibitors (letrozole, anastrozole, exemestane).[74] The choice to add a chemotherapeutic agent to endocrine therapy has become a more nuanced decision-making process in recent years. Multiple genetic tests like MammaPrint, Oncotype-Dx, ProSigna, and EndoPredict have been approved to guide clinical treatment decisions based on the gene expression of 12-50 genes in the tumor tissue. These gene expression analysis tests categorize the reoccurrence risk of the cancer into “low-” and “high-risk” and calculate the risk of recurrence in percent over 10 years. In patients with a low-risk, ER-positive, HER2-negative tumor, and 0-3 involved lymph nodes, chemotherapy can safely be avoided.[79] If the risk of recurrence is >10% in 10 years, chemotherapy is generally recommended. The standard treatment regimen should include an anthracycline and a taxane for high-risk patients. Specifically, the anthracycline doxorubicin and the cytostatic cyclophosphamide in combination with taxane docetaxel were found to be superior compared to docetaxel and cyclophosphamide in high-risk Her2-negative patients. For low-risk patients, anthracycline can be omitted due to studies showing equal or better results with a combination of cyclophosphamide and docetaxel.[83,84]

1.7.4.3.2 PARP inhibitor and Her2-directed therapies

If the patient has a germline *BRCA1* or *BRCA2* mutation, PARP inhibitors are a first-line option for triple-negative BC patients or a second-line option after endocrine treatment for luminal BC patients with advanced disease.[79] For HER2-positive breast cancer, neoadjuvant chemotherapy and targeted anti-HER2 therapies have established themselves as the standard of care.[79] These targeted therapies include trastuzumab, trastuzumab deruxtecan, trastuzumab emtansine, pertuzumab, lapatinib, and neratinib.[74,79] Trastuzumab and pertuzumab are monoclonal antibodies targeting different epitopes on HER2, which block the receptor for intracellular signaling.[85,86] Trastuzumab deruxtecan is an ADC that combines an anti-HER2 antibody with the topoisomerase-I inhibitor exatecan.[87] Trastuzumab emtansine also belongs to the category of ADC and combines an anti-HER2 antibody with the tubulin-binding agent maytansine.[86,87] ADCs have shown great promise in clinical trials and offer a new type of therapeutic agent that aims to reduce the side effects of the strong cytotoxic agents by attaching them to antibodies that target surface markers specifically expressed on tumor cells.[87] Lapatinib and neratinib are both small-molecule drugs that enter the tumor cell and inhibit the tyrosine kinase domain of the human epidermal growth factor 2 receptor.[88,89] Lapatinib is given in combination with other HER2 targeting therapies like trastuzumab as a second-line treatment option. The recommendation for treatment duration of anti-HER2 targeted therapies is no less than 1 year. [79]

1.7.4.4 p53-based therapies

With 30 % of all breast cancer cases, *TP53* is the gene with the highest mutation rate.[90] For triple-negative breast cancer, the *TP53* mutation rate rises to up to 80 % of cases.[26] Recently, *TP53* mutations have been associated with shorter overall survival in metastatic breast cancer across all subtypes.[91] In breast cancer patients with wild-type p53, mainly in the luminal-like subtype, p53 activity is downregulated by other means, such as overexpression of MDM2 or MDMX. In p53-mutant cancers, the current predominant therapeutic approaches are to either restore mutant p53, remove mutant p53, inhibit mutant p53 GOF pathways, or induce synthetic lethality. In wild-type p53 cancers, the focus is on inhibiting MDM2 or MDMX-mediated p53 degradation.[90] While there are many clinical trials currently being conducted, no p53-based therapy has been approved by the Food and Drug Administration (FDA) or European Medicines Ageny (EMA) so far.[92]

1.8 Ovarian cancer

1.8.1 Incidence

In 2022, ovarian cancer (OC) was the most lethal gynecologic cancer, with 206,839 deaths worldwide. The incidence, with 324,398 cases worldwide, was the 18th highest among all cancer types and the 8th most common cancer among women.[70] The highest age-standardized incidence and mortality rates of OC were in Eastern Europe and Northern Europe, while the age-standardized incidence and mortality were lowest in Middle Africa and the Caribbean.[70] Epithelial ovarian cancer (EOC) has an estimated average 5-year survival rate of 45.6 % across all stages.[93] OC arises mostly in women over 40 years of age, of which 90 % of cases are EOC. Most OC diagnoses under the age of 40 are germ cell ovarian cancer.[94] OC appears mainly sporadically, with 5-10 % of cases being of familial origin.[95] However, germline mutations in the *BRCA1* and *BRCA2* genes increase the risk of OC by 44 % and 27 %, respectively, compared to the general population. Mutations in the genes *BRIP1*, *RAD1C,* and *RAD1D* have also been associated with a higher risk of developing OC of 5.8 %, 5.2 %, and 12 %, respectively. Mutations in other genes, like *BARD1*, *CHEK2*, *MRE11A*, *RAD50*, *PALB2,* and *ATM,* have also been linked to the development of OC. All these genes are involved in the homologous recombination (HR)-mediated pathway of DNA repair. Besides these genetic risk factors, hormonal risk factors, like the number of ovulatory cycles, have been associated with OC. This includes early menarche, late menopause, nulliparity, and endometriosis as risk factors, while pregnancy, breastfeeding, or the long-term use of oral contraceptives lower the risk of OC. Additional possible risk factors that have been described are obesity, diabetes, smoking, and the use of perineal talc.[96] The current scientific consensus postulates the fallopian tube as the origin tissue for high-grade serous ovarian cancer. Studies have been published that hint at a “p53 signature” as the earliest recognizable precursor lesion. This small stretch of 10-30 p53-mutated cells on the fallopian epithelium then evolves through clonal expansion, somatic mutations, and methylation change into serous tubal intraepithelial carcinoma (STIC). STIC then progresses into high-grade serous ovarian cancer (HGSOC).[97] A mathematical model indicates that the emergence of a p53 signature and dormant STIC may take up to 20 years or more, while the progression from STIC to HGSOC may happen in a shorter time frame of 6 years.[98] This current model of HGSOC development could explain the high amount of *TP53* mutations present in upwards of 96 % of HGSOC cases.[99]

1.8.2 Diagnosis

A contributing factor to the low survival rate of OC is the late diagnosis. Only around 13 % of serous ovarian cancers are diagnosed at an early stage. There are currently no standardized or effective screening strategies in place for the early detection of OC. Additionally, by the time a patient becomes symptomatic, the disease is found at an advanced stage in 75-80 % of cases.[96] Even then, most symptoms of OC are unspecific and can be associated with a multitude of different gastrointestinal, urological, or other diseases.[95] Symptoms can include abdominal pain, bloating, nausea, constipation, diarrhea, acid reflux, urinary frequency, vaginal bleeding or fatigue. [96] The patient presents clinically with an adnexal mass on imaging or pelvic examination.[95]

1.8.3 Histology and Staging

The World Health Organization (WHO) has defined a framework for histologically categorizing ovarian cancer, which is also supported by the International Federation of Gynecology and Obstetrics (FIGO).[100] Histologically different OC show significant differences in origin, molecular composition, progression, and treatment response, among other factors.[101] The WHO categories are depicted in Figure 3.

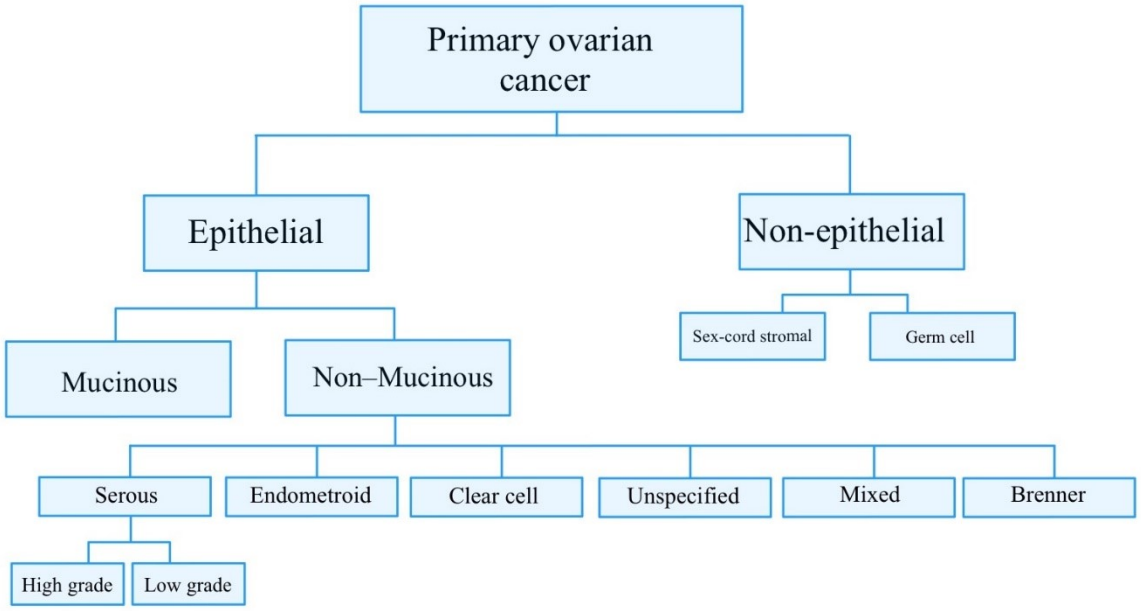

Figure 3: Classification of ovarian cancer histology focusing on epithelial ovarian cancer. Adapted from Gaona-Luviano et al. (2020)[95] and Berek et al. (2021)[100]

Additionally, the FIGO has defined a framework for staging disease progression for OC (Table 4).[100]

Table 4: FIGO classification for staging OC disease[100]

Stage I	**Tumor confined to ovaries or fallopian tube(s)**	**T1 N0 M0**
IA	Tumor limited to 1 ovary (capsule intact) or fallopian tube; no tumor surface; no malignant cells in ascites or washings	T1a N0 M0
IB	Tumor limited to both ovaries (capsules intact) or fallopian tubes; no tumor on surface; no malignant cells in the ascites or washings	T1b N0 M0
IC	Tumor limited to 1 or both ovaries or fallopian tubes, with any of the following:	
IC1	Surgical spill	T1c1 N0 M0
IC2	Capsule ruptured before surgery or tumor on surface	T1c2 N0 M0
IC3	Malignant cells in the ascites or peritoneal washings	T1c3 N0 M0
Stage II	Tumor involves 1 or both ovaries or fallopian tubes with pelvic extension or peritoneal cancer	T2 N0 M0
IIA	Extension and/or implants on uterus and/or fallopian tubes and/or ovaries	T2a N0 M0
IIB	Extension to other pelvic intraperitoneal tissues	T2b N0 M0
Stage III	Tumor involves 1 or both ovaries or fallopian tubes, or peritoneal cancer, with confirmed spread to the peritoneum outside the pelvis and/or metastasis to the retroperitoneal lymph nodes	T1-3 N0-1 M0
IIIA1	Positive retroperitoneal lymph nodes only:	T1-2 N1 -M0
IIIA1(i)	Metastasis up to 10 mm in greatest dimension	
IIIA1(ii)	Metastasis more than 10 mm in greatest dimension	
IIIA2	Microscopic extrapelvic peritoneal involvement with or without positive retroperitoneal lymph nodes	T3a2 N0-1 M0
IIIB	Macroscopic peritoneal metastasis beyond the pelvis up to 2 cm in greatest dimension, with or without metastasis to the retroperitoneal lymph nodes	T3b N0/N M0
IIIC	Macroscopic peritoneal metastasis beyond the pelvis more than 2 cm in greatest dimension, with or without metastasis to the retroperitoneal	T3c N0/N1 M0

	lymph nodes (includes extension of tumor to capsule of liver and spleen without parenchymal involvement of either organ)	
Stage IV	Distant metastasis excluding peritoneal metastases	Any T, any N, M1
Stage IVA	Pleural effusion with positive cytology	
Stage IVB	Parenchymal metastases and metastases to extra-abdominal organs (including inguinal lymph nodes and lymph nodes outside of the abdominal cavity)	

1.8.4 Therapy

1.8.4.1 Surgery – "Debulking"

The most important indicator for the successful treatment of OC is the outcome of the surgical cytoreduction or "debulking". The goal of this treatment is to remove all disseminated tumor mass in the pelvic region of the patient. Often, this includes the complete removal of tumor tissue, reproductive organs, the sigmoid colon, the peritoneum, and the omentum. While the successful outcome of the surgery is defined by the complete resection of the tumor mass with no macroscopic residual disease, a realistically feasible, optimal surgical outcome is defined as less than 1 cm of macroscopic tumor tissue remaining.[96] In some patients who are not good surgical candidates, three to four cycles of neo-adjuvant chemotherapy might be given first, followed by interval debulking surgery and additional chemotherapy.[100]

1.8.4.2 Chemotherapy

FIGO recommends adjuvant chemotherapy for all patients with Stage II disease and higher. The standard is 6 cycles of platinum-based combination chemotherapy with carboplatin or cisplatin and paclitaxel or docetaxel. Currently the efficacy and safety of intraperitoneal chemotherapy and hyperthermic intraperitoneal chemotherapy are evaluated in multiple clinical trials.[100] However, considering the current state of knowledge, both treatment options have not sufficiently proven a benefit over intravenous chemotherapy and are not recommended to replace the standard of care.[102]

1.8.4.3 Targeted Therapy

Bevacizumab is a humanized monoclonal antibody targeted against vascular endothelial growth factor and is, therefore, an angiogenesis inhibitor.[93] The clinical trials GOG 218 and ICON7 have

established Bevacizumab as a possible first-line treatment in combination with standard chemotherapy with an improvement in progression-free survival, but not in overall survival.[100,103] Another recent option for maintenance therapy belongs to the class of Poly (ADP-Ribose) polymerase (PARP) inhibitors. In tumors with a defect in homologous DNA repair (e.g. through a *BRCA1*/*BRCA2* mutation), the cells become over-reliant on Poly (ADP-Ribose) polymerase-mediated base excision repair in the event of spontaneous DNA damage. By inhibiting PARP, the cells accumulate DNA damage, which induces cell death. This process is described as synthetic lethality and an ideal mechanism to target cancer cells due to the underlying first mutation, which makes it specific for cancer cells. The three PARP inhibitors currently approved by the FDA for maintenance treatment in ovarian cancer are olaparib, niraparib, and rucaparib.[104]

1.8.4.4 Relapse

An estimated 80 % of ovarian cancer patients relapse at some stage during treatment. Recurrence is typically asymptomatic and detected by an increase in CA125 levels. The standard treatment procedure for recurrent disease is standard platinum-based chemotherapy, since around 50 % of patients still possess platinum-sensitive disease in recurrence. Other options like gemcitabine, etoposide, and topotecan are also available although the response rate at this stage is around 10-15 %. Eventually, around 80-90 % of patients with advanced disease will become treatment-resistant.[96] This underscores the critical need for innovative treatment approaches, including a potential p53-based approach due to the high p53 mutation rates of 96 % in HGSOC. Current p53-based approaches can be roughly categorized into five categories: viral p53 therapies, liposomal p53 therapies, nanoparticle p53 therapies, small molecular p53 therapies and peptide p53 therapies. While these approaches have generally shown great promise in preclinical studies, further research for clinical application is needed.[99]

1.9 Aims of this thesis

This work is generally separated into two projects.

(1) The first project aims to elucidate ReACp53 sensitivity in breast cancer cell lines.
(2) The second project involves the quantification of p53 aggregation in ovarian cancer tissue to determine its potential as a prognostic biomarker.

2 Methods and Materials

2.1 Cell culture maintenance

The cell line panel used in this study consists of 16 established breast cancer cell lines and the cell line HBL-100 of unknown origin, shown in Table 1. Additionally, the cell lines A-431, HBL-100, and OVCAR-3 were used as controls for immunofluorescence and Proximity Ligation Assay staining, respectively.

Table 5: Overview of cell lines.

Cell line	**Tissue of origin[1]**	**Molecular subtype[2,105]**	**p53 mutational status[3]**
Hs578T	Invasive breast carcinoma	Triple-negative	p.Val157Phe
MDA-MB-468	Breast adenocarcinoma, derived from pleural infusion metastasis	Triple-negative	p.Arg273His
MDA-MB-231	Breast adenocarcinoma, derived from pleural infusion metastasis	Triple-negative	p.Arg280Lys
BT-20	Invasive breast carcinoma	Triple-negative	p.Lys132Gln
BT-549	Invasive breast carcinoma	Triple-negative	p.Arg249Ser
MDA-MB-157	Breast carcinoma, derived from pleural infusion metastasis	Triple-negative	c.261_286del
MDA-MB-436	Invasive breast carcinoma, derived from pleural infusion metastasis	Triple-negative	c.612_613ins
MDA-MB-453	Breast adenocarcinoma, derived from pericardial effusion	Her2-positive	p.His368delinsGln
SK-BR-3	Breast adenocarcinoma, derived from pleural infusion metastasis	Her2-positive	p.Arg175His
UACC-893	Invasive breast carcinoma	Her2-positive	p.Arg342*
T-47D	Invasive breast carcinoma, derived from pleural infusion metastasis	Luminal A	p.Leu194Phe
Cama-1	Breast adenocarcinoma, derived from pleural infusion metastasis	Luminal A[106]	p.Arg280Thr
MCF-7	Invasive breast carcinoma, derived from pleural infusion metastasis	Luminal A	wild-type
BT-474	Invasive breast carcinoma	Luminal B	p.Glu285Lys
ZR-75-30	Invasive breast carcinoma, derived from ascites metastasis	Luminal B	wild-type
MDA-MB-361	Breast adenocarcinoma, derived from brain metastasis	Luminal B	p.Glu56*
*HBL-100**	Unknown origin		wild-type
A-431	Skin squamous cell carcinoma		p.Arg273His
OVCAR-3	High-grade ovarian serous adenocarcinoma, derived from ascites metastasis		p.Arg248Gln

[1]www.cellosaurus.org
[2]https://www.atcc.org
[105]Witt et al. (2023), doi:10.3390/life13122311
[3]https://tp53.cancer.gov/search_cell_lines, www.cellosaurus.org accessed 09/2024

The cell line MDA-MB-468 was kindly gifted by Klaus Czerwenka (Department of Pathology, Medical University of Vienna). The remaining cell lines were purchased from the American Type Culture Collection (Manassas, Virginia). All cell lines were tested regularly for *Mollicutes* (*Mycoplasma*, *Acholeplasma*, *Spiroplasma*) contamination with the Venor®GeM Classic kit from Minerva Biolabs GmbH (Berlin, Germany, 11-1025). Cells were grown in RPMI 1640 medium (Gibco, Thermo Fisher Scientific, Massachusetts USA, 21875-034 500ml) supplemented with 10 % fetal bovine serum (FBS, Gibco, 10270106) and 1 % Penicillin/Streptomycin (PS, Gibco, 15140122). Cell flasks were kept at 37° C in a BBD 6220 CO_2 humidified incubator (Thermo Fisher Scientific) with a CO_2 concentration of 5 %. All cell culture handling was done under sterile conditions in a Biowizard Silver Line Biosafety Cabinet (Kojair Tech Oy, Vilppula, Finland). Cells were passaged and harvested using Trypsin/EDTA (Gibco, 25300-062) at 80 % confluency. The old medium was removed, and cells were washed with 1x PBS w/o Mg^{2+} and Ca^{2+} (Gibco, 12559069). For a T25 flask, 1 ml of 0.05 % Trypsin/EDTA was added and incubated for at least 4 minutes at 37° C until cells lifted. To inactivate the Trypsin/EDTA, the volume of complete medium added was at least twice the volume of Trypsin/EDTA, and the cell suspension was either passaged or harvested for further analysis.

The "reactivating p53" ReACp53 peptide was kindly gifted by Dr. Alice Soragni, University of California, Los Angeles. The peptide was aliquoted to avoid multiple freeze-thaw cycles.

2.2 ReACp53 IC_{50} measurement

After cell harvest, the cells were centrifuged at 200 rcf for 8 min, then the supernatant was removed, and the cells were resuspended in 1 ml of RPMI 1640 medium. 10 µl of the cell suspension mixed 1:1 with Trypan blue (Life Technologies, Thermo Fisher Scientific, T10282) was used to count the number of cells with the LUNA cell counter II (Logos Biosystems, Anyang South Korea, L4002). Cells were then diluted with RPMI 1640 medium to 7000 cells per 200 µl. 200 µl cell suspension was seeded per well into a 96-well plate (Figure 4). After 24-hour incubation at 37° C, the medium was removed, and the wells were washed with FBS-free RMPI 1640 medium with 1 % PS. After washing, 0-40 µM ReACp53 was added, as depicted in Figure 1. Cells were incubated with ReACp53 for 24 hours at 37° C. Then, the EZ4U assay (Biomedica Immunoassays, Vienna, Austria, BI-5000) was performed. The detection reagent SUB substrate was dissolved in 2.5 ml ACT activator solution, pre-warmed to 37° C, and 20 µl was added to the 200 µl cell suspension. After 4 hours, absorption rates were measured in a Fluostar Optima plate reader (BMG Labtech, Ortenberg Germany) at 450 nm. Each cell line was tested in three technical replicates in three independent experiments. For the analysis, first the blank values were

subtracted in Microsoft Excel® (2016). Absorbance values were normalized by defining the untreated cells as 100% viability. Survival curves were generated by analyzing the normalized cell survival data with the "non-linear fit of log dose vs response curve" analysis option in GraphPad Prism (Version 6.01).

	blank	0	40	30	20	15	10	7,5	5	2,5	1,250	0,625	µM ReACp53
	1	2	3	4	5	6	7	8	9	10	11	12	
A	PBS	PBS	PBS	PBS	PBS	PBS	PBS	PBS	PBS	PBS	PBS	PBS	
B	Media	Media + cells	Media + Cells + Drug	Media + Cells + Drug	Media + Cells + Drug	Media + Cells + Drug	Media + Cells + Drug	Media + Cells + Drug	Media + Cells + Drug	Media + Cells + Drug	Media + Cells + Drug	Media + Cells + Drug	Cell line 1
C	Media	Media + cells	Media + Cells + Drug	Media + Cells + Drug	Media + Cells + Drug	Media + Cells + Drug	Media + Cells + Drug	Media + Cells + Drug	Media + Cells + Drug	Media + Cells + Drug	Media + Cells + Drug	Media + Cells + Drug	
D	Media	Media + cells	Media + Cells + Drug	Media + Cells + Drug	Media + Cells + Drug	Media + Cells + Drug	Media + Cells + Drug	Media + Cells + Drug	Media + Cells + Drug	Media + Cells + Drug	Media + Cells + Drug	Media + Cells + Drug	
E	PBS	PBS	PBS	PBS	PBS	PBS	PBS	PBS	PBS	PBS	PBS	PBS	

Figure 4: Pipetting scheme of ReACp53 IC_{50} value measurement

2.3 ReACp53 treatment and cell fixation

When cells reached 80 % confluency, they were harvested and separated into two different cell culture T12.5 flasks. After a 24-hour incubation, the flasks were washed with FBS-free medium. ReACp53 was diluted with FBS-free medium to a final concentration of 6 µM, and 2 ml of the ReACp53 was added to one T12.5 flask. The cells in the second flask were covered with FBS-free medium to act as untreated controls. After 24 hours of ReACp53 incubation, the cells were harvested and centrifuged at 200 rcf for 8 minutes. After removal of the supernatant, the cell pellets were washed in 1x PBS and centrifuged at 200 rcf for 8 minutes. After removal of the supernatant, the cell pellet was resuspended in 3.7 % formaldehyde/1xPBS (FA/PBS) for fixation and incubated for 10 minutes at room temperature (RT). Then, the cell suspension was centrifuged at 400 rcf for 5 minutes. The 3.7 % FA/PBS solution was removed, and the cell pellets were resuspended in 1x PBS and stored at 4° C. For IF staining and PLA, the cells were counted and diluted to 15.000 cells per 200 µl with 1x PBS. Cytospins were prepared using Poly-L-lysine slides and single-use cytofunnels (Epredia, Michigan, USA, 11972345). 200 µl of the cell suspension was added to a cytofunnel and was centrifuged at 1,200 rcf for 5 minutes (Shandon Cytospin 2, Epredia). After centrifugation, the slides were left to dry overnight in the fume hood and then stored at -20° C for a minimum of six hours.

2.4 Antibodies

All antibodies used in the following experimental protocols are listed in Table 6.

Table 6: Overview of antibodies.

Antibody	*Company*	*Catalog Nr*	*Clone*	*Isotype*	*Primary labelled?*
Anti-p53 antibody	Santa Cruz Biotechnology	sc-126	DO-1	Mouse IgG2a	/
Anti-p63 antibody	Cell Signaling	39692	D9L7L	Rabbit IgG	/
Anti-p73 antibody	Cell Signaling	14620	D3G10	Rabbit IgG	/
Anti-oligomer A11 antibody	Merck Millipore	AB9234	Polyclonal	Rabbit	/
Anti-fibril OC antibody	Merck Millipore	AB2286	Polyclonal	Rabbit	/
panCK-antibody	Invitrogen	MA5-18156	C-11	Mouse IgGK1	488 nm fluorophores
Anti-CK19 antibody	Invitrogen	MA5-18158	A53-B/A2	Mouse IgG2a k	488 nm fluorophores
Anti-Cleaved-Caspase-3 antibody	Cell Signaling	#9669	Asp175	Rabbit	488 nm fluorophores
Anti-mouse IgG2a 488 antibody	Invitrogen	A-21131	Polyclonal	Goat IgG	488 nm fluorophores
Anti-rabbit IgG 594 antibody	Invitrogen	A-11072	Polyclonal	Goat IgG	594 nm fluorophores

2.5 Immunofluorescence staining

For the p53 and p63 immunofluorescence (IF) staining the cell line A-431 was used as control, and for the p73 IF staining the cell line HBL-100 was used as control. The slides were first warmed to room temperature (RT), and the staining area was marked with a liquid-repellent Dako marker (Agilent Technologies, Santa Clara USA, S2002). The cells were rehydrated in 1x PBS for 2 minutes and then placed in 0.5 % Triton/PBS for 10 minutes for permeabilization. After permeabilization, the cells were washed with 1x PBS three times for 4 minutes each. All incubation steps were performed in a humidity chamber. Cells were blocked with Ultra V-Block (Thermo Fisher Scientific, TA-060-PBQ) for 7 minutes and rinsed with Milli-Q water. The primary antibodies p53 and p63 were diluted 1:200 in Dako diluent (Agilent Technologies, S202230-2), and the primary antibody p73 was diluted 1:50 in Dako diluent (Table 6). The primary antibodies were added to the cells and incubated overnight at 4° C for a minimum of 12 hours. For the negative control slides, Dako diluent without primary antibodies was added to the slides. After primary antibody incubation, the slides were washed with 1x PBS-Tween (0.05 %) three times for three minutes each. Then, the secondary antibodies anti-mouse-488 and anti-rabbit-549 (both diluted 1:1000 in 5 % bovine serum albumin/PBS) were added and incubated for one hour at RT. Subsequently, the slides were washed with 1x PBS three times for three minutes each. 4′,6-Diamidin-2-phenylindol (DAPI) (Merck KGaA, Darmstadt, Germany) was

diluted to a concentration of 0.125 µg/ml, added for 5 minutes at RT, and rinsed off with Milli-Q water. Finally, each slide was mounted with Flouromount G mounting medium (Invitrogen, Massachusetts USA, 00-4958-02) and left at RT to dry for a minimum of 30 minutes.

2.6 Proximity Ligation Assay staining

For the PLA, two different antibody combinations were tested. The primary antibody anti-p53, together with either primary antibody A11 or primary antibody OC, was combined. Each cell line was stained with both combinations. The negative control was done without any primary antibody, while the p53 negative control included only the diluted p53 DO-1 antibody and the A11 and/or OC primary NC only included the respective polyclonal antibody, as depicted in Figure 5.

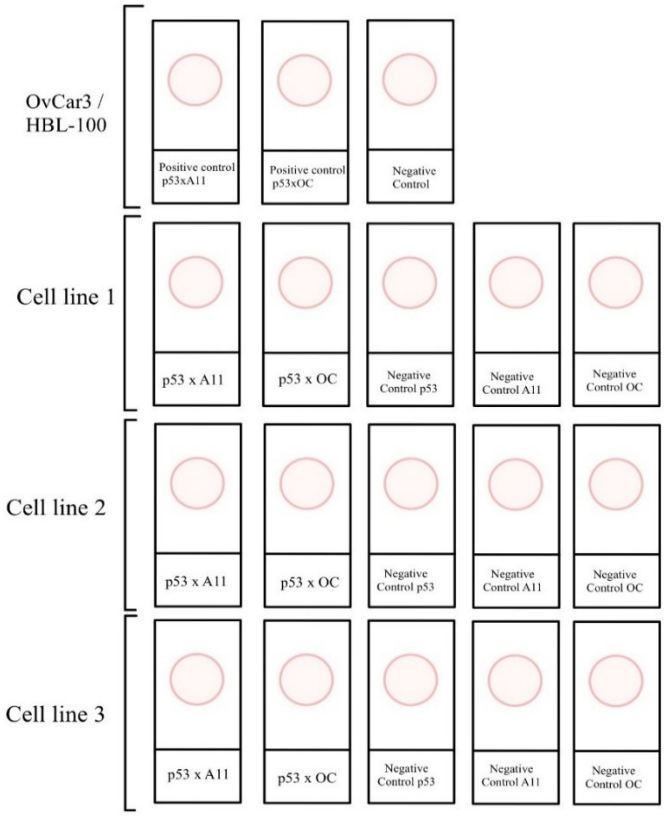

Figure 5: Scheme of sample types used in one PLA staining.

The kit used for PLA staining was the NaveniFlex Cell MR Red (Navinci Diagnostics, Uppsala Sweden, NC.R.100.2.Red). OVCAR-3 cell line was used as control cells. In three staining rounds, the cell line HBL-100 was additionally included as a control cell line. Pretreatment of the slides was done as described above in Chapter 2.5. In brief, three cell lines were rehydrated, permeabilized, and blocked. Three cell lines were blocked with Duolink Blocker (Sigma, DUO082007-8ml), and the remaining cell line panel was blocked with NaveniFlex Blocking Buffer. The blocking efficiency of both agents was evaluated to ensure comparability. PLA staining was done according to the manufacturer's protocol. All incubation steps were performed in a humidity chamber at 37°C unless otherwise stated. Blocking was performed for 1 hour. Then, the anti-p53 antibody was diluted 1:500, and the antibodies OC and A11 were diluted 1:1000 and incubated overnight at 4° C for a minimum of 12 hours. The next day, slides were rinsed with 1x TBS-Tween (TBS-T, 0.05%) and then washed in 1x TBS-T for 15 minutes at RT. After washing, the probes were diluted 1:60 with Diluent 2, added to the slides, and incubated for one hour. 1x TBS-T was pre-warmed to 37° C and then used to rinse and wash slides after the probe incubation for 15 minutes. After washing with pre-warmed 1x TBS-T, Reaction 1 (Ligation step shown in Figure 6) solution was made by diluting Buffer 1 1:5 in ddH_2O and Enzyme 1 1:40 with the Buffer 1 solution. Then, reaction 1 was added and incubated for 30 minutes. After Reaction 1, the slides were washed in 1x TBS-T for 5 minutes, and Reaction 2 (Rolling Circle Amplification step shown in Figure 6) was made by diluting Buffer 2 1:5 in ddH_2O and Enzyme 2 1:40. To avoid bleaching the fluorophores, all the following steps were done in the dark. Reaction 2 was incubated for 90 minutes. After Reaction 2, the slides were washed with TBS for 2 minutes, and counterstaining was done with primary 488-labeled antibody anti-Cleaved-Caspase 3. The antibody was diluted 1:50 in Dako Diluent, and antibody incubation was done overnight at 4° C for a minimum of 12 hours. After the counterstaining, slides were washed with TBS for 2 minutes, and DAPI was added for 5 minutes at RT. Afterwards, the slides were washed twice for 10 minutes with 1x TBS and once for 15 minutes with 0.1x TBS. After washing, the slides were mounted with Flouromount G mounting medium and left to dry at RT for a minimum of 30 minutes before they were stored short-term at 4° C and long-term at -20° C. The staining process is shown schematically in Figure 6.

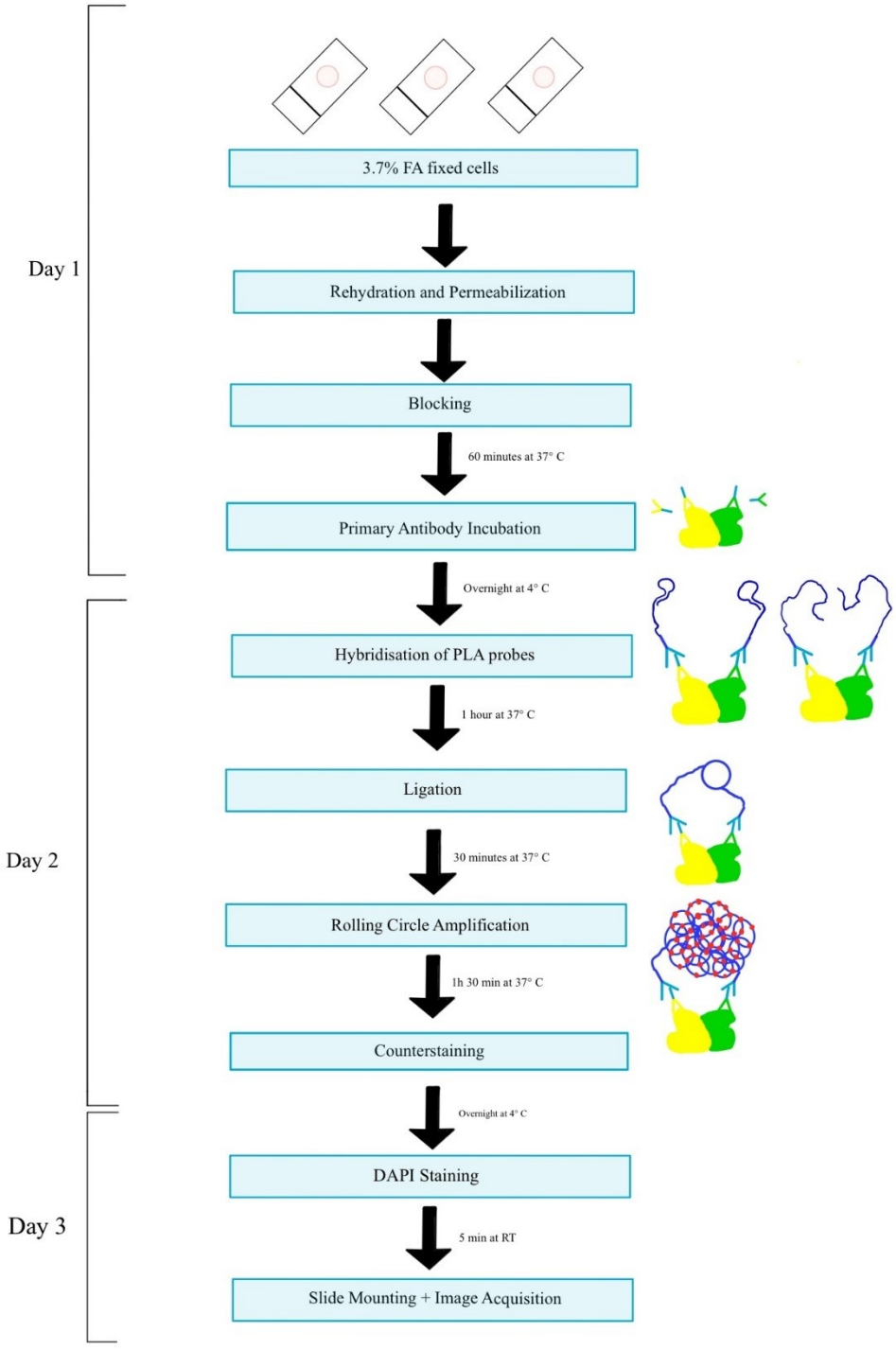

Figure 6: Flowchart of the Proximity Ligation Assay Cell MR Kit protocol

2.7 Real-time PCR

The real-time PCR was done by Eva Schuster and Dr. Eva Obermayr, who kindly provided me with the data for this work. Cell pellets were collected as described in Chapter 2.1. and stored at -80 °C until further processing. For RNA extraction, the AllPrep DNA/RNA Mini Kit (Qiagen, 80204) was used. The RNA extraction process was followed as described in the AllPrep DNA/RNA Mini Kit Handbook, version November 2005. RNA concentrations were measured with the QuantiFluor RNA System (Promega, Wisconsin, USA). For the reverse transcription into complimentary DNA (cDNA) with the SuperScript VILO Mastermix (Invitrogen, 11755-250) 500 ng of RNA was used per sample. The PCR was done in the GeneAmp PCR System 2700 (Applied Biosystems, Massachusetts, USA, A24811) with the following cycle settings: 25 °C for 10 minutes, 42 °C for 60 minutes, 85 °C for 5 minutes, 4 °C storage. For the quantification of target gene expression, real-time PCR was done with the TaqMan™ Gene Expression Assay (Thermo Fisher Scientific, 4331182). The mastermix used for the real-time PCR was the TaqMan™ Universal Master Mix (Applied Bioscience, 4440098). The Taqman Assay ID of the commercially available primers (Thermo Fisher Scientific) used are depicted in Table 7. The primers and probes for full-length p53, Δ40p53 and Δ133p53 were ordered from Thermo Fisher Scientific. The primer and probe sequences are depicted in Table 8. The real-time PCR was done with the QuantStudio™ 7 Flex Real-Time PCR System (Thermo Fisher Scientific, 4485701) with the following cycle settings: 50 °C for 2 minutes, 95 °C for 10 minutes, 40x 95 °C for 15 seconds and 60 °C for 1 minute. The duplicate samples were averaged using the QuantStudio Software (Thermo Fisher Scientific, v.1.6.1).

Table 7: TaqMan™Assay IDs of commercially available primers used for the real-time PCR.

Primer Target	Taqman Assay ID
B2M	Hs99999907_m1
TP63	Hs00978340_m1
TP73	Hs01056231_m1

Table 8: Sequences of primers and probes ordered from Thermo Fisher Scientific for the real-time PCR.

Primer Target	Forward primer	Reverse Primer	Probe Sequence
FLp53	TGGAAACTACTTC-CTGAAAACAACG	ACAGCATCAAA-TCATCCATTGC	TCTGTCCCCCT-TGCCGTCCCA
Δ40p53	TGTCTTTCAGACT-TCCTGAAAACAAC	ACAGCATCAAA-TCATCCATTGC	TCTGTCCCCCT-TGCCGTCCCA
Δ133p53	CTTGTGCCCTGA-CTTTCAACTCT	CAGTTGGCAAAA-CATCTTGTTGAG	TCTCCTTCCTCTTCCT-ACAGTACTCCCCTGC

2.8 Tissue Microarray assembly

Four Tissue Microarrays (TMAs), which included a total of 96 patients, were prepared as part of the EUDARIO ("European Trial on enhanced DNA Repair Inhibition in Ovarian Cancer") clinical trial (EudraCT-Number: 2017-004058-40). The EUDARIO/ENGOTov-48 included 120 patients with platinum-sensitive relapsed high-grade serous, high-grade endometroid, undifferentiated epithelial ovarian, or carcinosarcoma, fallopian tube or primary peritoneal cancer.

Three additional TMAs, with a total of 59 patients, were kindly prepared by the Department of Pathology, Medical University Vienna (Prof. Gerda Hofstetter). Patients for the TMAs prepared by the Department of Pathology were chosen based on the following criteria:

I. Ovarian cancer diagnosis with at least 5 years of follow-up
II. No other cancer diagnosis 5 years before ovarian cancer diagnosis
III. Primary tumor tissue available

For the TMAs prepared as part of the EUDARIO clinical trials, two 1.5 mm cores per patient were punched from FFPE patient tumor tissue and added to the paraffin block. The TMAs prepared by the Department of Pathology included three 1 mm cores per patient. After preparation, the TMAs were cut into 4 µm slices and applied to Superfrost slides. For each TMA a hematoxylin-eosin (H&E) staining, an immunohistochemistry (IHC) staining with the anti-p53 DO-1 antibody, and a Proximity Ligation assay with the two antibody combinations p53xA11 and p53xOC, was performed. The H&E staining was performed by the Department of Pathology.

2.9 Preparation of Tissue Microarrays for Staining

Formalin-fixed paraffin embedded (FFPE) OVCAR-3 cells were used for technical controls. The slides were incubated at 58° C for one hour and then placed in xylol for 5 minutes twice. Then, the slides were placed in descending alcohol concentrations in the following order: twice in 100 % ethanol for 3 minutes each, once in 96 % ethanol for 1 minute, once in 80 % ethanol for 1 minute, and once in 70 % ethanol for 1 minute. Subsequently, the slides were placed in Milli-Q water for 5 minutes. Heat-induced epitope retrieval was performed by placing the slides in a staining jar with Tris-EDTA (10 mM Tris Base, 1 mM EDTA Solution, 0.05% Tween 20, pH 9.0) buffer. The jar was wrapped in cling film and small holes were made in the top to allow for a pressure release. The jar was microwaved for 2.5 minutes at 850 W, followed by 11 minutes at 160 W. Then, the slides were left to cool for 30 minutes at RT with 1x PBS added after 15 minutes. Subsequently, the slides were washed in 1x PBS twice for 3 minutes each. The staining area was marked with a liquid-repellent Dako marker.

2.10 Immunohistochemistry staining of Tissue Microarrays

The TMAs were stained by immunohistochemistry staining to determine the total amount of p53 protein in the patient tissues. The tissue area was quenched with an endogenous peroxidase-blocking solution (Agilent Dako, S2023) for 10 minutes at RT. The slides were washed with Milli-Q water twice for 3 minutes. Then, the tissue was treated with Ultra-V blocking reagent (Agilent Dako, TA-060-PBQ.) for 7 minutes. The blocking solution was tapped off the slides, and the anti-p53 antibody was diluted 1:100 in Dako Antibody diluent (Agilent Dako, S0809) and added to the slides. To the negative controls Dako Antibody diluent without primary antibody was added. The primary antibody was left to incubate overnight at 4° C. The next day, the slides were washed with 1x PBS-Tween (0.05 %) three times for 3 minutes each. The negative controls were washed separately. Then, the Dako Link biotinylated secondary antibody (Agilent Dako, K0675) was added for 15 minutes at RT. The slides were rinsed and washed with 1x PBS-Tween (0.05 %) twice for 3 minutes each. Dako Streptavidin Peroxidase solution (Agilent Dako, K0675) was added to the tissue for 15 minutes. The slides were washed with 1x PBS-Tween (0.05 %) twice for 3 minutes each. 1 ml of Dako DAB Substrate Buffer and 20 µl of DAB (3,3'-Diaminobenzidine) Chromogen (Agilent Dako, K3468) were mixed and added to the tissue for 2 minutes or until brown staining was visible in the positive control. Afterwards, the slides were washed with Milli-Q water three times for 3 minutes each and carefully wiped. The counterstaining was done with the filtered haematoxylin Gill III (Merck KGaA, 1.05174.0500) for 10 seconds, and the slides were placed into a box under flowing distilled water for 15 minutes. To mount the slides, Kaiser's Glyceringelatine (Merck KGaA, 109242) was used. The stained slides were kept at RT until analysis.

2.11 Proximity Ligation Assay staining of Tissue Microarrays

To determine the amount of p53 aggregation in patient tissue, the TMAs were stained with the NaveniFlex MR Red (Navinci Diagnostics, NF.MR.100.1) in the p53 x A11 and p53 x OC antibody combinations. After the slide preparation described in Chapter 2.9, the tissue area was treated with Duolink® Blocker (Sigma-Aldrich, DUO082007-8ml). The PLA was performed as described before with minor changes. Unless otherwise stated, all incubation steps were performed in a humidity chamber at 37°C. In brief, the PLA probes were diluted 1:40 with Diluent 2 and incubated for one hour. After washing with TBS-T, Reaction A solution was made by diluting Buffer A 1:5 in ddH2O and Enzyme A 1:40 with the Buffer A solution. Reaction A (Hybridisation step shown in Figure 7) was then added to the slides and incubated for 60 minutes. Reaction B (Ligation step shown in Figure 7) was prepared by diluting Buffer B 1:5 in ddH2O and Enzyme B 1:40 in Reaction B solution, added to the slides, and incubated for 30 minutes. Reaction C (Rolling

Circle Amplification step shown in Figure 7) was prepared by diluting Buffer C with Texas Red fluorophore oligonucleotides 1:5 in ddH2O, and Enzyme C was diluted 1:40 with the Buffer C solution. Reaction C was incubated for 90 minutes. Counterstaining was done with primary 488-labeled anti-Cytokeratin (pan reactive 4, 5, 6, 8, 10, 13, 18) antibody and 488-labeled anti-Cytokeratin-19 antibody. Both antibodies and DAPI (50 µg/ml) were diluted 1:100 in Dako Diluent, and the incubation was done for 45 minutes. After washing, slides were mounted with Flouromount G mounting medium and left to dry at RT for a minimum of 30 minutes.

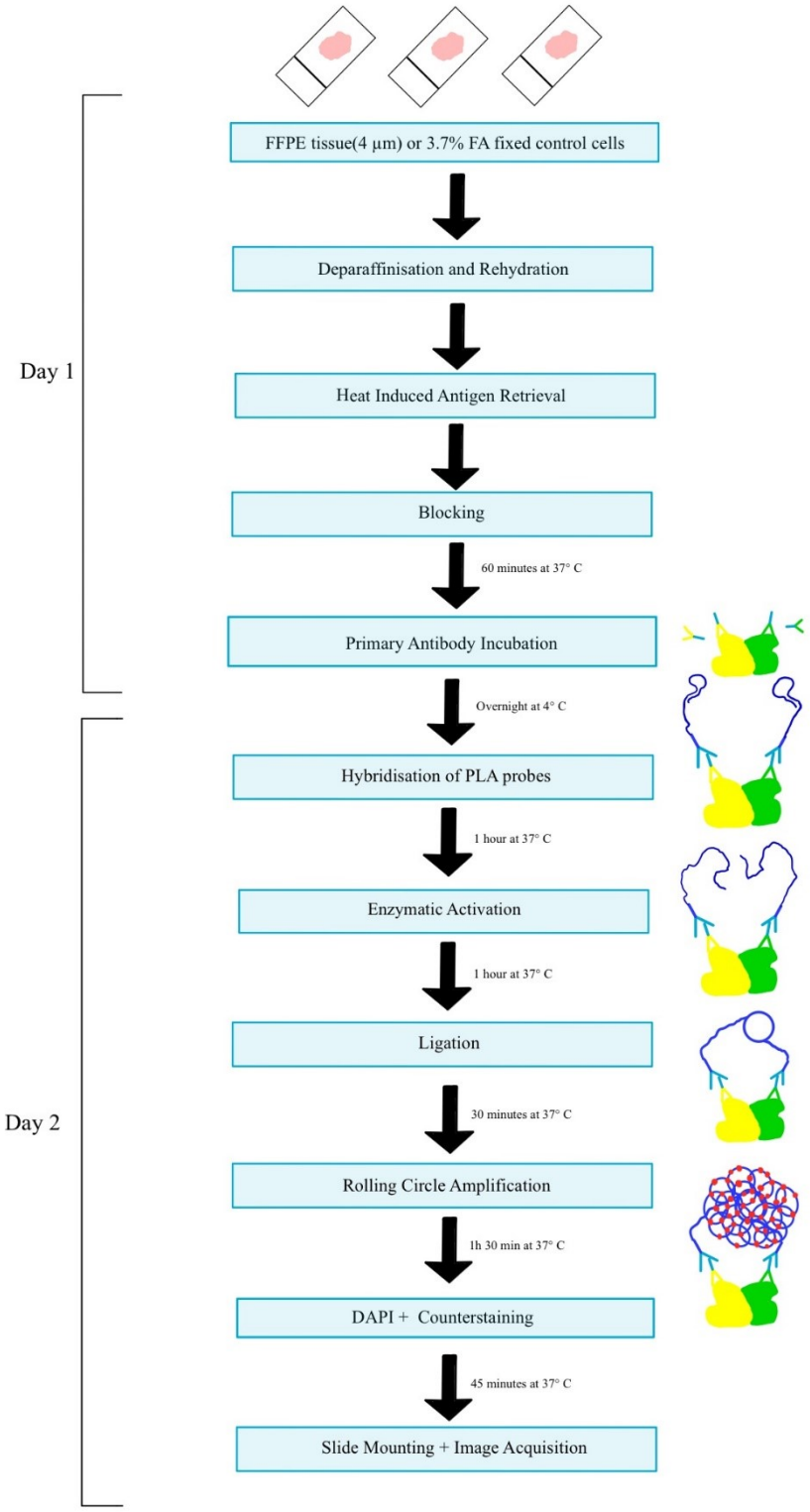

Figure 7: Flowchart of the Proximity Ligation Assay MR Kit protocol

2.12 Image Acquisition and Analysis

The microscope used for image analysis was the Olympus BX53F2/53/43 with a Hamamatsu C11440-36U camera. Pictures were taken with a gain of 14.60 db. The exposure time for the DAPI channel (359/465 nm wavelength) was 5 ms, and the exposure time for the TRITC (544/576 nm wavelength) and FITC (494/519 nm wavelength) varied between 100-200 ms. All slides stained within one experiment were imaged with the same exposure time. For the image analysis of the IF staining, the images were first pre-processed with the software ImageJ 1.54g[107] by merging the single channel images to a composite image (DAPI = blue, TRITC = red, FITC = green). To quantify the fluorescence signal, the images were analyzed in QuPath (Version 0.5.1)[108]. For this, the publicly available documentation protocol "Multiplexed Analysis" from QuPath 0.5.1[1] was followed. First, images loaded into QuPath were set as "Fluorescence Images". Then a full image annotation was applied. The cellular detection was conducted using the settings shown in Table 9. The threshold for analysis was set at 50 cells per image. The range of cells captured was from 60 cells up to 528 cells per image. The depicted threshold was for the category "Cell: Mean". Then, within the function "Create Single Measurement Classifier", a detection threshold for the TRITC and FITC channels was set. The settings are depicted in Table 9. To determine the extent of change in p53, p63, and p73 protein expression before and after ReACp53 treatment, intensity values were averaged, and a fold change of fluorescence intensity was calculated with the average intensity output by QuPath in Microsoft Excel. To determine p53 positive and p53 negative cell lines, the average intensity output of the untreated cell lines was calculated and a threshold using the negative controls was set for p53 positivity. Cell lines with final untreated p53 intensities above zero were classified as p53 positive.

$$(\text{Untreated cells p53 intensity}) - (\text{average NC} + 3\text{x SD}) = \text{final untreated cells p53 intensity}$$

For the image analysis of the PLA, the images were first pre-processed with ImageJ 1.54g[107] to remove background signaling with a Rolling Ball threshold of 5 to 20 pixels, depending on the amount of background signal. Only images with a strong background signal that distorted the signal detection were pre-processed. After the background removal, the image layers were merged. Again, to quantify the PLA signals, the images were analyzed in QuPath. First, images loaded into QuPath were set as "Fluorescence Images". Then a full image annotation was applied. The cell detection and subcellular detection were conducted with the settings shown in Table 9. The values of the negative controls were subtracted from the sample values.

[1]https://qupath.readthedocs.io/en/stable/docs/tutorials/multiplex_analysis.html (accessed: 09/2024)

$$(\text{ReACp53 treated p53xA11}) - (\text{NC p53} + \text{NC A11}) = \text{final ReACp53 treated p53xA11}$$

To determine the extent of change in p53 aggregation levels before and after ReACp53 treatment, the fold change of quantified PLA signals was calculated in Microsoft Excel. All graphs were produced with GraphPad Prism 6.01 and R 4.3.3./RStudio 2023.12.1.

To determine the change of cleaved Caspase 3 positive cells, a single Measurement Classifier was set, similar to the immunofluorescence analysis of p53, p63, and p73. The number of cells declared as positive was used to calculate (1) whether ReACp53 treatment caused an increase, no change, or decrease in cleaved Caspase 3 positive cells and (2) the fold change between before and after ReACp53 treatment. The depicted threshold in Table 9 was used for the category "Nucleus:Mean".

Table 9: Settings for Image Analysis in QuPath. CC3 = cleaved Caspase 3

Cellular detection		Single Measurement Classifier		Subcellular detection	
Detection channel	Blue	Object Filter	Detections(all)	Detection threshold (Channel 1)	30
Use opening by reconstruction	Yes	Channel Filter	No filter	Detection threshold (Channel 2)	-1
Background radius	30 px	Measurement	p53 OR p63 OR p73 OR CC3	Detection threshold (Channel 3)	-1
Median filter radius	0 px	Threshold	70 OR 80 OR 80 OR 250	Smooth before detection	Yes
Sigma	10 px	Above Threshold	p53 OR p63 OR p73 OR CC3	Split by intensity	Yes
Minimum area	10 px^2	Below Threshold	/	Split by shape	Yes
Maximum area	4000 px^2			Expected spot size	3 px^2
Threshold	10			Min spot size	1 px^2
Split by shape	Yes			Max spot size	200 px^2
Cell expansion	50 px			Include clusters	No
Include cell nucleus	Yes				
Smooth boundaries	Yes				
Make measurements	Yes				

2.13 Statistical analysis

Patients were included when more than 50 % of available tissue was evaluable. Categories were manually assigned to each tissue. The most frequently assigned category for each patient was chosen as the final category. When different categories were assigned equally often to the same patient, the lower category was selected. Patient samples for both the PLA and IHC staining were put into four groups depending on the intensity of each staining. The four groups were: 0 (negative), 1 (weak), 2 (intermediate) and 3 (strong). For further analysis, the category 1 and 2 were merged together into "intermediate", while category 0 became "negative" and category 3 became "high".

All statistical testing of correlations and statistical significance was done in GraphPad Prism (Version 6.01). Statistical significance was defined as a p-value below 0.05. All tests were done two-sided. Statistical correlation was determined by Spearman correlation for the following variables: ReACp53 IC_{50} vs. Seprion-ELISA p53 aggregation quantity, the ΔCT values for FLp53, Δ40p53, Δ133p53, *TP63*, *TP73* vs. Seprion-ELISA p53 aggregation quantity, the ΔCT values vs ReACp53 IC_{50} values, the log2FC of cleaved Caspase 3 positive cells vs ReACp53 IC_{50} and log2FC of cleaved Caspase 3 positive cells vs log2FC of p53xA11 and p53xOC PLA. To determine statistically significant difference between two variable groups, Mann-Whitney U testing was applied. This was done to test significant differences for ReACp53 IC_{50} between histological subtypes, p53 mutational status, p53 mutation type, p53 IF positive vs negative cell lines and for the log2FC between p53xA11 and p53xOC and the log2FC between p53, p63 and p73.

Progression-free survival was calculated from the date of diagnosis to the date of either documented progression or last observation in months. Overall survival was calculated from date of diagnosis to the date of death or last observation in months. Kaplan-Meier progression-free and overall survival curves were generated, and statistical significance was calculated with the Mantel-Cox test. To calculate the correlation between PLA and IHC categories, a Chi-Square test was done.

Heatmaps were generated with R 4.3.3./RStudio 2023.12.1. For the heatmap depicting real-time PCR results, the ΔCT values were normalized per gene for comparability.

3 Results

3.1 ReACp53 IC_{50} measurements

In previous work from Kalina J. titled "Investigating the role of fibrillar p53 protein in breast cancer" (2021), the amount of p53 aggregates in breast cancer cell lines was quantified by the p53-Seprion-ELISA. To determine if the amount of p53 aggregation shows a correlation with the sensitivity to the p53-restoring small-peptide drug ReACp53 (Soragni et al.)[66], 16 breast cancer cell lines and HBL-100 were tested with an MTT assay (Figure 8).

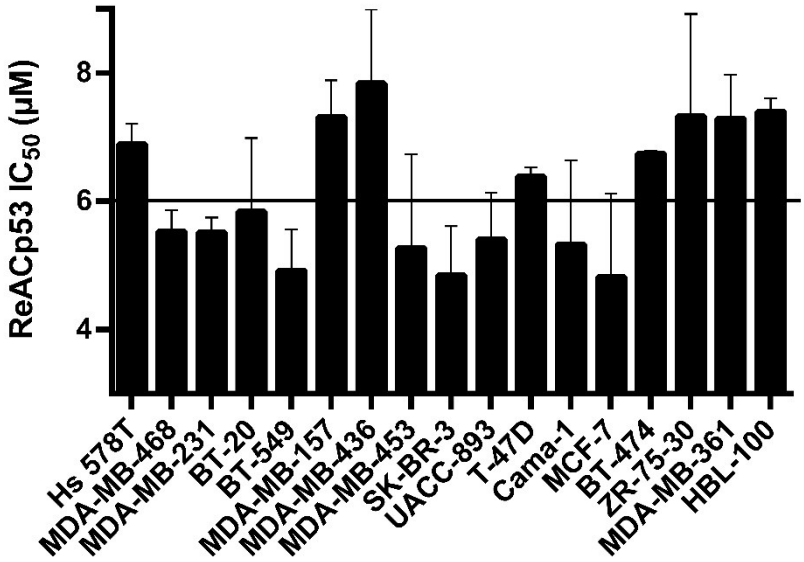

Figure 8: Bar graph depicting the ReACp53 IC_{50} results for every cell line in µM. Each cell line was tested in triplicates in three independent MTT assays. The IC_{50} values are depicted as the average mean and the error bars depict standard deviation.

The IC_{50} values for the 17 cell lines are between 4.7 µM (SK-BR-3) and 7.6 µM (MDA-MB-436). The average IC_{50} value of all cell lines is 6.12 with a standard deviation (SD) of 0.99. For a subset of cell lines, the effect of hormesis was observed where small concentrations of ReACp53 stimulated cells to an increase in MTT signal above 100 %. These cell lines include MDA-MB-157, T-47D, CAMA-1, BT-474 and UACC-893 and their cell viability curves are shown in Figure 9.

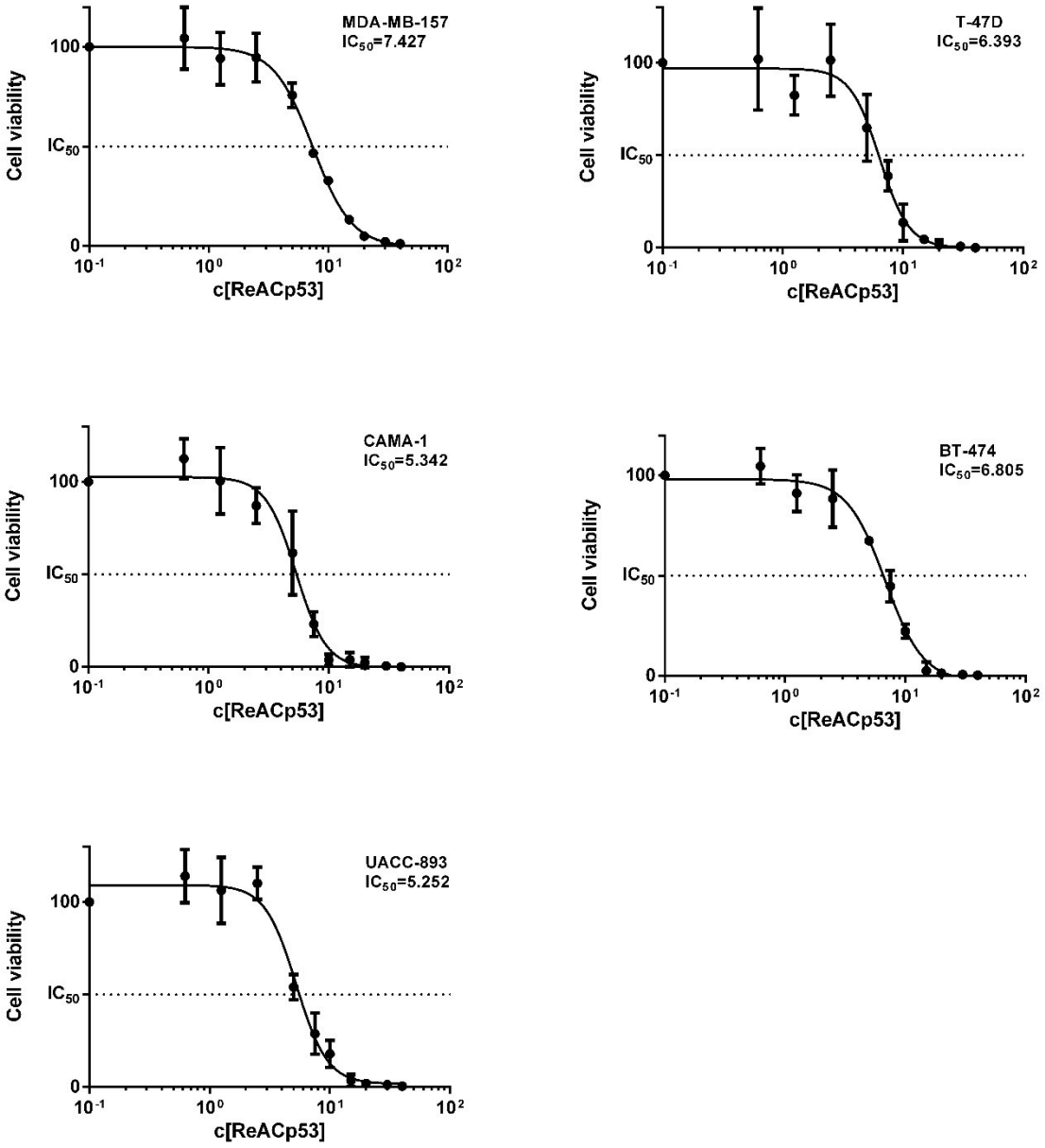

Figure 9: Cell viability curves of the five cell lines MDA-MB-157, T-47D, CAMA-1, BT-474 and UACC-893. X-axis depicts ReACp53 concentrations on a logarithmic scale and the y-axis shows cell viability in percent. Data points are shown as means with SD of triplicate measurements.

When analyzing the correlation between ReACp53 IC_{50} and the p53 aggregation measured by p53-Seprion-ELISA, no significant relationship was observed (p-value = 0.277, r-value = -0.246, Figure 10A). When separated into histological subtypes, ReACp53 IC_{50} values do differ, although not significantly. While the IC_{50} values of Her2+ cell lines cluster around 5.04 µM with an SD of 0.20 and Luminal B cell lines cluster around 7.13 µM with an SD of 0.25, the cell lines derived from triple-negative (TN) and Luminal B breast cancer do not seem to cluster around a specific value with SD of 0.99 and 0.57 respectively (Figure 10B). Since ReACp53 has been reported to act specifically in p53 mutant cells, we have compared wild-type p53 and p53 mutant cell lines. No

significant correlation of IC_{50} values was found between p53-mutated and wild-type p53 cell lines (p = 0.933). The mean of the two wild-type p53 cell lines was 6.24 as compared to the mean of the p53 mutated cell lines of 6.03 (Figure 10C). Since different types of *TP53* mutations affect p53 stability differently, we have compared the IC_{50} values of cell lines with different types of *TP53* mutation, categorized into DNA contact mutations, structural mutations, and "others", including indels and nonsense mutations. IC_{50} values do not significantly differ between the different types of *TP53* mutation, shown in Figure 10D. Although the type of mutation does not significantly influence IC_{50} values, the IC_{50} values of cell lines with a DNA contact mutation cluster around 5.48 µM with an SD of 0.1.

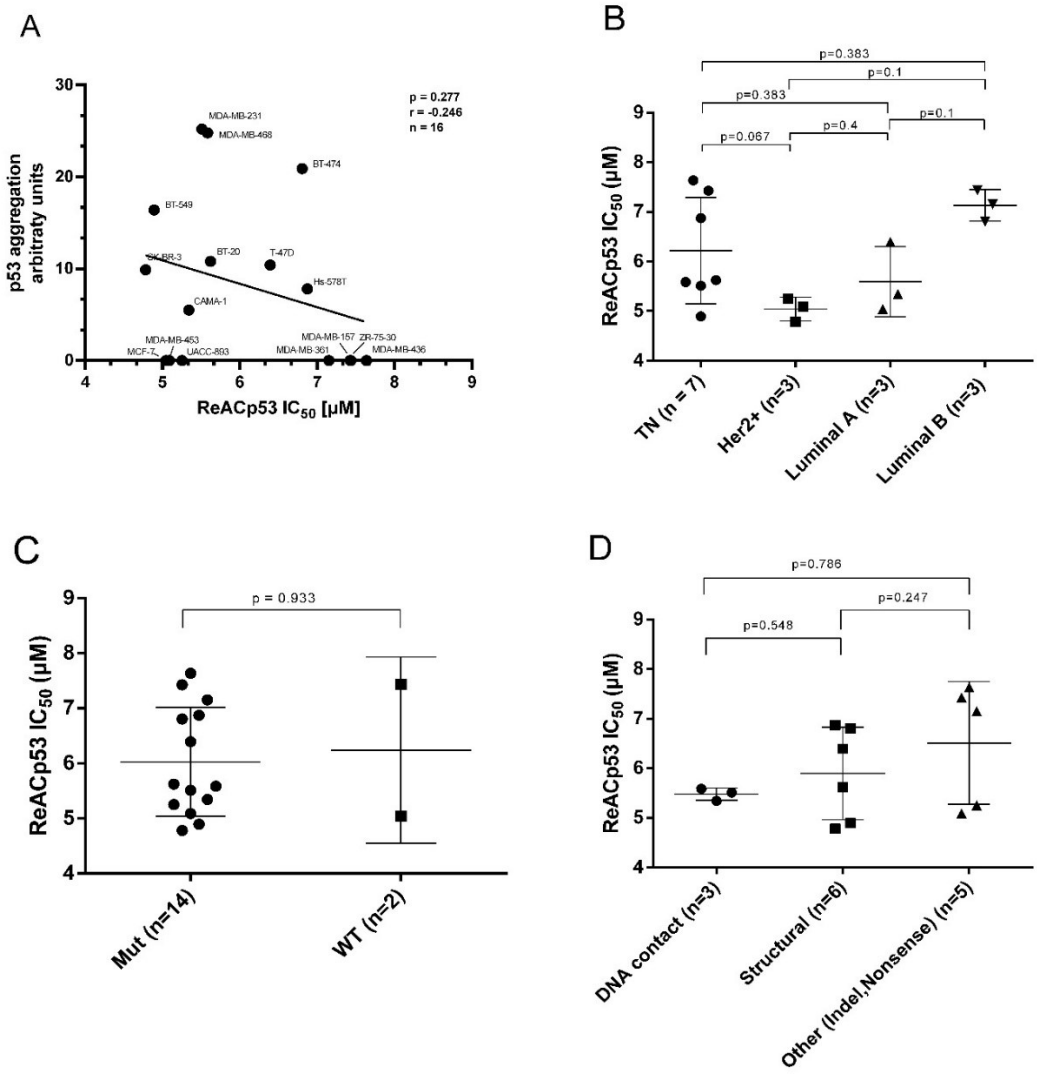

Figure 10: Statistical analysis of ReACp53 IC_{50} results. A) Scatter plot of the ReACp53 IC_{50} with p53 aggregation results from Seprion-ELISA. A Spearman correlation was used to determine correlation coefficient r and statistical significance. B) Comparison of the ReACp53 IC_{50} values between different histology subtypes. TN = triple negative C) Comparison of ReACp53 IC_{50} values between mutated and wild-type breast cancer cell lines. D) Comparison of ReACp53 IC_{50} values between different types of p53 mutations (DNA contact, structural, and Others, including indel and nonsense). For Figures B-D, Mann-Whitney-U- test was used to test for statistical significance. All IC_{50} values depicted are means.

ReACp53 IC_{50} values from this cell line panel are not statistically significantly influenced by histological subtype, *TP53* mutational status, or the type of *TP53* mutation. However, we have observed a clustering of IC_{50} values, with 8 out of 17 of cell lines having an IC_{50} value above 6.39 µM and 9 out of 17 having an IC_{50} value below 5.62 µM. The remaining work on ReACp53 was to elucidate the distinguishing factor between these two groups of cell lines and potentially find a contributing factor to ReACp53 sensitivity.

3.2 Real-time PCR results

Since Soragni et al. mention in their work potential off-target effects regarding p63 and p73 binding of ReACp53 due to their high sequence homology to p53, we first looked at these proteins on a transcriptional level.[66] Besides p53, p63, and p73, we additionally characterized the cell lines for their gene expression of the p53 isoforms Δ133p53 and Δ40p53 due to their possible implication in p53 aggregation formation. These results were then correlated with the amount of p53 aggregation measured by Seprion-ELISA and the ReACp53 IC_{50} values to determine if the gene expression of these proteins and isoforms is implicated in aggregation formation and ReACp53 sensitivity. For this purpose, real-time PCR (RT-PCR) was performed by Dr. Eva Obermayr and Eva Schuster, who kindly provided the resulting data for this work. Figure 11 shows a heatmap generated with the normalized CT values of full-length *TP53*, *TP63*, *TP73*, Δ133p53, and Δ40p53, which have been normalized to a housekeeping gene *B2M* (ΔCT). All ΔCT values have been multiplied by (-1) to reflect the correct relationship between ΔCT values and the number of transcripts. For *TP53,* the cell line BT-474 shows the highest ΔCT value (ΔCT = 0.087), while MDA-MB-436 shows the lowest ΔCT value (ΔCT = -7.343). *TP63* was expressed the most in relation to *B2M* in the cell line MDA-MB-453 (ΔCT = -4.542), while the lowest *TP63* ΔCT value was measured in HBL-100 cells (ΔCT = -14.855). TP73 expression was highest in the cell line MDA-MB-361 (ΔCT = -4.569) and lowest in the cell line MCF-7 (ΔCT = - 16.347). The isoform Δ133p53 had the highest ΔCT value in the cell line HBL-100 (ΔCT = -9.477) and the lowest ΔCT value in the cell line T-47D (ΔCT = -14.336). Lastly, the isoform Δ40p53 was expressed the most in relation to *B2M* in the cell line MDA-MB-231 (ΔCT = -3.819), while the lowest Δ40p53 ΔCT value was measured in the cell line MDA-MB-361 (ΔCT = -10.822).

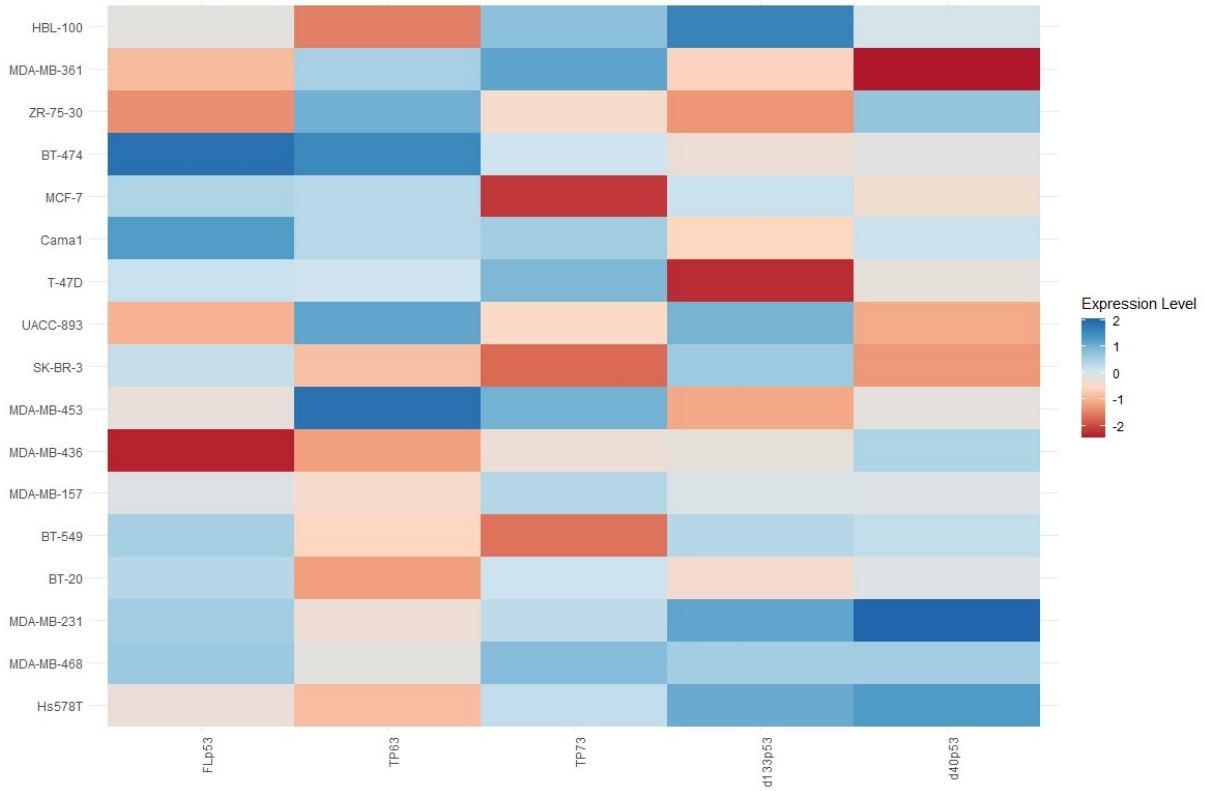

Figure 11: Heatmap of the RT-PCR results for the expression of full-length TP53 (FLp53), TP63, TP73 and the p53 isoforms Δ133p53 and Δ40p53. Results are normalized per gene. All CT-values have been standardized to the housekeeping gene B2M (ΔCT values) and have been multiplied by (-1).

The ΔCT values were then tested for a correlation with each cell line's quantity of p53 aggregation and ReACp53 IC_{50} values. The results are depicted in Tables 10 and 11, respectively.

*Table 10: Table depicting the results of a Spearman correlation test between the ΔCT values of FLp53, TP63, TP73, and the isoforms Δ133p53 and Δ40p53 that have been normalized against the housekeeping gene B2M and p53 aggregation measured by Seprion-ELISA. ** P-value<0.01*

Comparison	**ΔCT FLp53 vs p53 Aggregation**	**ΔCT TP63 vs p53 Aggregation**	**ΔCT TP73 vs p53 Aggregation**	**ΔCT Δ133p53 vs p53 Aggregation**	**ΔCT Δ40p53 vs p53 Aggregation**
Correlation coefficient r	0.625	-0.404	0.124	0.45	0.345
p-value	0.009	0.108	0.634	0.070	0.175
Significance	**	Not significant	Not significant	Not significant	Not significant

*Table 11: Table depicting the results of a Spearman correlation test between the ΔCT values of FLp53, TP63, TP73 and the isoforms Δ133p53, and Δ40p53 that have been referenced against the housekeeping gene B2M and IC_{50} values of ReACp53. * P-value<0.05*

Comparison	**ΔCT FLp53 vs IC_{50} ReACp53**	**ΔCT TP63 vs IC_{50} ReACp53**	**ΔCT TP73 vs IC_{50} ReACp53**	**ΔCT Δ133p53 vs IC_{50} ReACp53**	**ΔCT Δ40p53 vs IC_{50} ReACp53**
Correlation coefficient r	-0.487	-0.179	0.321	-0.207	0.325
p-value	0.048	0.492	0.209	0.425	0.203
Significance	*	Not significant	Not significant	Not significant	Not significant

For both, p53 aggregation quantities and IC_{50} values, only the gene expression of full-length p53 showed a significant correlation. The correlation between FLp53 and p53 aggregation is positive, therefore showing that the more *TP53* is expressed in a cell line, the more p53 aggregation can be measured. In contrast, the IC_{50} of ReACp53 is negatively correlated with the amount of *TP53* expression, showing that a cell line is more sensitive to ReACp53 treatment when it expresses more *TP53*. These correlations are depicted in Figure 12.

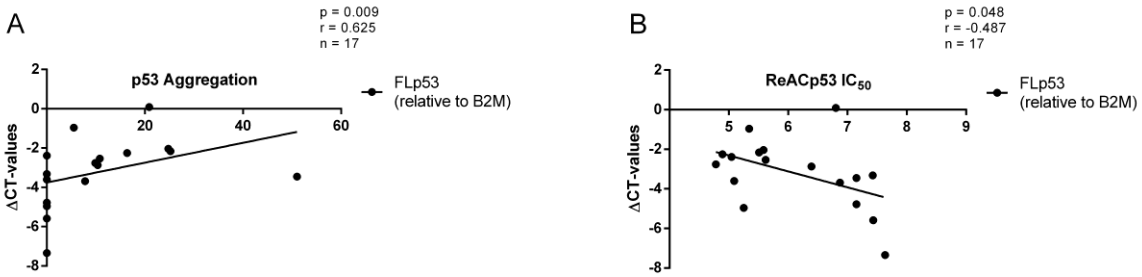

Figure 12: Scatter plots depicting the correlation between ΔCT values of full-length TP53 and A) p53 aggregation and B) IC_{50} values of ReACp53. Correlation was tested with a Spearman Correlation test.

3.3 Proximity Ligation Assay and Immunofluorescence results

Due to the high sequence similarity in the ReACp53 binding sequence between p53, p63, and p73, this work aims to show whether ReACp53 has an influence not only on the amount of oligomer and fibrillary p53 aggregation but also on the total protein level of p53, p63 and p73. This was done by staining the cell line panel before and after ReACp53 treatment with Proximity Ligation Assay in two antibody combinations, p53xA11 and p53xOC, and staining the cell line panel before and after ReACp53 treatment with immunofluorescence with primary antibodies binding p53, p63 and p73. Figure 13 depicts representative microscope images of the PLA stainings of the triple-negative cell line MDA-MB-231. For this cell line, a decline in p53 oligomers and p53 fibrils after ReACp53 treatment was observed.

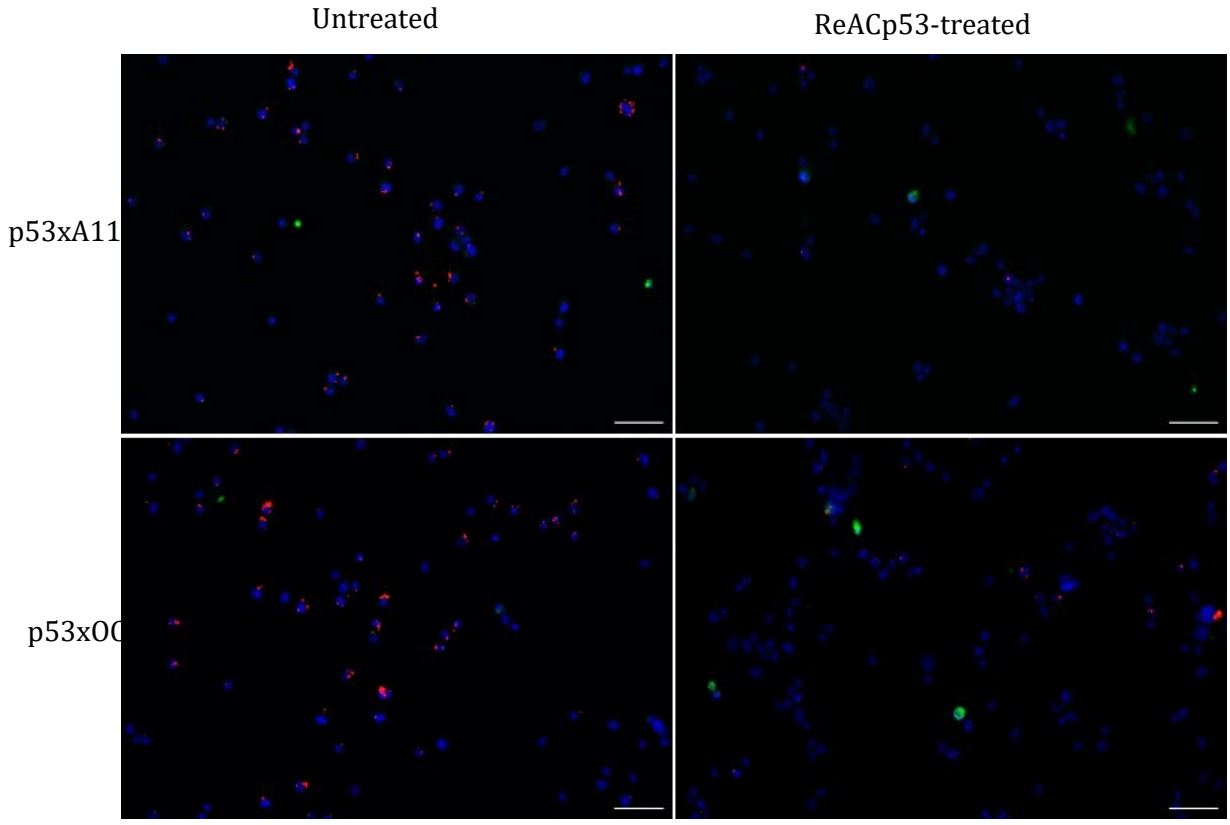

Figure 13: Representative microscope imaging of MDA-MB-231 PLA staining before and after ReACp53 treatment. Pictures were made with an exposure time for DAPI at 5 ms, TRITC at 100 ms and FITC at 100 ms. Blue = DAPI, red = PLA signal, green = Cleaved-Caspase 3 signal. The scale bar depicts 50 µm.

For the immunofluorescence staining of p53, p63, and p73, microscopic imaging of the cell line MDA-MB-468 is shown representatively in Figure 14. The triple-negative cell line MDA-MB-468 has shown an increase in total p53 and p63 protein levels and a decrease in p73 protein.

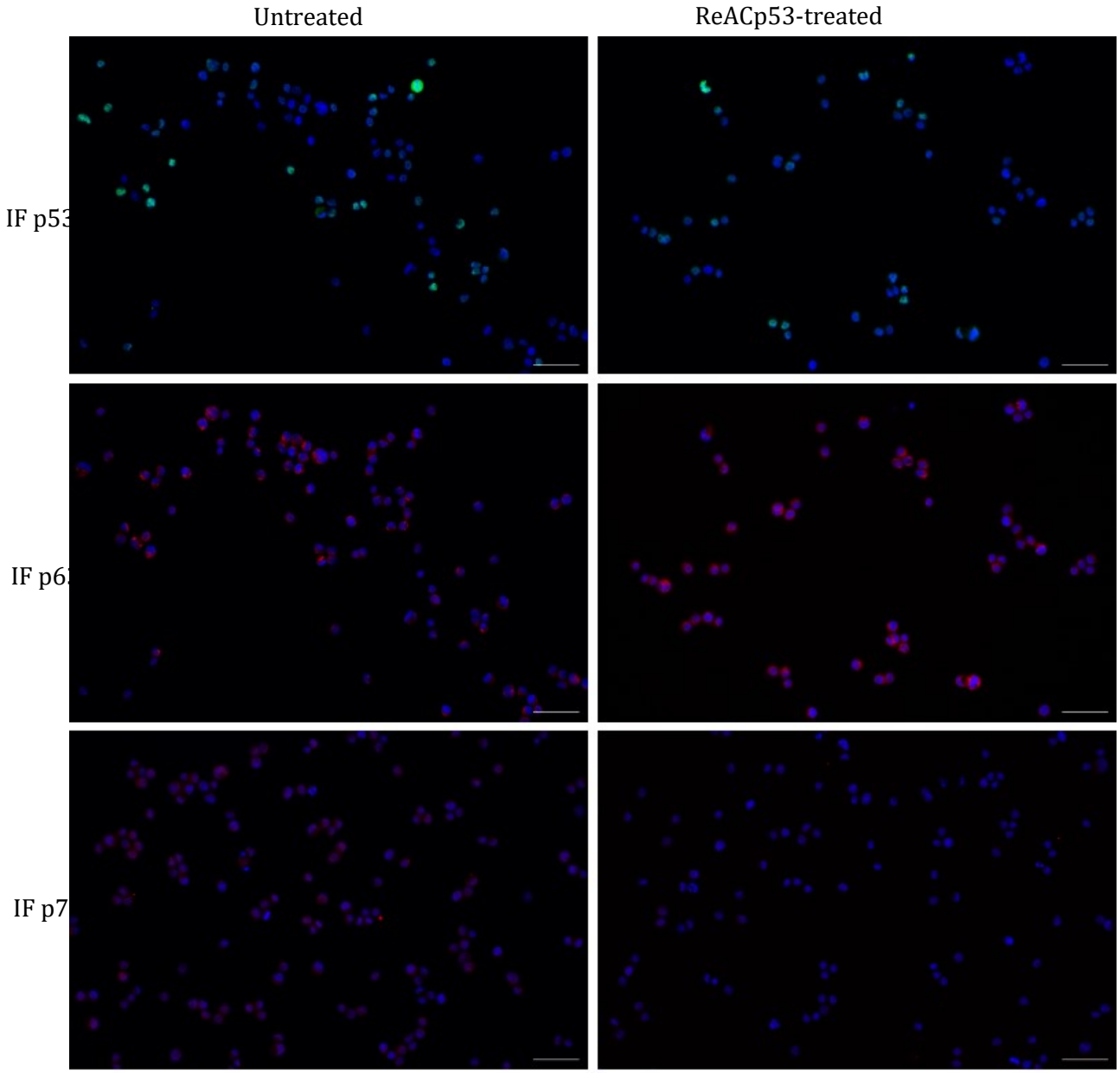

Figure 14: Representative microscope imaging of MDA-MB-468 immunofluorescence staining before and after ReACp53 treatment. Pictures were made with an exposure time for DAPI at 5 ms, TRITC at 100 ms and FITC at 50 ms. Blue = DAPI. Immunofluorescence signal for p53 is depicted in green, while immunofluorescence signal for p63 and p73 is depicted in red respectively. The scale bar depicts 50 µm.

To re-examine the association between the amount of total p53 protein and the IC_{50} values of ReACp53, the values of the p53 immunofluorescence staining of the untreated cells were used to determine p53 positive and p53 negative cell lines. Figure 15 shows the difference of ReACp53 IC_{50} values between p53 positive and p53 negative cell lines. While the average mean IC_{50} of p53 negative cell lines is higher than the average mean IC_{50} of positive cells, this difference did not reach statistical significance (p = 0.156).

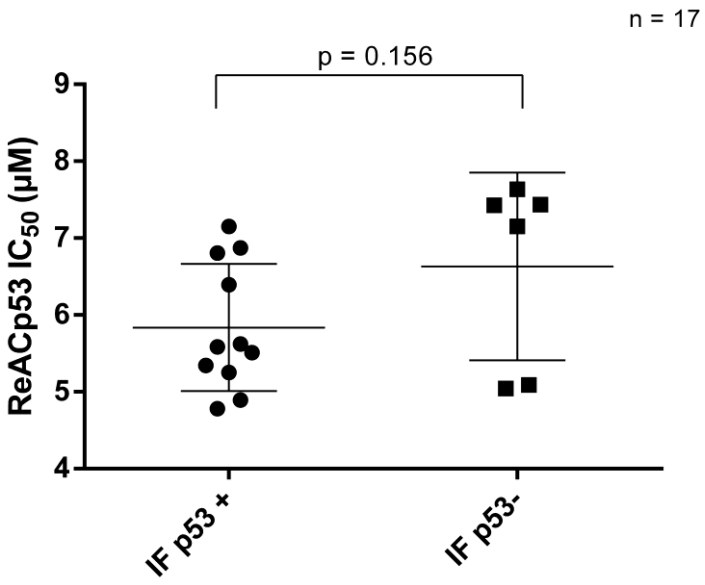

Figure 15: Comparison of ReACp53 IC_{50} values between IF p53-positive and IF p53-negative cell lines. Statistical significance was determined with a Mann-Whitney-U test.

The change in PLA and IF signal for all cell lines was calculated as the $\log_2$ of the fold change (log2FC) and is depicted in Figure 16. The average log2FC for p53xA11 PLA staining throughout the 17 cell lines is -0.45, while for p53xOC, the average log2FC is -0.61 (Figure 16A). This translates to an average reduction of p53 oligomer signal of 26 % and an average reduction of p53 fibril signal of 34 % by ReACp53 treatment (p-value = 0.936). Figures 16C and 16D depict the log2FC for each cell line individually.

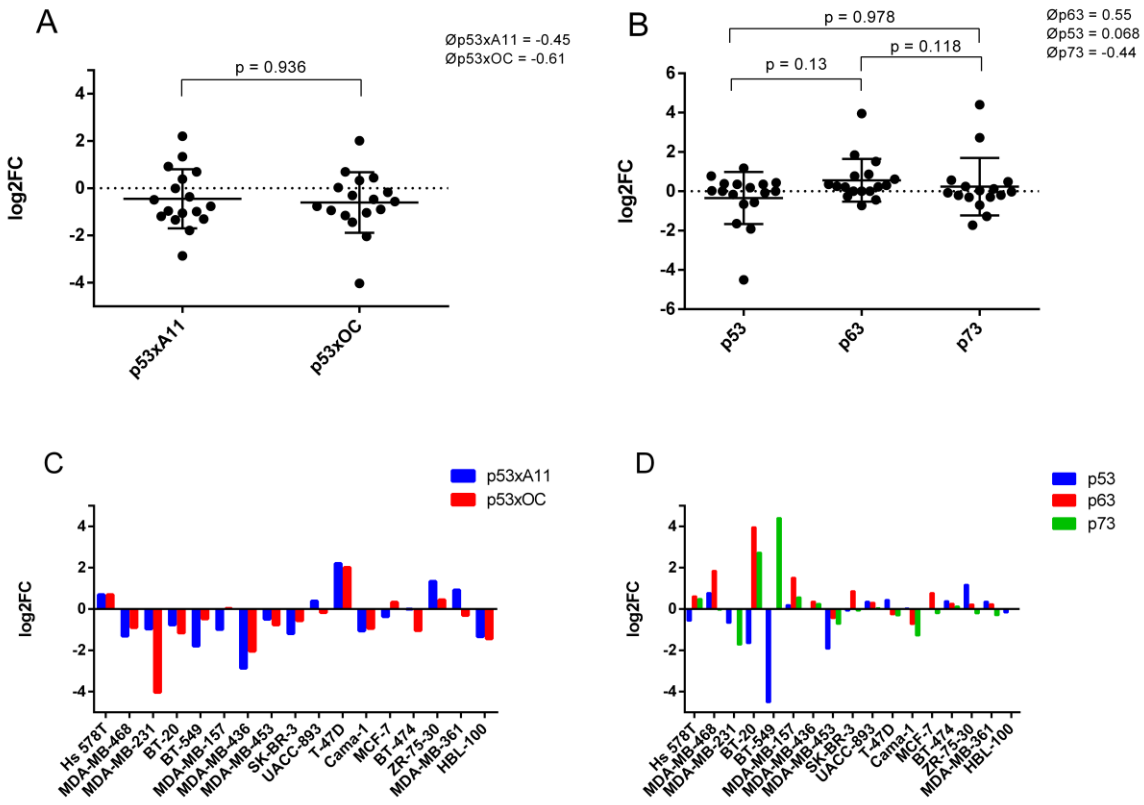

Figure 16: Visualization of proximity ligation assay and immunofluorescence results. A) Comparison of the log2FC values from the p53xA11 and p53xOC staining. P-value was calculated with Mann-Whitney-U test. B) Comparison of the log2FC values of the immunofluorescence staining of p53, p63, and p73. P-values were calculated with Mann-Whitney U test. C) Bar graph depicting the log2FC values of the PLA staining. D) Bar graph depicting the log2FC values for the immunofluorescence staining.

Immunofluorescence results show that while on average total p53 levels seem to be only minimally increased (log2FC = 0.066) by ReACp53 treatment, total p63 increases (log2FC = 0.55) after ReACp53 treatment whereas total p73 decreases (log2FC = -0.44) (Figure 16B). These log2FC values translate to an increase of p53 by 4.83 %, an increase of p63 by 46.41 %, and a decrease of p73 by 26.29 %.

3.4 Cleaved Caspase-3 results

To elucidate whether ReACp53 treatment induces apoptosis in the cell lines, we counterstained with an anti-cleaved Caspase 3 antibody after the PLA. In Table 12, an overview of the results is presented. The change of cleaved Caspase 3 positive cells before and after ReACp53 treatment was converted into a heatmap (Figure 17). The only cell line showing a decrease in both PLA stainings is CAMA-1, with the majority of cell lines showing either an increase or no change of apoptotic cells after ReACp53 treatment.

Table 12: Overview of the amount of cells positive for Cleaved-Caspase 3. Results are standardized to the total amount of cells visible per image.

	p53xA11		**p53xOC**	
Cell Line	Untreated	ReACp53 treated	Untreated	ReACp53 treated
Hs-578T	0	0.046	0.031	0.013
MDA-MB-468	0	0.037	0	0.008
MDA-MB-231	0	0	0	0
BT-20	0	0.024	0	0.03
BT-549	0	0.072	0.011	0.035
MDA-MB-157	0	0.012	0.01	0.006
MDA-MB-436	0	0.012	0	0.015
MDA-MB-453	0	0	0	0
SK-BR-3	0.009	0.035	0.007	0.019
UACC-893	0	0	0.016	0.047
T-47D	0	0	0	0
CAMA-1	0.023	0	0.044	0.023
MCF-7	0	0	0	0
BT-474	0.018	0.017	0	0.019
ZR-75-30	0	0	0	0
MDA-MB-361	0	0	0	0
HBL-100	0	0.047	0	0.044

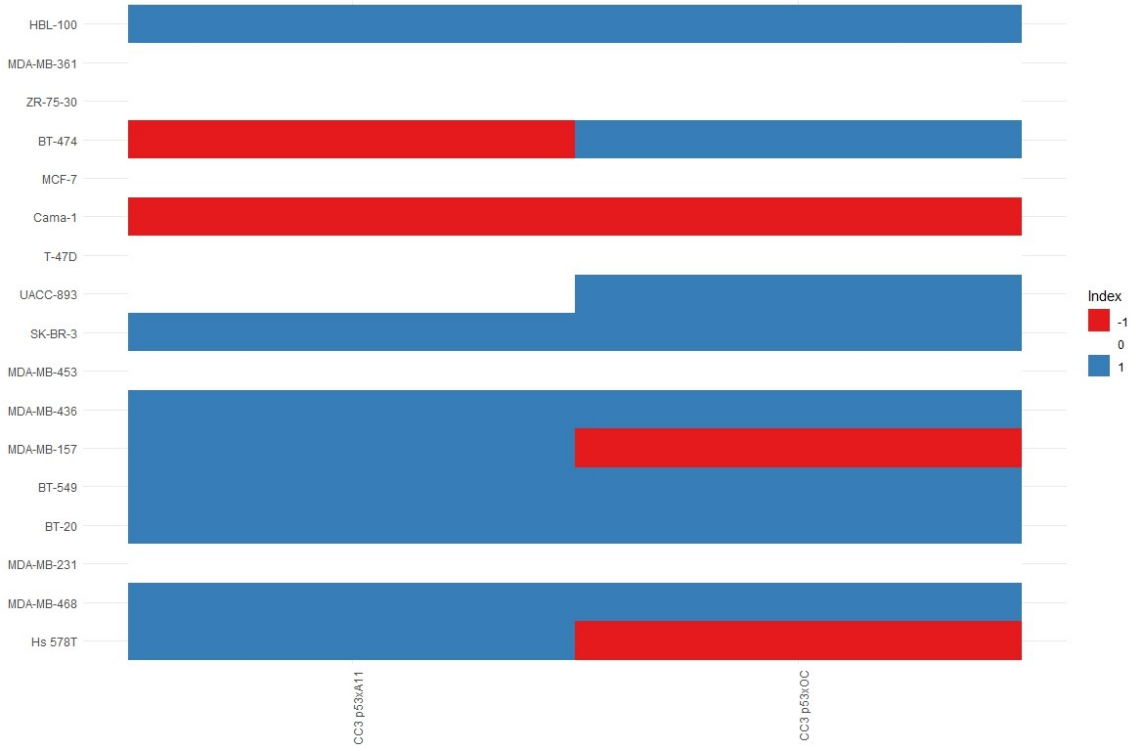

Figure 17: Heatmap depicting the changes in cleaved Caspase 3 signal across the cell lines after ReACp53 treatment. The left column depicts the changes for the p53xA11 PLA staining, while the right column depicts the changes for the p53xOC PLA staining. An index of 1 indicates an increase in cleaved Caspase 3 positive cells, while a 0 indicates no change and -1 indicates a decrease in cleaved Caspase 3 positive cells.

The logarithmic fold change (log2FC) of cleaved Caspase 3 staining was calculated for each cell line and correlated with ReACp53 IC_{50} values and log2FC from the respective PLA staining (Figure 18). Both correlations for the cleaved Caspase 3 staining and the IC_{50} are not statistically significant, with a p-value of 0.705 (r = 0.099) for the p53xA11 staining and a p-value of 0.929 (r = 0.023) for the p53xOC staining, suggesting that the change in apoptotic cells is not correlated with the cell lines sensitivity to ReACp53 (Figure 18A and 18B). In contrast, the log2FC values of p53xA11 are negatively correlated with the log2FC of cells positive for Cleaved-Caspase-3 (p = 0.035, r = -0.513), indicating that a decrease of p53 oligomers corresponds to an increase of apoptotic cells. The association between log2FC values of p53xOC and the log2FC of cleaved Caspase 3 positive cells is also significantly corelated (p = 0.012, r = -0.576), indicating that the reduction of p53 fibrils also corresponds to an increase of apoptotic cells (Figure 18C and 18D).

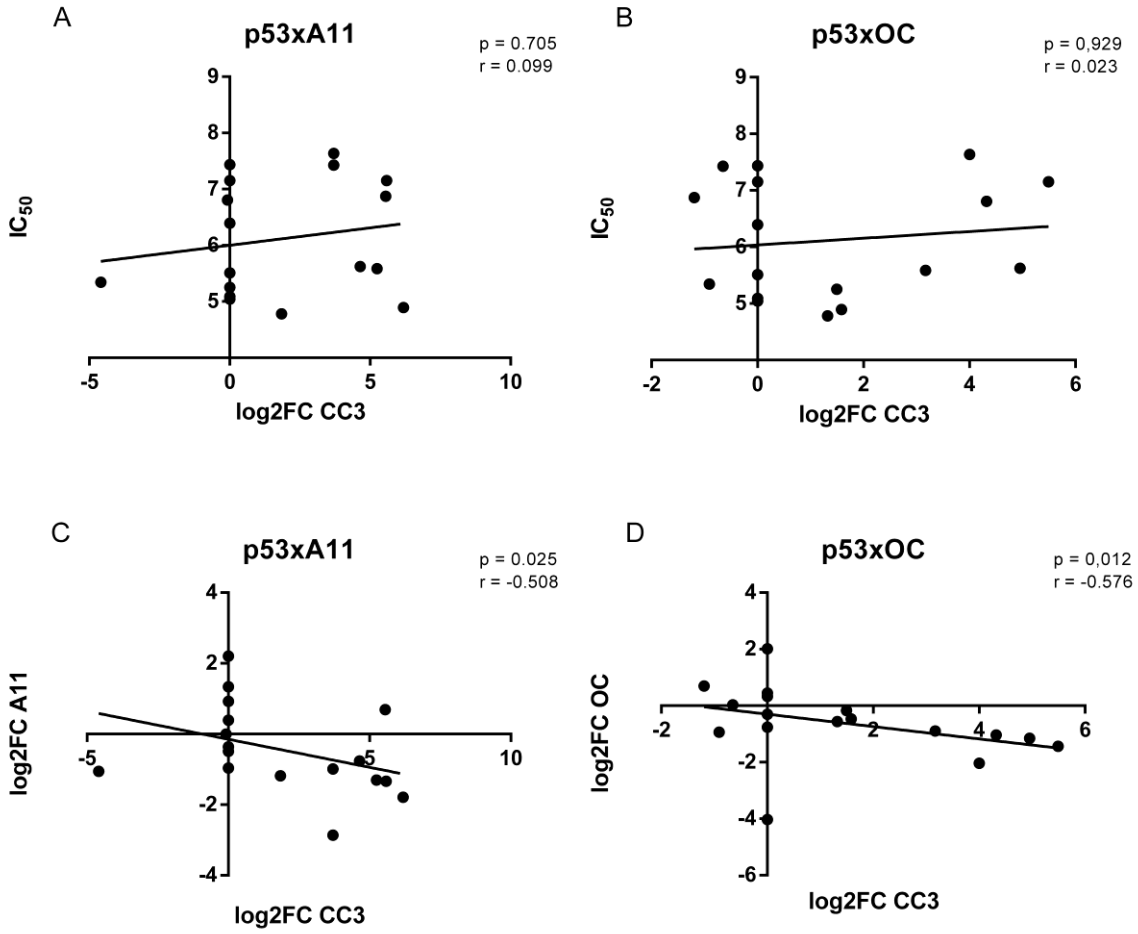

Figure 18: Scatter plots illustrating the correlation between log2FC in Cleaved-Caspase-3 signal in both p53xA11 and p53xOC stainings and A, B) their corresponding ReACp53 IC_{50} and C, D) log2FC. Statistical testing was done with Spearman correlation.

3.5 Association of p53 aggregation with patient survival

The second aim of this thesis is to verify an association between p53 aggregation and patient survival in serous ovarian cancer in a patient cohort of over 400 patients. Due to time constraints, this work presents the preliminary results from 154 patients. Table 13 shows an overview of the clinical data available from patients included in this study.

Table 13: Overview of patient data included in this study.

# patients	154
Median age at diagnosis	60 years
Age range	17-85 years
# FIGO (2014) Stage 0	7
# FIGO (2014) Stage I	0
# FIGO (2014) Stage II	6
# FIGO (2014) Stage III	130
# patients progressed	121
Mean PFS	7.5 months
# patients deceased	82
Mean OS	21 months

To determine the total p53 protein content in the patient tissues, tissue microarrays were stained with p53 IHC. Out of 154 patients, we obtained 139 evaluable tissue samples out of which 125 showed a positive nuclear p53 staining. The 139 evaluable patients were categorized into the following order: 14 patients in the category "negative" (9.1 %), 74 patients in the category "intermediate" (53.2 %), and 51 patients in the category "high" (33.1 %) (Figure 19).

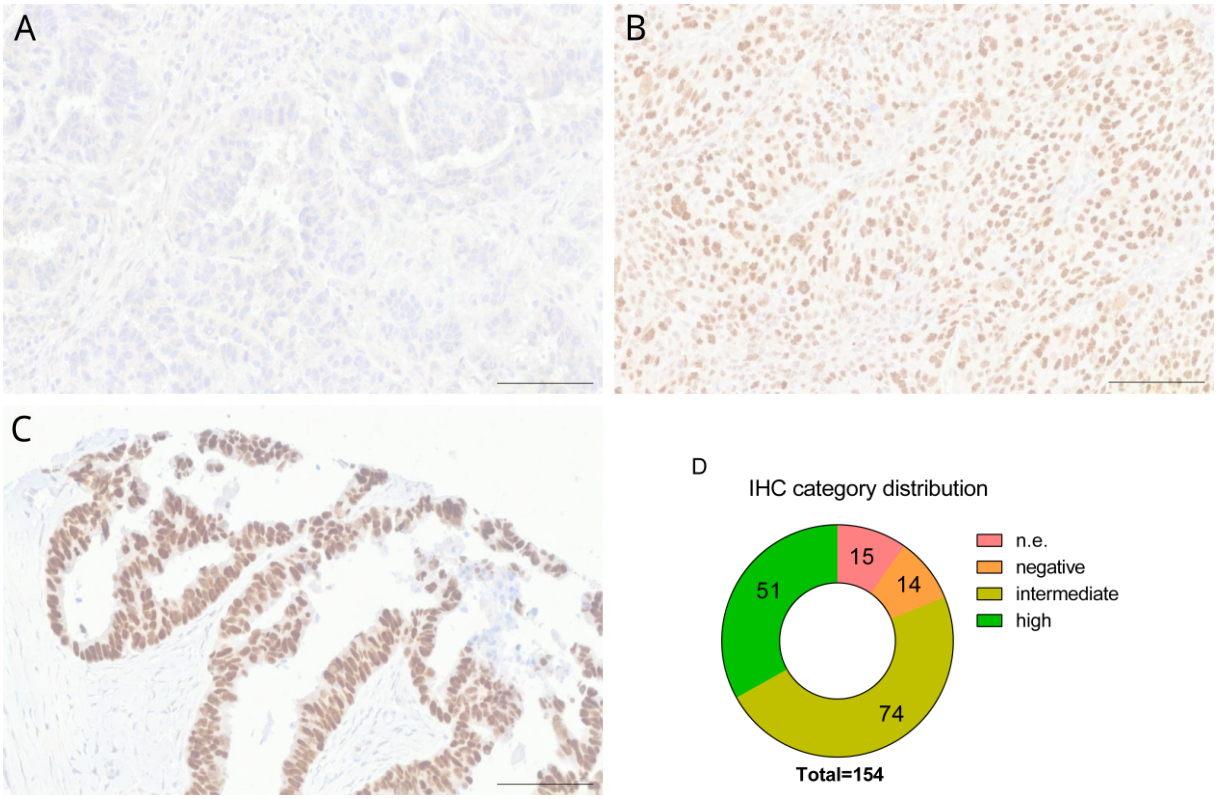

Figure 19: Classification of p53 IHC categories and their distributions in the patient cohort. A) Light-field microscope image of a patient tissue categorized as "negative". B) Light-field microscope images of patient tissues categorized as "intermediate". C) Light-field microscope image of a patient tissue categorized as "high". All images were taken with 20x magnification. Scale bar depicts 100 µm. D) Donut graph depicting the distribution of categories among the patient cohort. n.e. = not evaluable.

To determine whether the IHC p53 staining is a prognostic marker for progression-free survival (PFS) and overall survival (OS), the IHC categories "negative", "intermediate" and "high" were analyzed with a Mantel-Cox test. For both PFS and OS, there was no significant difference between the IHC categories (PFS: p = 0.514 and OS: p = 0.848, Figure 20).

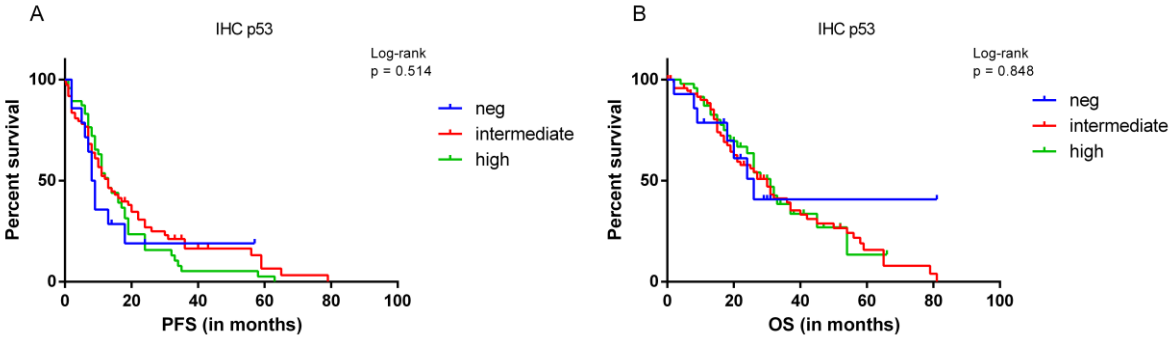

p53 IHC category	Neg.	Interm.	High
# patients	14	74	51
Median PFS	8.5	13	13

p53 IHC category	Neg.	Interm.	High
# patients	14	74	51
Median OS	26	30	31

Figure 20: Survival curves of A) progression-free survival (PFS) and B) overall survival (OS) of p53 IHC category results. Mantel-Cox test was used to determine statistical significance. Table below depicts the number of patients in each category and the median survival of patients in that respective category.

Previous studies have shown the prognostic impact of p53 aggregation in cancer. Against the current consensus, Heinzl et al. have shown that serous ovarian cancer patients with higher p53 aggregation have longer progression-free survival using the p53-Seprion-ELISA.[48] To test this correlation, we have stained the tissue microarrays of 154 ovarian cancer patient samples with PLA in two antibody combinations: p53xA11 and p53xOC. Representative images of the staining categories are shown in Figure 21A-C.

For the p53xA11 staining, 138 patients were categorized into the three staining intensities in the following distribution: 41 patients in the category "negative" (29.7 %), 69 patients in the category "intermediate" (50 %), and 28 patients in the category "high" (20.3 %), as shown in Figure 21D. For the p53xOC staining, 130 patients were categorized into the three staining intensities in the following order: 30 patients in the category "negative" (23 %), 64 patients in the category "intermediate" (49.2 %), and 36 patients in the category "high" (27.7 %), as shown in Figure 21E.

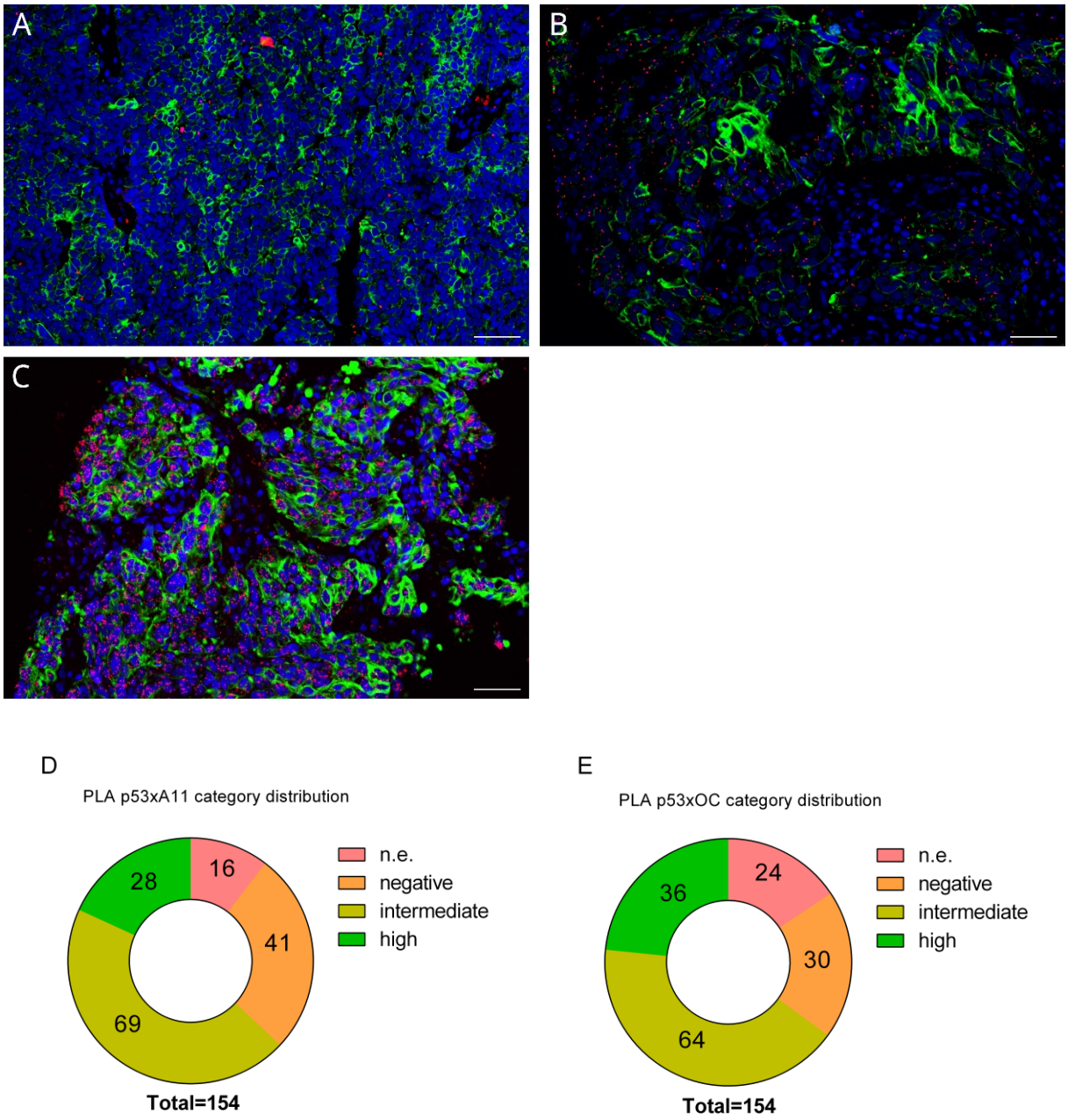

Figure 21: Classification of PLA intensity categories and their distributions in the patient cohort. A) Fluorescence microscope image of a patient tissue categorized as "negative". B) Fluorescence microscope images of patient tissues categorized as "intermediate". C) Fluorescence microscope image of a patient tissue categorized as "high". Blue = DAPI, Red = PLA points (p53xA11), Green = Cytokeratin-staining. All images were taken with 20x magnification. Scale bar depicts 50 µm. D) Donut graph depicting the distribution of p53xA11 staining categories among the patient cohort. E) Donut graph depicting the distribution of p53xOC staining categories among the patient cohort. n.e. = not evaluable.

Table 14: Chi-square table depicting the correlation between the IHC and PLA staining categories. P-values determined by Chi-square testing are <0.0001 for both.

	A11 negative	**A11 intermediate**	**A11 high**
IHC negative	8	6	0
IHC intermediate	27	37	6
IHC high	4	25	20
	OC negative	**OC intermediate**	**OC high**
IHC negative	7	6	0
IHC intermediate	18	36	12
IHC high	3	21	23

To examine the overlap of categories between IHC and PLA staining, a Chi-square test was done. Both, the association between IHC and the p53xA11 PLA staining and the association between IHC and the p53xOC staining, were significantly correlated with a p-value below 0.0001 for both each. However, there are 31 patients who showed a positive IHC signal but were negative for oligomer p53 aggregation and 21 patients who showed a positive IHC signal but were negative for fibril aggregation. Similarly, 6 patients in both PLA stainings each showed intermediate oligomer or fibril p53 aggregation but had a negative p53 IHC staining (Table 14).

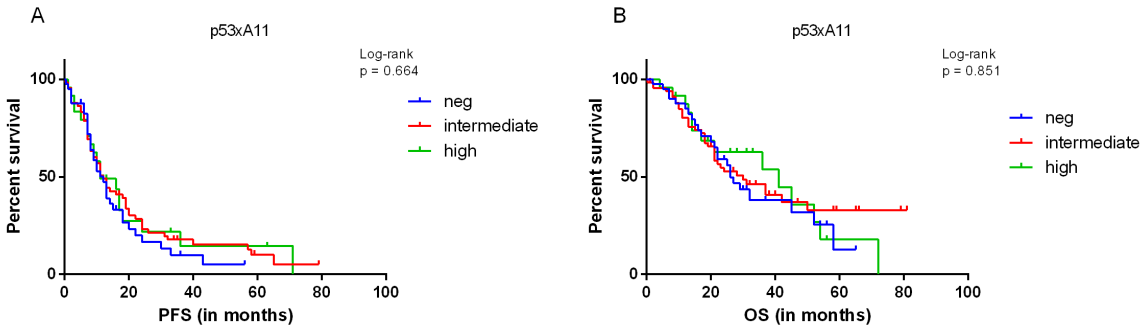

p53xA11 category	**Neg.**	**Interm.**	**High**	**p53xA11 category**	**Neg.**	**Interm.**	**High**
# patients	41	69	28	**# patients**	41	69	28
Median PFS	12	12	11	**Median OS**	26	30	41

Figure 22: Survival curves of A) progression-free survival and B) overall survival of p53xA11 PLA category results. Mantel-Cox test was used to determine statistical significance. Table below depicts the number of patients in each category and the median survival of patients in the respective category.

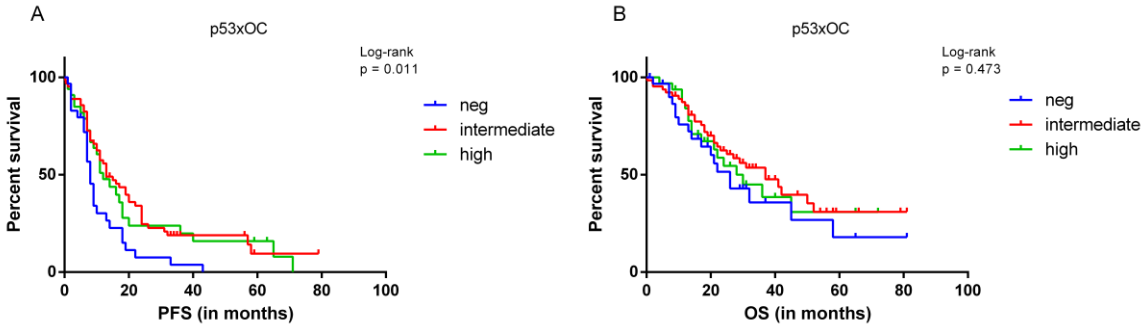

p53xOC category	Neg.	Interm.	High
# patients	30	64	36
Median PFS	8	13	12

p53xOC category	Neg.	Interm.	High
# patients	30	64	36
Median OS	26	37	28

Figure 23: Survival curves of A) progression-free survival and B) overall survival of p53xOC PLA category results. Mantel-Cox test was used to determine statistical significance. Table below depicts the number of patients in each category and the median survival of patients in the respective category.

Since the staining intensity of p53 IHC is not a prognostic marker for PFS or OS, the association of PLA staining with PFS and OS was evaluated using a Mantel-Cox test (Figure 22 and 23). The only association that achieved statistical significance ($p = 0.013$) is between the p53xOC staining and progression-free survival. The patient cohort with a negative p53 fibril staining had a median PFS of 8 months, while the patient cohort with an intermediate and high p53 fibril staining had a median PFS of 13 and 12 months respectively. Therefore, we show that patients with a positive p53 fibril staining have a prolonged progression-free survival.

4 Discussion

4.1 Comparing ReACp53 IC_{50} values with existing literature

In recent years, p53 aggregation has been found in a wide range of different cancer types. In 2010, Levy et al. have shown the presence of p53 aggregation in breast cancer patient tissues with co-immunofluorescence. The immunofluorescence staining was done with an anti-p53 (DO-1) antibody and anti-oligomer antibody A11.[49] However, the protein aggregation staining with A11 shows significantly more staining for protein aggregation than for stabilized p53. Therefore, protein aggregation besides p53 aggregation is present, and the simultaneous presence of p53 and protein aggregation signal does not necessarily confirm the presence of a p53 aggregate molecule.[60] This is improved with the Proximity Ligation Assay, where a signal is only produced when the primary antibodies have bound within roughly 40 nm of each other.[62] In this thesis, we have successfully shown p53 aggregation presence in breast cancer cell lines covering all four histological subtypes with varying *TP53* mutational subtypes. This was done with Proximity Ligation Assay in two different antibody combinations, p53xA11 for the detection of p53 oligomers and p53xOC for the detection of p53 fibrils. Additionally, we have shown that p53 fibrils act as a prognostic marker for progression-free survival in ovarian cancer.

While there are currently no p53-based cancer therapies approved by the FDA or EMA, arsenic trioxide (ATO), which is approved for acute promyelocytic leukemia, has recently been shown to reduce unfolded p53 bound by the antibody Pa1620.[64] Many other p53-based therapies are currently in pre-clinical and clinical trials, with some targeting p53 aggregation.[92] For this work, the drug ReACp53, which was first designed and published by Soragni et al. in 2016[66], was chosen. The concept involves a small peptide that binds to an aggregation-prone sequence in the p53 protein, thereby facilitating the refolding into the wild-type state of p53 and subsequent stimulation of wild-type p53 activity, which in cancer cells involves the initiation of apoptosis.[66] ReACp53 has since then been tested in multiple different settings, including different types of cancer. In this work, for the 17 cell lines treated with ReACp53, IC_{50} values lie between 4.8 and 7.6 µM. Soragni et al. tested ReACp53-concentration-dependent cell viability on S1-GODL cells, a primary ovarian cancer cell line, which had an EC_{50} of 3.9 µM.[66] Neal et al. also tested ReACp53-concentration-dependent cell viability on ovarian cancer cell lines in combination with carboplatin. Out of the 8 tested cell lines, OvCar-3 (missense), OAW-28 (frameshift), Kuramochi (missense), and SNU-119(missense) show IC_{50} values between the concentrations of 5 and 7 µM. SKOV-3 (frameshift) and CaOV-3 (nonsense) show an IC_{50} between 7 and 10 µM ReACp53, while the remaining two cell lines, OvCar-4 (missense) and OvCar-8 (deletion), show an IC_{50} above 10

μM.[69] Zhang et al. investigated the effect of ReACp53 in mutant-p53 carrying cell models by measuring cell viability at 0.2, 1, 5 and 10 μM. For CWRR-1 (missense), the IC_{50} lies between 5 and 10 μM ReACp53, while the remaining three cell models, C4-2 (wild-type), PC-3 (frameshift), and DU-145 (missense), exhibit an IC_{50} above 10 μM.[68] Additionally, both Neal et al. and Zhang et al. have observed a protective effect of small concentrations of ReACp53 in their cell models. A similar observation can be made for multiple cell lines in the breast cancer cell line panel from this work, including MDA-MB-157, T-47D, CAMA-1, BT-474, and UACC-893.

4.2 ReACp53 sensitivity dependencies

The previously reported Seprion-ELISA results are comprehensive characterizations of the amount of p53 aggregates present in 16 breast cancer cell lines and HBL-100. No statistical correlation between the amount of p53 aggregation and the respective IC_{50} values was found. Additionally, the breast cancer cell lines have been separated into their respective histological subtypes, *TP53* mutational status, and mutational category. No statistical significance has been observed between the IC_{50} values and any of these categories in this work. Mutations have been categorized into "DNA-binding", "structural" and "others", which include indel or nonsense mutations. This work did not find a significant difference in ReAcCp53 IC_{50} for *TP53* mutational status. A possible reason for this could be that out of the 17 cell lines tested, only two cell lines are wild-type p53 carriers. In contrast to our results, the studies by Soragni, Neal, and Zhang showed that the sensitivity to ReACp53 is dependent on the *TP53* mutational status. Soragni et al. showed a ReACp53 specificity towards organoids grown from mutant p53 cell lines compared to wild-type p53 cell lines by observing more extensive signs of apoptotic and/or necrotic cell death in organoids with *TP53* mutation than in organoids with wild-type p53 or null cells. Additionally, ReACp53 only significantly affected gene expression in mutant p53 cells, with over 2400 transcripts differentially regulated in OvCar3 cells and over 700 transcripts differentially regulated in high-grade serous ovarian cancer sample cells, while wild-type p53 only had a few significantly different expressed transcripts. In xenografted mice models, only tumors from mutant p53-bearing cells responded to ReACp53 treatment, while p53 wild-type MCF-7 xenografts were unaffected by ReACp53 treatment. Furthermore, a significant increase of p21 and MDM2, transcriptional targets of p53, was only visible in OvCar3 but not MCF-7 xenografts after ReACp53 treatment.[66] Neal et al. demonstrated a reduced tumor burden in mice with OvCar3-based xenografts in comparison to p53-null SKOV-3 cells[69] Zhang et al. utilized an SDS-resistance assay to show reduced SDS-resistant p53 aggregate formation after treatment with 20 μM ReACp53 in DU145 and CWRR1, both p53-mutated prostate cancer cell lines, whereas in the wild-type p53 C4-2 cell line, no effect was observed. Additionally, certain effects of ReACp53 treatment, including the change of total p53 protein level, association of p53 with Bax, and mitochondrial

p53 staining, were only affected in mutant p53 cell lines.[68] However, in contrast to the previous findings from the study, Zhang et al. showed a reduced DNA synthesis rate after treatment with 10 µM ReACp53 through flow cytometry analysis for every cell line, regardless of *TP53* mutational status. They also reported a significant increase in total p21 protein levels in CWRR1 cells and a slight increase in DU145 and C4-2 cells, while p21 transcripts were increased in C4-2 and CWRR1 cells. These results point to a potential mutational-independent function of ReACp53.[68] In a poster abstract, Sartini et al. describe how they found that organoids established from four different sarcoma lines show a marked susceptibility towards ReACp53, irrespective of the *TP53* mutational status of the organoids.[109]

To assess the efficacy of ReACp53, multiple studies have tried to evaluate the amount of change in p53 aggregation in response to ReACp53 treatment. We have shown that treatment of 6 µM ReACp53 reduced PLA signals for both antibody combinations (p53 oligomers and p53 fibrils). Soragni et al. determined the change in p53 level from ReACp53 treatment by staining unfolded p53 with the antibody PAb240, a surrogate marker for p53 aggregation. After treatment of the patient-derived cell line S1 GODL cells with 10 µM ReACp53, they observed a decrease in unfolded p53 with less than 10 % of Pab240 positive cells present.[66] Zhang et al. showed a reduction of SDS-resistant p53 in DU145 and CWRR1 cells when treated with 20 µM ReACp53.[68] While both methods from Soragni and Zhang can only classify total p53 aggregation, we have shown that both p53 oligomers and fibrils can be reduced through ReACp53 treatment. Additionally, Soragni et al. reported a localization shift of total p53 from a cytosolic, punctate staining to a nuclear p53 staining upon ReACp53 treatment.[66] Similarly, Zhang et al. show that ReACp53 treatment led to a 30 % increase in cells with nuclear p53. In CWRR1 cells, ReACp53 treatment also led to an increase in mitochondrial p53 staining.[68]

Besides PLA staining of p53 oligomers and fibrils, this work also analyzed changes in total protein levels of p53 by ReACp53 treatment with IF staining. We saw a slight increase in total p53, which stands in contrast to previously published results from Soragni et al. and Zhang et al., who both observed a decrease in total p53 protein after ReACp53 treatment. Soragni et al. added Nutlin-3, a p53-MDM2 interaction inhibitor, to S1 GODL cells treated with ReACp53 and observed higher p53 levels, which points to MDM2 degradation of p53 after ReACp53 treatment.[66] Zhang et al. observed higher MDM2 levels in the immunoprecipitated p53 fraction of ReACp53-treated CWRR1-cells.[68] Therefore, both have observed a higher p53-MDM2 interaction after ReACp53 treatment. The small increase in total p53 that we have observed points towards the possibility that p53 is not degraded by MDM2 after ReACp53 in the breast cancer cell lines. One possible explanation for the potential lack of MDM2 degradation could be the *TP53* mutations present in

14 of the breast cancer cell lines, which may obstruct the p53-MDM2 binding site even after ReACp53-mediated native folding.[110,111]

4.3 ReACp53 increases Cleaved-Caspase 3 positive cells

To determine if ReACp53 restores wild-type p53 function to initiate apoptosis, we examined the amount of cleaved Caspase 3 cells before and after ReACp53 treatment. The majority of cell lines showed increased cleaved Caspase 3 signal, which correlated significantly with the decrease of p53 oligomer and fibril aggregates. However, the total amount of cleaved Caspase 3 positive cells was low, with a maximum of 7.2 % of cells for BT-549. Soragni et al. stained OvCar3 and S1 GODL cells with YO-PRO-1, an early apoptosis marker, and propidium iodide, a late apoptotic cell marker, in response to ReACp53 treatment. The increase of these apoptosis markers was dose-dependent, but cell viability was only partially recovered by the pan-caspase inhibitor QV-OPh.[66] Neal et al. analyzed ReACp53 and Carboplatin synergy. While the treatment with ReACp53 did increase the percentage of apoptotic cells, the increase of apoptotic cells from both the Carboplatin treatment and the combination treatment was stronger. Furthermore, this was validated on protein level, with the apoptosis marker cleaved PARP increased only slightly from the ReACp53 treatment compared to Carboplatin and the combination, while Cleaved Caspase 3 from the ReACp53 treatment was not visible in the Western Blot. A potential explanation for the low amount of Cleaved-Caspase 3 positive cells in this work could be the rapid process of apoptosis initiation.[112] However cleaved Caspase 3 signal was detected in the cell line A2780 for over 72 hours after cisplatin treatment.[112,113] Another possible explanation for the low amount of cleaved Caspase 3 positive cells we have observed could be that ReACp53 initiates apoptosis through a cleaved Caspase 3 independent pathway, e.g. through Apoptosis-Inducing Factor (AIF).[114] This would also potentially explain the partial cell viability recovery by pan-caspase inhibition that Soragni et al. have observed.[66] Additionally, the total amount of cells analyzed was greatly limited by the image frame. For future studies, the amount of analyzed cells needs to be increased by either taking multiple images or scanning the complete slide.

4.4 ReACp53 reduces p53 aggregation and influences p63 and p73 protein levels

Since we have determined that ReACp53 IC_{50} values are not dependent on mutational status, we investigated other potential mechanisms that could explain the differences in ReACp53 sensitivity in our cell lines. The two p53-family members, p63 and p73, show high homology to p53 in the binding region of ReACp53, which makes them susceptible to "off-target" ReACp53 binding. To analyze these potential off-target effects of ReACp53, we have performed RT-PCR to determine *TP63* and *TP73* transcript levels and stained the cell lines before and after ReACp53 treatment with p63 and p73 immunostaining. For *TP63* and *TP73* transcript levels, we have found no significant correlation with ReACp53 IC_{50} values, nor with log2FC of both p53xA11 and p53xOC stainings. Therefore, the level of gene expression does not predict ReACp53 sensitivity nor the amount of p53 aggregation reduction. However on protein level, we observed an increase in total p63 and a decrease in total p73, which is in line with Soragni et al., who has shown that ReACp53 leads to an increase in p63 expression and protein level and a decrease in p73 expression and protein level in both OvCar3 and S1 GODL cells.[66] Palanikumar et al. have designed the tripyridylamide ADH-6 that has been shown to dissolve p53 aggregates. Transcriptome analysis of oligopyridylamide-treated MIA PaCa-2 cells also showed a reduction of TP73 expression after ADH-6 treatment.[63] Zeng et al. theorize that the isoform ΔNp73 could be responsible for the anti-tumoral activity of ReACp53 in wild type p53 cells through induction of co-aggregation that is dissolved by ReACp53 regardless of p53 mutational status. The overexpression of ΔNp73 in wild type-p53 HEK239T cells increased Thioflavin T staining, which simultaneously made them more susceptible to ReACp53 treatment.[115]

4.5 The interplay between p53 isoforms, p53 aggregation and ReACp53 sensitivity

To further characterize the cell line panel and elucidate potential off-target effects of ReACp53, the cell lines were analyzed for their amount of full length-p53 and the isoforms Δ133p53 and Δ40p53 by RT-PCR. As mentioned in the introduction, a major aggregation-prone region is located at aa 252-258. Therefore, both isoforms retain the possibility to form p53 aggregates. We have observed a significant positive correlation only between p53 aggregation and the amount of gene expression of full length p53. Further, the association between sensitivity to ReACp53 and the expression levels of full-length p53, Δ40p53, and Δ133p53 was analyzed. Only the amount of full-length p53 expression was significantly correlated to IC_{50} values of ReACp53. In contrast, we have

not seen a correlation between the amount of the two p53 isoforms. This could indicate that the two p53 isoforms are not involved in p53 aggregate formation in these cell lines and, therefore, are not involved in ReACp53 sensitivity. In contrast to our work, Melo dos Santos et al. have confirmed that the loss of the first transactivation domain confers an affinity for aggregation of Δ40p53 in endometrial carcinoma cells.[116] Not only is Δ40p53 implicated in p53 aggregation, Hofstetter et al. show that elevated Δ40p53 expression presented an independent prognostic marker for recurrence-free survival in mucinous ovarian cancer.[7] Avery-Kiejda et al. show that Δ40p53 expression is highly correlated with the triple-negative breast cancer subtype, which is a clinically aggressive subtype.[117] The Δ133p53 isoform was also shown to be implicated in p53 aggregation formation, with Lei et al. showing that Δ133p53 has a higher solvent accessible surface area (SASA) than wild-type p53, indicating a higher aggregation propensity. This effect seems to be especially pronounced for the hydrophobic region of aa 251-257, where SASA is much larger in the Δ133p53 isoform than for the same region in the wild-type p53.[118] This hydrophobic region is also the target of ReACp53.[66] Bischof et al. have also demonstrated that high expression of Δ133p53 acts as an independent prognostic marker for improved overall survival in ovarian cancer.[119] Additionally, Arsic et al. describe intricate mechanisms of the interplay between the Δ133p53 isoform and ΔNp63 that affect intracellular mobility, the epithelial-to-mesenchymal transition, and invasiveness.[120]

4.6 P53 aggregation as an independent biomarker in ovarian cancer

The stabilization of p53, determined by p53 IHC, has long been recognized as a prognostic marker in multiple cancer types. In this work, 154 patients diagnosed with serous ovarian cancer were stained with immunohistochemistry to assess the amount of total p53 protein present in the ovarian cancer tissue. There was no significant association between the p53 staining and either PFS or OS. De Graeff et al. analyzed 476 patients diagnosed with epithelial ovarian cancer for their p53 positivity through IHC staining with the DO-7 antibody clone. When patients were separated into their origin countries (Scotland and Netherlands), univariate analysis showed that positive p53 staining is associated with shorter PFS and OS for both cohorts. However, this association did not hold up for the multivariate analysis for neither PFS or OS.[121] This aligns with our results, that p53 stabilization is not a prognostic marker in ovarian cancer. This is likely due to the high percentage of ovarian cancer patients (96 %) having *TP53* mutations, resulting in most patients testing positive for p53 in IHC.[99] This is also reflected in our patient cohort, where out of 140 evaluable patient tissues, 126 patients (90 %) stained positive for p53 in IHC.

To verify whether p53 aggregation is a suitable prognostic marker in contrast to IHC based on previous work from our research group (Heinzl et al.[48]), we stained 154 patient tissues with PLA

to detect p53 oligomers and p53 fibrils. While the categories of IHC staining and PLA staining did correlate, there was a considerable number of patients who were p53 aggregation negative but IHC positive. In this work, the amount of p53 oligomers detected in ovarian cancer tissue was not a prognostic factor for neither PFS nor OS. In contrast, the amount of p53 fibrils was a prognostic factor for PFS, with p53 fibril-positive patients showing longer PFS than p53 fibril-negative patients (Median PFS: 13 months vs 8 months).

De Smet et al. have shown that for colon cancer and glioblastoma, the presence of p53 in nuclear inclusion bodies (p53-nIB) is associated with a worse prognosis for disease-free and overall survival. While they were able to quantify their results into five subcategories, statistical significance was only specified for the comparison between patients with p53-nIB in over 50 % of tumor cells, and soluble p53.[122] Iwahashi et al. analyzed 121 HGSOC patients with p53 IHC staining. Patients who were p53 IHC positive for both nucleus and cytoplasm had worse prognosis for both progression-free and overall survival than patients with complete p53 aggregation absence or patients who were only nuclear p53 IHC positive. The p53 aggregation was then confirmed by co-IF consisting of an anti-p53 antibody and ProteoStat, an amyloid binding fluorophore in 14 patients with positive nuclear and cytoplasmic p53 IHC staining.[123] Nishitsuji et al. used the same staining method of co-IF with an anti-p53 antibody and ProteoStat for lung squamous cell carcinoma and showed similar results to Iwahashi et al. Patients with nuclear and cytoplasmic positive co-IF staining had significantly worse outcomes for both progression-free and overall survival than patients with p53 negative and p53 nuclear staining.[124] However, as already mentioned before, co-immunofluorescence is not a sensitive method for p53 aggregation detection. Additionally, Iwahashi et al. did not directly confirm the relation between p53 aggregation and patient survival.[123] Heinzl et al. analyzed fresh-frozen serous ovarian cancer tissue from 123 patients with Seprion-ELISA to determine the amount of p53 aggregation. Due to the possible quantification of Seprion-ELISA, p53 aggregation results were separated into three categories: negative, moderate, and high. High p53 aggregation compared to moderate or low p53 aggregation was an independent prognostic factor for longer PFS and OS in multivariate analysis. Heinzl et al. theorize that this effect might be due to the high levels of p53 aggregation stimulating an immune response. Additionally, the apoptosis markers cleaved PARP and cleaved Caspase 3 were elevated for high p53 aggregation tissue. [48]

5 Conclusion & Outlook

To summarize, we have identified p53 aggregates in oligomer and fibril states in a panel of breast cancer cell lines with the Proximity Ligation Assay. For the drug ReACp53, IC_{50} values were determined for 17 cell lines in total. These IC_{50} values lie in a range of 4.8 to 7.6 µM, which is close to previously reported IC_{50} values of other cancer cell lines. The IC_{50} values are not significantly associated with previously measured p53 aggregation quantity, total p53 protein quantity, histological subtype, *TP53* mutational status or the type of *TP53* mutation. Previously published data on ReACp53 shows a sensitivity dependence on *TP53* mutational status, which we were not able to reproduce. However, our panel of cell lines only included two wild-type p53 cell lines. To accurately reflect this relation, more wild-type p53 breast cancer cell lines need to be analyzed.

Although ReAcp53 reduces aggregated p53, total p53 is not reduced after treatment. While other studies have shown p53-MDM2 interaction after ReACp53 treatment, the slight increase of total p53 questions whether the p53 degradation process is functional in our cell lines. Future work could elucidate the p53 degradation mechanism after re-folding aggregated p53 and whether this is MDM2-mediated. Additionally, the identification of the cellular location of a PLA signal would be a feasible next step to identify whether ReACp53 changes the cellular localization of p53 protein in breast cancer cell lines. While total p53 quantity is slightly increased, total p63 is increased and total p73 is decreased upon ReACp53 treatment, which is in line with previously published results. ReACp53 also increases the amount of cells positive for cleaved Caspase 3, showing that ReACp53 is capable of inducing apoptosis. However, the total amount of cells positive for cleaved Caspase 3 was relatively small, which could allude to either a different apoptosis signal pathway or a different type of cell death that is activated upon ReACp53 treatment. By inhibiting Caspase 3 during ReACp53 treatment and measuring cell death with an MTT assay, the importance of Caspase 3 during ReACp53-triggered cell death could be analyzed. For further characterization, we have analyzed the cell line panel regarding their gene expression level of full-length p53, the isoforms Δ40p53 and Δ133p53, p63 and p73. The amount of expression of full-length p53 correlates directly with the IC_{50} values of ReACp53. In this work, the gene expression of these proteins was only evaluated in untreated cell lines. Bulk RNA-sequencing of the cell lines before and after ReACp53 treatment could elucidate the effect of ReACp53 not only on transcription directly but also show if p53 is able to regulate transcription of target genes after refolding. While this has been shown in ovarian cancer cell lines, it is unclear whether this is also the case for breast cancer cell lines and if this is a consistent effect throughout 16 breast cancer cell lines that cover a wide range of histological subtypes and different *TP53* mutations.[66]

Besides the effect of ReACp53 treatment on breast cancer cell lines, this work also looked at p53 aggregation in ovarian cancer patient tissue and its relationship to progression-free and overall

survival. Through IHC staining, we first determined the amount of stabilized p53 protein present in ovarian cancer patient tissue. However, the amount of p53 IHC staining intensity did not show a correlation with neither PFS or OS. To determine the amount of p53 aggregation present in ovarian cancer patient tissue, Proximity Ligation Assay was used to stain the tissue to visualize p53 oligomer and fibril presence. Patient tissue was again separated into three subcategories based on staining intensity. To remove human error and bias, in future analyses this process should be done by computer software. This makes it easier to set intensity thresholds for each category and not only standardize categories for inter-tumor heterogeneity but also for intra-tumor heterogeneity. For p53 oligomers, no statistical correlation with PFS or OS could be found. However, fibrillary p53 aggregation was a prognostic biomarker for PFS but not OS, which is in line with Heinzl et al. but contradicts previous findings. Even though these results reached statistical significance with 154 patients included, the patient cohort needs to be further expanded in the future to solidify these results.

Therefore, this work shows both a prognostic effect of p53 aggregation for progression-free survival in ovarian cancer and shows that ReACp53 reduces p53 aggregation in breast cancer cell lines. It remains to be seen, whether ReACp53 is a more effective treatment option than the prognostic effect that p53 aggregation offers.

6 List of abbreviations

AA	Amino acid
ADC	Antibody-Drug Conjugate
APR	Aggregation-prone region
ATO	Arsenic trioxide
BC	Breast cancer
BCS	Breast conserving surgery
CC3	Cleaved Caspase 3
CTD	C-terminal domain
DAB	3,3'-Diaminobenzidine
DAPI	4'6-Diamidin-2-phenylindol
DBD	DNA-binding domain
DN	Dominant negative
ELISA	Enzyme-linked immunoabsorbant assay
EMA	European Medicines Agency
EOC	Epithelial ovarian cancer
ER	Estrogen receptor
FA	Formaldehyd
FBS	Fetal bovine serum
FDA	Food and Drug Administration

FFPE	Formalin-fixed, paraffin embedded
FIGO	International Federation of Gynecology and Obstetrics
FLp53	Full-length p53
GOF	Gain-of-function
H&E	Hematoxylin-eosin
HER2	Human epidermal growth factor receptor 2
HGSOC	High-grade serous ovarian cancer
HR	Homologous recombination
HRP	Horseradish peroxidase
IC_{50}	Inhibitory concentration 50 %
IF	Immunofluorescence
IHC	Immunohistochemistry
LOF	Loss-of-function
Log2FC	Log_2 foldchange
MOMP	Mitochondrial outer membrane permeabilization
NMR	Nuclear magnetic resonance
OC	Ovarian cancer
OD	Oligomerization domain
OS	Overall survival

P53-nIB	P53 nuclear inclusion bodies
PARP	Poly-(ADP-Ribose) Polymerase
PFS	Progression-free survival
PLA	Proximity Ligation Assay
PR	Progesteron receptor
PRR	Proline-rich region
PS	Pencillin-Streptamycin
PTM	Post-translational modification
ReACp53	Re-Active p53
RT	Room temperature
RT-PCR	Real-time PCR
SASA	Solvent accessible surface area
SD	Standard deviation
STIC	Serous tubal intraepithelial carcinoma
TAD1	Transactivation domain 1
TAD2	Transactivation domain 2
TBS-T	TBS-Tween
TMA	Tissue Microarray
TN	Triple-negative
WHO	World Health Organization

7 List of Figures

8 List of Tables

9 Literature

1. Solares MJ, Kelly DF. Complete Models of p53 Better Inform the Impact of Hotspot Mutations. *Int J Mol Sci*. 2022;23(23):15267. doi:10.3390/ijms232315267

2. Saha T, Kar RK, Sa G. Structural and sequential context of p53: A review of experimental and theoretical evidence. *Prog Biophys Mol Biol*. 2015;117(2-3):250-263. doi:10.1016/j.pbiomolbio.2014.12.002

3. Khoury MP, Bourdon JC. The Isoforms of the p53 Protein. *Cold Spring Harb Perspect Biol*. 2010;2(3):a000927-a000927. doi:10.1101/cshperspect.a000927

4. Uversky V. p53 Proteoforms and Intrinsic Disorder: An Illustration of the Protein Structure–Function Continuum Concept. *Int J Mol Sci*. 2016;17(11):1874. doi:10.3390/ijms17111874

5. Arlt C, Ihling CH, Sinz A. Structure of full-length p53 tumor suppressor probed by chemical cross-linking and mass spectrometry. *PROTEOMICS*. 2015;15(16):2746-2755. doi:10.1002/pmic.201400549

6. Vieler M, Sanyal S. p53 Isoforms and Their Implications in Cancer. *Cancers*. 2018;10(9):288. doi:10.3390/cancers10090288

7. Hofstetter G, Berger A, Berger R, et al. The N-Terminally Truncated p53 Isoform Δ40p53 Influences Prognosis in Mucinous Ovarian Cancer. *Int J Gynecol Cancer*. 2012;22(3):372-379. doi:10.1097/IGC.0b013e31823ca031

8. Zhao L, Sanyal S. p53 Isoforms as Cancer Biomarkers and Therapeutic Targets. *Cancers*. 2022;14(13):3145. doi:10.3390/cancers14133145

9. Mehta S, Campbell H, Drummond CJ, et al. Adaptive homeostasis and the p53 isoform network. *EMBO Rep*. 2021;22(12):e53085. doi:10.15252/embr.202153085

10. Ha JH, Prela O, Carpizo DR, Loh SN. p53 and Zinc: A Malleable Relationship. *Front Mol Biosci*. 2022;9:895887. doi:10.3389/fmolb.2022.895887

11. Liu Y, Su Z, Tavana O, Gu W. Understanding the complexity of p53 in a new era of tumor suppression. *Cancer Cell*. 2024;42(6):946-967. doi:10.1016/j.ccell.2024.04.009

12. Hafner A, Bulyk ML, Jambhekar A, Lahav G. The multiple mechanisms that regulate p53 activity and cell fate. *Nat Rev Mol Cell Biol*. 2019;20(4):199-210. doi:10.1038/s41580-019-0110-x

13. Nagpal I, Yuan ZM. The Basally Expressed p53-Mediated Homeostatic Function. *Front Cell Dev Biol*. 2021;9:775312. doi:10.3389/fcell.2021.775312

14. Horn HF, Vousden KH. Coping with stress: multiple ways to activate p53. *Oncogene*. 2007;26(9):1306-1316. doi:10.1038/sj.onc.1210263

15. Kruse JP, Gu W. Modes of p53 Regulation. *Cell*. 2009;137(4):609-622. doi:10.1016/j.cell.2009.04.050

16. Hernández Borrero LJ, El-Deiry WS. Tumor suppressor p53: Biology, signaling pathways, and therapeutic targeting. *Biochim Biophys Acta BBA - Rev Cancer*. 2021;1876(1):188556. doi:10.1016/j.bbcan.2021.188556

17. Cheng Q, Chen J. Mechanism of p53 stabilization by ATM after DNA damage. *Cell Cycle*. 2010;9(3):472-478. doi:10.4161/cc.9.3.10556

18. Brázda V, Fojta M. The Rich World of p53 DNA Binding Targets: The Role of DNA Structure. *Int J Mol Sci*. 2019;20(22):5605. doi:10.3390/ijms20225605

19. Fischer M. Gene regulation by the tumor suppressor p53 – The omics era. *Biochim Biophys Acta BBA - Rev Cancer*. 2024;1879(4):189111. doi:10.1016/j.bbcan.2024.189111

20. Chipuk JE, Bouchier-Hayes L, Kuwana T, Newmeyer DD, Green DR. PUMA Couples the Nuclear and Cytoplasmic Proapoptotic Function of p53. *Science*. 2005;309(5741):1732-1735. doi:10.1126/science.1114297

21. Dashzeveg N, Yoshida K. Cell death decision by p53 via control of the mitochondrial membrane. *Cancer Lett*. 2015;367(2):108-112. doi:10.1016/j.canlet.2015.07.019

22. Kalkavan H, Green DR. MOMP, cell suicide as a BCL-2 family business. *Cell Death Differ*. 2018;25(1):46-55. doi:10.1038/cdd.2017.179

23. Vousden KH, Lane DP. p53 in health and disease. *Nat Rev Mol Cell Biol*. 2007;8(4):275-283. doi:10.1038/nrm2147

24. Marques MA, De Oliveira GAP, Silva JL. The chameleonic behavior of p53 in health and disease: the transition from a client to an aberrant condensate scaffold in cancer. Mukhopadhyay S, ed. *Essays Biochem*. 2022;66(7):1023-1033. doi:10.1042/EBC20220064

25. Cai BH, Hsu YC, Yeh FY, et al. P63 and P73 Activation in Cancers with p53 Mutation. *Biomedicines*. 2022;10(7):1490. doi:10.3390/biomedicines10071490

26. Naeimzadeh Y, Tajbakhsh A, Fallahi J. Understanding the prion-like behavior of mutant p53 proteins in triple-negative breast cancer pathogenesis: The current therapeutic strategies and future directions. *Heliyon*. 2024;10(4):e26260. doi:10.1016/j.heliyon.2024.e26260

27. Osterburg C, Dötsch V. Structural diversity of p63 and p73 isoforms. *Cell Death Differ*. 2022;29(5):921-937. doi:10.1038/s41418-022-00975-4

28. Rodriguez Calleja L, Lavaud M, Tesfaye R, et al. The p53 Family Members p63 and p73 Roles in the Metastatic Dissemination: Interactions with microRNAs and TGFβ Pathway. *Cancers*. 2022;14(23):5948. doi:10.3390/cancers14235948

29. Chen Y, Peng Y, Fan S, Li Y, Xiao ZX, Li C. A double dealing tale of p63: an oncogene or a tumor suppressor. *Cell Mol Life Sci*. 2018;75(6):965-973. doi:10.1007/s00018-017-2666-y

30. Maeso-Alonso L, López-Ferreras L, Marques MM, Marin MC. p73 as a Tissue Architect. *Front Cell Dev Biol*. 2021;9:716957. doi:10.3389/fcell.2021.716957

31. Marshall CB, Beeler JS, Lehmann BD, et al. Tissue-specific expression of p73 and p63 isoforms in human tissues. *Cell Death Dis*. 2021;12(8):745. doi:10.1038/s41419-021-04017-8

32. Rozenberg JM, Zvereva S, Dalina A, et al. Dual Role of p73 in Cancer Microenvironment and DNA Damage Response. *Cells*. 2021;10(12):3516. doi:10.3390/cells10123516

33. Woodstock DL, Sammons MA, Fischer M. p63 and p53: Collaborative Partners or Dueling Rivals? *Front Cell Dev Biol*. 2021;9:701986. doi:10.3389/fcell.2021.701986

34. Candi E, Smirnov A, Panatta E, et al. Metabolic pathways regulated by p63. *Biochem Biophys Res Commun*. 2017;482(3):440-444. doi:10.1016/j.bbrc.2016.10.094

35. Ramos H, Raimundo L, Saraiva L. p73: From the p53 shadow to a major pharmacological target in anticancer therapy. *Pharmacol Res*. 2020;162:105245. doi:10.1016/j.phrs.2020.105245

36. Xu Y, Yang X, Xiong Q, Han J, Zhu Q. The dual role of p63 in cancer. *Front Oncol*. 2023;13:1116061. doi:10.3389/fonc.2023.1116061

37. Balchin D, Hayer-Hartl M, Hartl FU. In vivo aspects of protein folding and quality control. *Science*. 2016;353(6294):aac4354. doi:10.1126/science.aac4354

38. Kulkarni P, Leite VBP, Roy S, et al. Intrinsically disordered proteins: Ensembles at the limits of Anfinsen's dogma. *Biophys Rev*. 2022;3(1):011306. doi:10.1063/5.0080512

39. Ezzat K, Sturchio A, Espay AJ. Proteins Do Not Replicate, They Precipitate: Phase Transition and Loss of Function Toxicity in Amyloid Pathologies. *Biology*. 2022;11(4):535. doi:10.3390/biology11040535

40. Houben B, Rousseau F, Schymkowitz J. Protein structure and aggregation: a marriage of necessity ruled by aggregation gatekeepers. *Trends Biochem Sci*. 2022;47(3):194-205. doi:10.1016/j.tibs.2021.08.010

41. Zhang Z, Huang G, Song Z, Gatch AJ, Ding F. Amyloid Aggregation and Liquid–Liquid Phase Separation from the Perspective of Phase Transitions. *J Phys Chem B*. 2023;127(28):6241-6250. doi:10.1021/acs.jpcb.3c01426

42. Willbold D, Strodel B, Schröder GF, Hoyer W, Heise H. Amyloid-type Protein Aggregation and Prion-like Properties of Amyloids. *Chem Rev*. 2021;121(13):8285-8307. doi:10.1021/acs.chemrev.1c00196

43. Kwan K, Castro-Sandoval O, Gaiddon C, Storr T. Inhibition of p53 protein aggregation as a cancer treatment strategy. *Curr Opin Chem Biol*. 2023;72:102230. doi:10.1016/j.cbpa.2022.102230

44. Ghosh S, Ghosh D, Ranganathan S, et al. Investigating the Intrinsic Aggregation Potential of Evolutionarily Conserved Segments in p53. *Biochemistry*. 2014;53(38):5995-6010. doi:10.1021/bi500825d

45. Li J, Guo M, Chen L, Chen Z, Fu Y, Chen Y. p53 amyloid aggregation in cancer: function, mechanism, and therapy. *Exp Hematol Oncol*. 2022;11(1):66. doi:10.1186/s40164-022-00317-7

46. Petronilho EC, Pedrote MM, Marques MA, et al. Phase separation of p53 precedes aggregation and is affected by oncogenic mutations and ligands. *Chem Sci*. 2021;12(21):7334-7349. doi:10.1039/d1sc01739j

47. Bullock AN, Fersht AR. Rescuing the function of mutant p53. *Nat Rev Cancer*. 2001;1(1):68-76. doi:10.1038/35094077

48. Heinzl N, Maritschnegg E, Koziel K, et al. Amyloid-like p53 as prognostic biomarker in serous ovarian cancer—a study of the OVCAD consortium. *Oncogene*. 2023;42(33):2473-2484. doi:10.1038/s41388-023-02758-8

49. Levy CB, Stumbo AC, Ano Bom APD, et al. Co-localization of mutant p53 and amyloid-like protein aggregates in breast tumors. *Int J Biochem Cell Biol*. 2011;43(1):60-64. doi:10.1016/j.biocel.2010.10.017

50. De Oliveira GAP, Petronilho EC, Pedrote MM, et al. The Status of p53 Oligomeric and Aggregation States in Cancer. *Biomolecules*. 2020;10(4):548. doi:10.3390/biom10040548

51. Ghosh S, Salot S, Sengupta S, et al. p53 amyloid formation leading to its loss of function: implications in cancer pathogenesis. *Cell Death Differ*. 2017;24(10):1784-1798. doi:10.1038/cdd.2017.105

52. Ferretti GDS, Quarti J, Dos Santos G, Rangel LP, Silva JL. Anticancer Therapeutic Strategies Targeting p53 Aggregation. *Int J Mol Sci*. 2022;23(19):11023. doi:10.3390/ijms231911023

53. Silva JL, Cino EA, Soares IN, Ferreira VF, A. P. De Oliveira G. Targeting the Prion-like Aggregation of Mutant p53 to Combat Cancer. *Acc Chem Res*. 2018;51(1):181-190. doi:10.1021/acs.accounts.7b00473

54. Scheckel C, Aguzzi A. Prions, prionoids and protein misfolding disorders. *Nat Rev Genet*. 2018;19(7):405-418. doi:10.1038/s41576-018-0011-4

55. Forget KJ, Tremblay G, Roucou X. p53 Aggregates Penetrate Cells and Induce the Co-Aggregation of Intracellular p53. Tatzelt J, ed. *PLoS ONE*. 2013;8(7):e69242. doi:10.1371/journal.pone.0069242

56. Billant O, Friocourt G, Roux P, Voisset C. p53, A Victim of the Prion Fashion. *Cancers*. 2021;13(2):269. doi:10.3390/cancers13020269

57. Housmans JAJ, Wu G, Schymkowitz J, Rousseau F. A guide to studying protein aggregation. *FEBS J*. 2023;290(3):554-583. doi:10.1111/febs.16312

58. Gan SD, Patel KR. Enzyme Immunoassay and Enzyme-Linked Immunosorbent Assay. *J Invest Dermatol*. 2013;133(9):1-3. doi:10.1038/jid.2013.287

59. Maritschnegg E, Heinzl N, Wilson S, et al. Polymer-Ligand-Based ELISA for Robust, High-Throughput, Quantitative Detection of p53 Aggregates. *Anal Chem*. 2018;90(22):13273-13279. doi:10.1021/acs.analchem.8b02373

60. Heinzl N, Koziel K, Maritschnegg E, et al. A comparison of four technologies for detecting p53 aggregates in ovarian cancer. *Front Oncol*. 2022;12:976725. doi:10.3389/fonc.2022.976725

61. Yang-Hartwich Y, Bingham J, Garofalo F, Alvero AB, Mor G. Detection of p53 Protein Aggregation in Cancer Cell Lines and Tumor Samples. In: Mor G, Alvero AB, eds. *Apoptosis and Cancer: Methods and Protocols*. Springer New York; 2015:75-86. doi:10.1007/978-1-4939-1661-0_7

62. Söderberg O, Gullberg M, Jarvius M, et al. Direct observation of individual endogenous protein complexes in situ by proximity ligation. *Nat Methods*. 2006;3(12):995-1000. doi:10.1038/nmeth947

63. Palanikumar L, Karpauskaite L, Al-Sayegh M, et al. Protein mimetic amyloid inhibitor potently abrogates cancer-associated mutant p53 aggregation and restores tumor suppressor function. *Nat Commun*. 2021;12(1):3962. doi:10.1038/s41467-021-23985-1

64. Chen S, Wu JL, Liang Y, et al. Arsenic Trioxide Rescues Structural p53 Mutations through a Cryptic Allosteric Site. *Cancer Cell*. 2021;39(2):225-239.e8. doi:10.1016/j.ccell.2020.11.013

65. Ferraz Da Costa DC, Campos NPC, Santos RA, et al. Resveratrol prevents p53 aggregation *in vitro* and in breast cancer cells. *Oncotarget*. 2018;9(49):29112-29122. doi:10.18632/oncotarget.25631

66. Soragni A, Janzen DM, Johnson LM, et al. A Designed Inhibitor of p53 Aggregation Rescues p53 Tumor Suppression in Ovarian Carcinomas. *Cancer Cell*. 2016;29(1):90-103. doi:10.1016/j.ccell.2015.12.002

67. Lei J, Cai M, Shen Y, Lin D, Deng X. Molecular dynamics study on the inhibition mechanisms of ReACp53 peptide for p53–R175H mutant aggregation. *Phys Chem Chem Phys*. 2021;23(40):23032-23041. doi:10.1039/D1CP03094A

68. Zhang Y, Xu L, Chang Y, et al. Therapeutic potential of ReACp53 targeting mutant p53 protein in CRPC. *Prostate Cancer Prostatic Dis*. 2020;23(1):160-171. doi:10.1038/s41391-019-0172-z

69. Neal A, Lai T, Singh T, et al. Combining ReACp53 with Carboplatin to Target High-Grade Serous Ovarian Cancers. *Cancers*. 2021;13(23):5908. doi:10.3390/cancers13235908

70. Bray F, Laversanne M, Sung H, et al. Global cancer statistics 2022: GLOBOCAN estimates of incidence and mortality worldwide for 36 cancers in 185 countries. *CA Cancer J Clin*. 2024;74(3):229-263. doi:10.3322/caac.21834

71. Maajani K, Jalali A, Alipour S, Khodadost M, Tohidinik HR, Yazdani K. The Global and Regional Survival Rate of Women With Breast Cancer: A Systematic Review and Meta-analysis. *Clin Breast Cancer*. 2019;19(3):165-177. doi:10.1016/j.clbc.2019.01.006

72. Smolarz B, Nowak AZ, Romanowicz H. Breast Cancer—Epidemiology, Classification, Pathogenesis and Treatment (Review of Literature). *Cancers*. 2022;14(10):2569. doi:10.3390/cancers14102569

73. Giaquinto AN, Sung H, Miller KD, et al. Breast Cancer Statistics, 2022. *CA Cancer J Clin*. 2022;72(6):524-541. doi:10.3322/caac.21754

74. Łukasiewicz S, Czeczelewski M, Forma A, Baj J, Sitarz R, Stanisławek A. Breast Cancer—Epidemiology, Risk Factors, Classification, Prognostic Markers, and Current Treatment Strategies—An Updated Review. *Cancers*. 2021;13(17):4287. doi:10.3390/cancers13174287

75. Løberg M, Lousdal ML, Bretthauer M, Kalager M. Benefits and harms of mammography screening. *Breast Cancer Res*. 2015;17(1):63. doi:10.1186/s13058-015-0525-z

76. McDonald ES, Clark AS, Tchou J, Zhang P, Freedman GM. Clinical Diagnosis and Management of Breast Cancer. *J Nucl Med*. 2016;57(Supplement 1):9S-16S. doi:10.2967/jnumed.115.157834

77. Peintinger F. National Breast Screening Programs across Europe. *Breast Care*. 2019;14(6):354-358. doi:10.1159/000503715

78. Katsura C, Ogunmwonyi I, Kankam HK, Saha S. Breast cancer: presentation, investigation and management. *Br J Hosp Med*. 2022;83(2):1-7. doi:10.12968/hmed.2021.0459

79. Harbeck N, Penault-Llorca F, Cortes J, et al. Breast cancer. *Nat Rev Dis Primer*. 2019;5(1):66. doi:10.1038/s41572-019-0111-2

80. Karim AM, Eun Kwon J, Ali T, et al. Triple-negative breast cancer: epidemiology, molecular mechanisms, and modern vaccine-based treatment strategies. *Biochem Pharmacol*. 2023;212:115545. doi:10.1016/j.bcp.2023.115545

81. Ciruelos E, Pérez-García JM, Gavilá J, Rodríguez A, De La Haba-Rodriguez J. Maintenance Therapy in HER2-Negative Metastatic Breast Cancer: A New Approach for an Old Concept. *Clin Drug Investig*. 2019;39(7):595-606. doi:10.1007/s40261-019-00790-9

82. Martínez-Sáez O, Prat A. Current and Future Management of HER2-Positive Metastatic Breast Cancer. *JCO Oncol Pract*. 2021;17(10):594-604. doi:10.1200/OP.21.00172

83. Jones S, Holmes FA, O'Shaughnessy J, et al. Docetaxel With Cyclophosphamide Is Associated With an Overall Survival Benefit Compared With Doxorubicin and Cyclophosphamide: 7-Year Follow-Up of US Oncology Research Trial 9735. *J Clin Oncol*. 2009;27(8):1177-1183. doi:10.1200/JCO.2008.18.4028

84. Nitz U, Gluz O, Clemens M, et al. West German Study PlanB Trial: Adjuvant Four Cycles of Epirubicin and Cyclophosphamide Plus Docetaxel Versus Six Cycles of Docetaxel and Cyclophosphamide in HER2-Negative Early Breast Cancer. *J Clin Oncol*. 2019;37(10):799-808. doi:10.1200/JCO.18.00028

85. Richard S, Selle F, Lotz JP, Khalil A, Gligorov J, Soares DG. Pertuzumab and trastuzumab: the rationale way to synergy. *An Acad Bras Ciênc*. 2016;88(suppl 1):565-577. doi:10.1590/0001-3765201620150178

86. Barzaman K, Karami J, Zarei Z, et al. Breast cancer: Biology, biomarkers, and treatments. *Int Immunopharmacol*. 2020;84:106535. doi:10.1016/j.intimp.2020.106535

87. Dumontet C, Reichert JM, Senter PD, Lambert JM, Beck A. Antibody–drug conjugates come of age in oncology. *Nat Rev Drug Discov*. 2023;22(8):641-661. doi:10.1038/s41573-023-00709-2

88. Moreira C, Kaklamani V. Lapatinib and breast cancer: current indications and outlook for the future. *Expert Rev Anticancer Ther*. 2010;10(8):1171-1182. doi:10.1586/era.10.113

89. Park JW, Liu MC, Yee D, et al. Adaptive Randomization of Neratinib in Early Breast Cancer. *N Engl J Med*. 2016;375(1):11-22. doi:10.1056/NEJMoa1513750

90. Marvalim C, Datta A, Lee SC. Role of p53 in breast cancer progression: An insight into p53 targeted therapy. *Theranostics*. 2023;13(4):1421-1442. doi:10.7150/thno.81847

91. Meric-Bernstam F, Zheng X, Shariati M, et al. Survival Outcomes by *TP53* Mutation Status in Metastatic Breast Cancer. *JCO Precis Oncol*. 2018;(2):1-15. doi:10.1200/PO.17.00245

92. Hassin O, Oren M. Drugging p53 in cancer: one protein, many targets. *Nat Rev Drug Discov*. 2023;22(2):127-144. doi:10.1038/s41573-022-00571-8

93. Oronsky B, Ray CM, Spira AI, Trepel JB, Carter CA, Cottrill HM. A brief review of the management of platinum-resistant–platinum-refractory ovarian cancer. *Med Oncol*. 2017;34(6):103. doi:10.1007/s12032-017-0960-z

94. Webb PM, Jordan SJ. Epidemiology of epithelial ovarian cancer. *Best Pract Res Clin Obstet Gynaecol*. 2017;41:3-14. doi:10.1016/j.bpobgyn.2016.08.006

95. Gaona-Luviano P, Medina-Gaona LA, Magaña-Pérez K. Epidemiology of ovarian cancer. *Chin Clin Oncol*. 2020;9(4):47-47. doi:10.21037/cco-20-34

96. Lisio MA, Fu L, Goyeneche A, Gao Z hua, Telleria C. High-Grade Serous Ovarian Cancer: Basic Sciences, Clinical and Therapeutic Standpoints. *Int J Mol Sci*. 2019;20(4):952. doi:10.3390/ijms20040952

97. Shih IM, Wang Y, Wang TL. The Origin of Ovarian Cancer Species and Precancerous Landscape. *Am J Pathol*. 2021;191(1):26-39. doi:10.1016/j.ajpath.2020.09.006

98. Wu R, Wang P, Lin S, et al. Genomic landscape and evolutionary trajectories of ovarian cancer precursor lesions. *J Pathol*. 2019;248(1):41-50. doi:10.1002/path.5219

99. Wallis B, Bowman KR, Lu P, Lim CS. The Challenges and Prospects of p53-Based Therapies in Ovarian Cancer. *Biomolecules*. 2023;13(1):159. doi:10.3390/biom13010159

100. Berek JS, Renz M, Kehoe S, Kumar L, Friedlander M. Cancer of the ovary, fallopian tube, and peritoneum: 2021 update. *Int J Gynecol Obstet*. 2021;155(S1):61-85. doi:10.1002/ijgo.13878

101. Wentzensen N, Poole EM, Trabert B, et al. Ovarian Cancer Risk Factors by Histologic Subtype: An Analysis From the Ovarian Cancer Cohort Consortium. *J Clin Oncol*. 2016;34(24):2888-2898. doi:10.1200/JCO.2016.66.8178

102. Harter P, Bogner G, Chiva L, et al. Statement of the AGO Kommission Ovar, AGO Study Group, NOGGO, AGO Austria, Swiss AGO, BGOG, CEEGOG, GEICO, and SFOG regarding the use of hyperthermic intraperitoneal chemotherapy (HIPEC) in epithelial ovarian cancer. *Bull Cancer (Paris)*. 2024;111(3):277-284. doi:10.1016/j.bulcan.2023.02.011

103. Sambasivan S. Epithelial ovarian cancer: Review article. *Cancer Treat Res Commun*. 2022;33:100629. doi:10.1016/j.ctarc.2022.100629

104. O'Malley DM, Krivak TC, Kabil N, Munley J, Moore KN. PARP Inhibitors in Ovarian Cancer: A Review. *Target Oncol*. 2023;18(4):471-503. doi:10.1007/s11523-023-00970-w

105. Witt BL, Tollefsbol TO. Molecular, Cellular, and Technical Aspects of Breast Cancer Cell Lines as a Foundational Tool in Cancer Research. *Life*. 2023;13(12):2311. doi:10.3390/life13122311

106. Albrecht J, Müller M, Hafstað V, et al. Dynamic methylation and expression of alternative promoters for oestrogen receptor alpha in cell line models of fulvestrant resistance. *Mol Oncol*. Published online August 6, 2024:1878-0261.13713. doi:10.1002/1878-0261.13713

107. Schneider CA, Rasband WS, Eliceiri KW. NIH Image to ImageJ: 25 years of image analysis. *Nat Methods*. 2012;9(7):671-675. doi:10.1038/nmeth.2089

108. Bankhead P, Loughrey MB, Fernández JA, et al. QuPath: Open source software for digital pathology image analysis. *Sci Rep*. 2017;7(1). doi:10.1038/s41598-017-17204-5

109. Sartini S, Le H, Soragni A. Protein aggregation in sarcoma as a target for therapy. *Cancer Res*. 2023;83(7_Supplement):2582-2582.

110. Nakamura S, Roth JA, Mukhopadhyay T. Multiple Lysine Mutations in the C-Terminal Domain of p53 Interfere with MDM2-Dependent Protein Degradation and Ubiquitination. *Mol Cell Biol*. 2000;20(24):9391-9398. doi:10.1128/MCB.20.24.9391-9398.2000

111. Poyurovsky MV, Katz C, Laptenko O, et al. The C terminus of p53 binds the N-terminal domain of MDM2. *Nat Struct Mol Biol*. 2010;17(8):982-989. doi:10.1038/nsmb.1872

112. Shaulov-Rotem Y, Merquiol E, Weiss-Sadan T, et al. A novel quenched fluorescent activity-based probe reveals caspase-3 activity in the endoplasmic reticulum during apoptosis. *Chem Sci*. 2016;7(2):1322-1337. doi:10.1039/C5SC03207E

113. Rehm M, Düßmann H, Jänicke RU, Tavaré JM, Kögel D, Prehn JHM. Single-cell Fluorescence Resonance Energy Transfer Analysis Demonstrates That Caspase Activation during Apoptosis Is a Rapid Process. *J Biol Chem*. 2002;277(27):24506-24514. doi:10.1074/jbc.M110789200

114. Bano D, Prehn JHM. Apoptosis-Inducing Factor (AIF) in Physiology and Disease: The Tale of a Repented Natural Born Killer. *eBioMedicine*. 2018;30:29-37. doi:10.1016/j.ebiom.2018.03.016

115. Zeng J, Soragni A, Ishizawa J, et al. Targeting Aggregation of Wilde-Type p53 and Mutant p53 with ReACp53 As a Novel Therapeutic Concept for AML. *Blood*. 2016;128(22):3944-3944. doi:10.1182/blood.V128.22.3944.3944

116. Melo Dos Santos N, De Oliveira GAP, Ramos Rocha M, et al. Loss of the p53 transactivation domain results in high amyloid aggregation of the Δ40p53 isoform in endometrial carcinoma cells. *J Biol Chem*. 2019;294(24):9430-9439. doi:10.1074/jbc.RA119.007566

117. Avery-Kiejda KA, Morten B, Wong-Brown MW, Mathe A, Scott RJ. The relative mRNA expression of p53 isoforms in breast cancer is associated with clinical features and outcome. *Carcinogenesis*. 2014;35(3):586-596. doi:10.1093/carcin/bgt411

118. Lei J, Qi R, Tang Y, et al. Conformational stability and dynamics of the cancer-associated isoform Δ133p53β are modulated by p53 peptides and p53-specific DNA. *FASEB J*. 2019;33(3):4225-4235. doi:10.1096/fj.201801973R

119. Bischof K, Knappskog S, Hjelle SM, et al. Influence of p53 Isoform Expression on Survival in High-Grade Serous Ovarian Cancers. *Sci Rep*. 2019;9(1):5244. doi:10.1038/s41598-019-41706-z

120. Arsic N, Slatter T, Gadea G, et al. Δ133p53β isoform pro-invasive activity is regulated through an aggregation-dependent mechanism in cancer cells. *Nat Commun*. 2021;12(1):5463. doi:10.1038/s41467-021-25550-2

121. De Graeff P, Hall J, Crijns APG, et al. Factors influencing p53 expression in ovarian cancer as a biomarker of clinical outcome in multicentre studies. *Br J Cancer*. 2006;95(5):627-633. doi:10.1038/sj.bjc.6603300

122. The Journal of Pathology - 2016 - De Smet - Nuclear inclusion bodies of mutant and wild-type p53 in cancer a hallmark of.pdf.

123. Iwahashi N, Ikezaki M, Komohara Y, et al. Cytoplasmic p53 aggregates accumulated in p53-mutated cancer correlate with poor prognosis. Furmanski P, ed. *PNAS Nexus*. 2022;1(3):pgac128. doi:10.1093/pnasnexus/pgac128

124. Nishitsuji K, Mito R, Ikezaki M, et al. Impacts of cytoplasmic p53 aggregates on the prognosis and the transcriptome in lung squamous cell carcinoma. *Cancer Sci*. 2024;115(9):2947-2960. doi:10.1111/cas.16252